David Taylor Research Center
Bethesda, MD 20084–5000

DTRC-89/038 January 1990

Ship Hydromechanics Department
Research and Development Report

Kelvin Wake Measurements Obtained on Five Surface Ship Models

by
Toby J. Ratcliffe
William T. Lindenmuth

DTRC-89/038 Kelvin Wake Measurements Obtained on Five Surface Ship Models

DISCLAIMER NOTICE

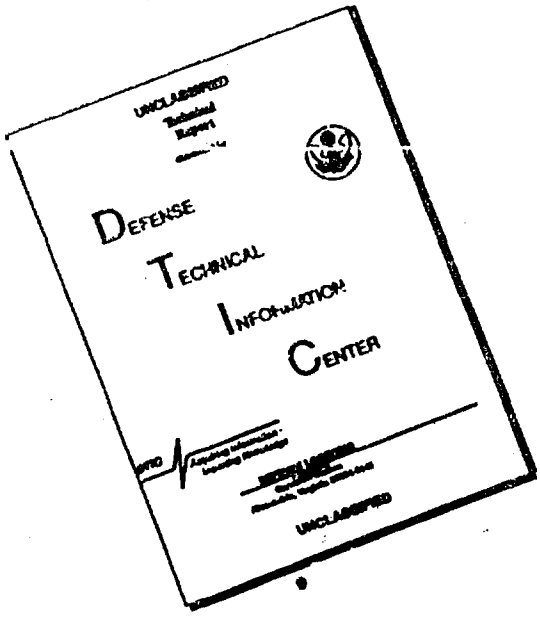

THIS DOCUMENT IS BEST QUALITY AVAILABLE. THE COPY FURNISHED TO DTIC CONTAINED A SIGNIFICANT NUMBER OF PAGES WHICH DO NOT REPRODUCE LEGIBLY.

MAJOR DTRC TECHNICAL COMPONENTS

CODE 011 DIRECTOR OF TECHNOLOGY, PLANS AND ASSESSMENT

12 SHIP SYSTEMS INTEGRATION DEPARTMENT

14 SHIP ELECTROMAGNETIC SIGNATURES DEPARTMENT

15 SHIP HYDROMECHANICS DEPARTMENT

16 AVIATION DEPARTMENT

17 SHIP STRUCTURES AND PROTECTION DEPARTMENT

18 COMPUTATION, MATHEMATICS & LOGISTICS DEPARTMENT

19 SHIP ACOUSTICS DEPARTMENT

27 PROPULSION AND AUXILIARY SYSTEMS DEPARTMENT

28 SHIP MATERIALS ENGINEERING DEPARTMENT

DTRC ISSUES THREE TYPES OF REPORTS:

1. **DTRC reports, a formal series,** contain information of permanent technical value. They carry a consecutive numerical identification regardless of their classification or the originating department.

2. **Departmental reports, a semiformal series,** contain information of a preliminary, temporary, or proprietary nature or of limited interest or significance. They carry a departmental alphanumerical identification.

3. **Technical memoranda, an informal series,** contain technical documentation of limited use and interest. They are primarily working papers intended for internal use. They carry an identifying number which indicates their type and the numerical code of the originating department. Any distribution outside DTRC must be approved by the head of the originating department on a case-by-case basis.

REPORT DOCUMENTATION PAGE

1a. REPORT SECURITY CLASSIFICATION UNCLASSIFIED	1b. RESTRICTIVE MARKINGS
2a. SECURITY CLASSIFICATION AUTHORITY	3. DISTRIBUTION/AVAILABILITY OF REPORT Approved for public release; distribution unlimited.
2b. DECLASSIFICATION/DOWNGRADING SCHEDULE	
4. PERFORMING ORGANIZATION REPORT NUMBER(S) DTRC–89/038	5. MONITORING ORGANIZATION REPORT NUMBER(S)
6a. NAME OF PERFORMING ORGANIZATION David Taylor Research Center 6b. OFFICE SYMBOL (If applicable) Code 1522	7a. NAME OF MONITORING ORGANIZATION
6c. ADDRESS (City, State, and ZIP Code) Bethesda, MD 20084–5000	7b. ADDRESS (City, State, and ZIP Code)
8a. NAME OF FUNDING/SPONSORING ORGANIZATION Chief of Naval Research, Office of Naval Technology 8b. OFFICE SYMBOL (If applicable)	9. PROCUREMENT INSTRUMENT IDENTIFICATION NUMBER
8c. ADDRESS (City, State, and ZIP Code) 800 N. Quincy St. Arlington, VA 22217	10 SOURCE OF FUNDING NUMBERS PROGRAM ELEMENT NO. 62543N; PROJECT NO. RS43–421S; TASK NO.; WORK UNIT ACCESSION NO. DN507164

11. TITLE (Include Security Classification)
KELVIN WAKE MEASUREMENTS OBTAINED ON FIVE SURFACE SHIP MODELS

12. PERSONAL AUTHOR(S)
Ratcliffe, Toby J. and Lindenmuth, William T.

13a. TYPE OF REPORT	13b. TIME COVERED	14. DATE OF REPORT (YEAR, MONTH, DAY)	15. PAGE COUNT
Final	FROM_____TO_____	1990 January	100

16. SUPPLEMENTARY NOTATION

17. COSATI CODES			18. SUBJECT TERMS (Continue on reverse if necessary and identify by block number)
FIELD	GROUP	SUB–GROUP	Kelvin Wake

19. ABSTRACT (Continue on reverse if necessary and identify by block number)

use single quotes

Experimental measurements of the Kelvin wake were obtained for five surface ship models representing an assortment of naval combatants, including a cruiser, an aircraft carrier, and three destroyers. Measurements were performed in the Carriage I basin at DTRC (David Taylor Research Center) using capacitance wave probes, a newly developed laser–slope meter, and close–range photogrammetry techniques. Data obtained from these measurement systems resulted in single point time–histories of wave height and slope as well as a series of sequential stereo snap–shots of the wave field generated by the towed model. All the models were tested without propulsion at a Froude number of 0.25, and similarities and differences in the wave patterns were documented and are discussed herein. In addition, Kelvin wake data were obtained for other conditions such as altered trim, speed variation, and with propulsion. The effect of these changes on the wave system is also discussed.

20. DISTRIBUTION/AVAILABILITY OF ABSTRACT	21. ABSTRACT SECURITY CLASSIFICATION
☐ UNCLASSIFIED/UNLIMITED ☒ SAME AS RPT ☐ DTIC USERS	UNCLASSIFIED

22a. NAME OF RESPONSIBLE INDIVIDUAL	22b. TELEPHONE (Include Area Code)	22c. OFFICE SYMBOL
Toby J. Ratcliffe	(202) 227–1638	Code 1522

CONTENTS

FIGURES

FIGURES (Continued)

FIGURES (Continued)

FIGURES (Continued)

TABLES

NOMENCLATURE

A/A_x	ratio of section area at a given station to maximum section area
AP	aft perpendicular
B/B_x	ratio of beam at a given to station to beam at the maximum section area
BL	baseline
C(w.y)+iS(w.y)	fourier transform of the wavecut record
C_w	wave resistance coefficient without truncation correction
$C_w(T)$	wave resistance coefficient with truncation correction
DWL	design waterline
E	amplitude of the free-wave spectra. $\sqrt{(F^2+G^2)}$
F	sine component of the free-wave spectra $$F(u)=\frac{4\sqrt{w^2-1}}{(2w^2-1)}\times\{C(w,y)\sin(uy)+S(w,y)\cos(uy)\}$$
F_n	Froude number. $V/\sqrt{gL}$
FP	forward perpendicular
g	gravitational constant
G	cosine component of the free-wave spectra $$G(u)=\frac{4\sqrt{w^2-1}}{(2w^2-1)}\times\{C(w,y)\cos(uy)+S(w,y)\sin(uy)\}$$
k_o	fundamental wave number. g/V^2
k_oL	$1/(F_n)^2$
L	length of model along DWL
η	wave height $$\int_{-\infty}^{\infty}\eta(x,y)\exp(iux)dx = C(w,y) + iS(w,y)\quad 0\le w<\infty$$

NOMENCLATURE (Continued)

U	transverse wave number, $\sec\theta \tan\theta$ $w\sqrt{w^2-1}$
V	ship or model speed
w	longitudinal wave number, $\sec\theta$
x	longitudinal distance from model FP to wave probe
y/B	transverse offset of wave probe from model centerline, non-dimensionalized by model beam
θ	angle from which the transverse wave number is computed: defined as the angle between the direction of wave propagation and the direction in which the ship/model is travelling (see figure)

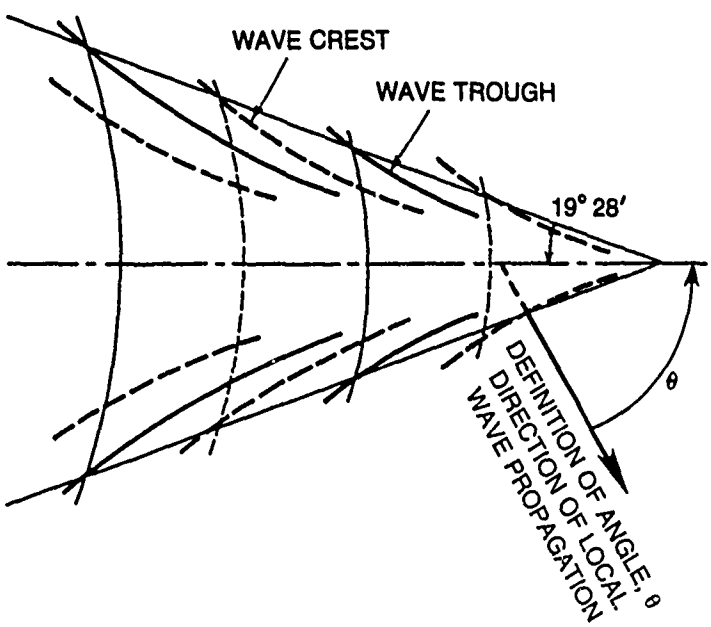

THIS PAGE INTENTIONALLY LEFT BLANK

ABSTRACT

Experimental measurements of the Kelvin wake were obtained for five surface ship models representing an assortment of naval combatants, including a cruiser, aircraft carrier and three destroyers. Measurements were performed in the Carriage 1 basin at DTRC (David Taylor Research Center) using capacitance wave probes, a newly developed laser-slope meter and close-range photogrammetry techniques. This resulted in single point time-histories of wave height and slope as well as a series of sequential stereo "snap-shots" of the wave field generated by the towed model. All the models were tested at a Froude number of 0.25 and similarities and differences in the wave patterns were documented and are discussed herein. In addition, Kelvin wake data were obtained for other conditions such as altered trim, speed variation and with or without propulsion. The effect of these changes on the wave system is also discussed.

ADMINISTRATIVE INFORMATION

This investigation was sponsored by the Chief of Naval Research, Office of Naval Technology OCNR 211 under the Ship and Submarine Technology Program, Program Element 62543N, ONT Thrust Area RS43-421S (SUSQSR), Surface Ship Hydrodynamic - Quieting Signature Reduction. The DTRC Work Unit Numbers are 1506-620 and 1506-810.

INTRODUCTION

Radar and optical images of ship wakes at sea have stirred an interest in obtaining model-scale Kelvin wake data. The distinctive Kelvin wave pattern consists of diverging and transverse waves as shown in Figure 1. These wave systems, manifested as surface disturbances, have unique characteristics. As shown in the figure, the included angle between the two divergent wave arms is 39 degrees. All components of the wave system parallel to the direction of travel of the ship have the same speed as the ship. The simplifed drawings of Figure 1 are good descriptions of the wave generation of a point source travelling through the water, however, in the case of a model or ship of finite length the wave system is more complicated and its details are influenced by the hull form characteristics.

In an effort to study these Kelvin wake details, five models were chosen for the experimental program, covering a range of naval combatant hull types: Model 5063 (Nimitz Class - CVN 68), Model 4645 (Charles Adams Class - DDG 2), Model 5201 (Virginia Class - CGN 38), Model 5359 (Kidd Class - DDG 993) and Model 5415, representing a prototype destroyer. For Model 5415, an extensive viscous wake data set already exists and the Kelvin wake measurements were obtained in the interest of forming a complete set of wake data for that hull form.

The Kelvin wake measurements performed on these models consisted of wave height time-history records obtained with capacitance wire probes, two-dimensional wave slope data obtained with a recently developed laser wave slope meter and "whole-field" wave height measurements obtained with a ceiling-mounted photogrammetric system. Each of these systems provides very unique information about the wave system generated by the model and the complete set of data is invaluable. A subset of this data has already been used to verify the results from numerical Kelvin wake computer code predictions.[1]

EXPERIMENTAL PROGRAM

All five ship models were tested at a speed corresponding to 20 knots as well as at a Froude number of 0.25 to observe similarities and differences in the Kelvin wake at identical Froude numbers.

Model 5063 (λ=33.058).representing the CVN 68, was tested as a drag body (without propulsion) at two Froude numbers: F_n=0.185 corresponding to a ship speed of 20 knots and F_n=0.25 corresponding to a ship speed of 27 knots.

Data were obtained on Model 4645 (λ=21.524) representing the DDG 2, over a range of Froude numbers from 0.25 to 0.31 (17.3 knots full scale to 21.3 knots full scale) in Froude number increments of 0.01. All data were obtained for the model run as a drag body. Two keel mounted sonar domes were in place on this model during the experiments.

In the case of Model 5201 (λ=24.064) representing the CGN 38, all the Kelvin wake data were obtained at a Froude number of 0.25 corresponding to a full scale ship speed of 20 knots. The model was tested at three trim conditions to observe the effect of trim on the Kelvin wake. The three trim conditions run were: operating trim (with and without propulsion), bow-down trim (with and without propulsion) and stern-down trim without propulsion.

The DDG 993 was represented by Model 5359 (λ=24.824) and data were collected at 20 speeds over a large range of Froude numbers, from F_n=0.20 to F_n=0.41, corresponding to ship speeds between 15.5 knots and 31.7 knots.

Finally, Model 5415 was tested, representing a prototype destroyer design with λ=24.824. The model was run at the same speeds for which viscous wake data were collected in a previous experiment: 20 knots (F_n=0.28) and 30 knots (F_n=0.41) with the addition of F_n=0.25.

Table 1 contains a list of hull form coefficients for each model while Figures 2-6 present sectional area curves and lines of form for all five models.

Table 2 documents the conditions at which each model was run as well as the appropriate model length and scale ratio.

EXPERIMENTAL APPARATUS

CAPACITANCE WAVE PROBE

A capacitance wire wave probe system was used to obtain longitudinal wave records along a track parallel to the model travel. The probes are fabricated at DTRC and each consists of a length of teflon-coated stainless steel cable. The overall probe diameter is 0.017 in. (0.44 mm). The probe and grounding wire are attached to a wave sensor circuit board mounted to a wave boom which suspends the wires in the water. For these experiments a square configuration of four wave probes was used. A diagram of the wave probe placement in the towing basin is shown in Figure 7. This set-up provided the option for deriving transverse and longitudinal wave slope from the height gauges. The longitudinal wavecut data were collected on a Perkin Elmer Model 70 Interdata computer and stored on 9-track magnetic tapes.

PHOTOGRAMMETRIC SYSTEM

Three sets of apparatus, unique to this research technique, were designed especially for use at DTRC and are discussed in the following paragraphs. Two views of the close-range photogrammetric system configuration are shown in Figure 8.

Towing Beam

An extended carriage towing beam is used to tow the ship model out from underneath the carriage so that an unobstructed view can be obtained from the ceiling mounted cameras. The towing beam is supported from the east vertical rails of Carriage I and is aligned with the centerline of the basin. The underside of the beam is identical to that on the standard towing carriage girder enabling model attachment by means of available towing brackets.

Cameras and Camera Carrier Assemblies

Two Hasselblad Model MK70 motorized metric cameras were used for these experiments. The cameras are equipped with Zeiss Biagon wide angle lenses with a nominal focal length of 1.57 in. (40 mm). A glass reseau plate with fiducial marks is permanently mounted at the film plane. This plate, along with the low distortion lens, are the two components which make this a "metric" camera recommended for photogrammetric data acquisition. Each camera was attached to a separate camera carrier assembly built to be lowered from the ceiling to the top of the carriage, facilitating the mounting of the cameras as well as loading and unloading of the film (2.76 in. (70 mm) Tri-X). The cameras were then raised up and locked to a fixture on the ceiling for the photographs to be taken. The movement of the camera carrier assemblies and the camera shutter triggering was initiated through a control panel located at the side of the basin. The cameras were mounted on the camera carrier assemblies at a tilt angle of 12 degrees toward each other. Although this resulted in a

"distorted" view. it was done in order to photogrammetrically enhance the vertical dimension of the stereopairs and thus significantly improve the wave height measurement resolution. Tilting also afforded maximum stereo coverage of the water surface.

Control Target Grid Assembly

It is necessary to have a calibrated "control" in every stereopair in order to obtain the most accurate results. For this towing tank application. the control grid was fabricated from PVC piping in two sections. one attached to the north wall of the basin. supporting 5 photogrammetric survey targets and one attached to the south wall supporting 10 targets. Figure 9 shows a photograph of the assembly in the basin along with a diagram indicating the dimensions of the structure. The targets were mounted on small diameter rods permanently attached to the PVC grid. Their x,y,z positions were determined by a National Bureau of Standards survey. When a set of photogrammetric experiments is completed. the targets are removed from the rods and the grid is lowered into the water to rest on the wall and bottom of the basin.

LASER WAVE SLOPE METER

The laser wave slope meter used in these experiments was developed at DTRC. A schematic of the system is shown in Figure 10. The system is composed of three items: a 15 mw helium-neon laser enclosed in a waterproof housing located at the bottom of the towing basin. a Sony CCD video camera located on the wave boom. and a DBA optical tracker which converts the location of the deflected laser beam on the ceiling to voltage signals representing x- and y- coordinates of position. The voltage signals are collected on the Perkin Elmer computer and stored on 9-track tape along with the wavecut data.

The advantage of such a system is its superior frequency response which is important in the detection of wave breaking and resolving other fine structure details of the model-generated wave pattern.

EXPERIMENTAL PROCEDURE

During the experiment the three sets of instrumentation - capacitance probes. photogrammetric system and laser slope meter were often in use simultaneously. The procedures which were used to collect the data will be described below for each system.

The computer data collection process for the capacitance probes and laser slope meter was triggered by a reflective "trip" attached to the underside of the carriage passing over a photocell mounted at the side of the basin. The photocell is positioned to insure that the maximum amount of data is collected before tank wall reflections occur. During each run. both the wavecut and slope data were collected at 100 Hz for 20 seconds and stored on 9-track magnetic tape.

In order to obtain stereopairs of the water surface, floating "seed" particles were distributed on the surface before each run. Computer card punch chips were used as the seeding material. After the chips were placed on the surface, the model was towed down the basin and a sequence of photographs were taken. Four reflective targets mounted on the carriage were sensed by an infrared scanner mounted on the basin wall to trigger the camera shutters and strobe lights as the model passed by. The shutters could also be triggered manually from the electrical control panel during any run. The camera shutters were set at 1/60th of a second at f/8. The strobe lights flashed each time with a duration of 1/1000th of a second and so it was actually the strobes which synchronized the stereopairs.

DATA ANALYSIS

Data analysis was required for the longitudinal wavecut and laser slope data as well as for the stereopairs. The nature of the analysis as well as associated accuracy issues will be discussed separately for each data set.

LONGITUDINAL WAVECUT ANALYSIS

The longitudinal wavecut data were analyzed on a DEC Microvax II using software originally used on the Interdata computer and rewritten for the Microvax. During the analysis, voltage data are converted to non-dimensional wave height and a Fourier transform is performed on the wavecuts to obtain free wave spectra. The software is documented in Reference 2. Tabular outputs and plots are then obtained of both the longitudinal wavecut, in dimensional and non-dimensional form, and the spectra. From the spectra, two wave resistance coefficients, C_W and $C_W(T)$ are calculated. C_W is the value of wave resistance calculated from the spectra representing the wavecut truncated before tank wall reflections occur. $C_W(T)$ includes an additional amount of wave resistance to account for the truncation of the wavecut. A thorough discussion of the methods of obtaining wave spectra and wave resistance from experimentally measured wave patterns is found in Reference 3. This reference also serves as the basis for the formulations used in wavecut data analysis at DTRC.

Data Accuracy

Three aspects of accuracy pertaining to the wave probe data have been examined to date: static calibration repeatability, wave record repeatability and probe contamination. Analysis of extensive repeat static calibrations performed on the capacitance probes during previous wavecut experiments yields an average error in the calibration factor of +/-0.5 %. This value results from nine calibrations of six wave probes. In an effort to examine the repeatability of the capacitance probe response to waves produced by the model during a run, two repeat wave records from the same probe were compared. For two model speeds, 4.36 knots and 11.65 knots, these comparisons yielded a

relative precision error (standard deviation) of 2 percent and 1.8 percent, respectively, referenced to the peak amplitude of the wave record. This error was obtained by calculating a standard deviation between two wave records using each of the 2000 data points in the record.

Probe contamination presented a problem for much of the experiment, manifesting itself as a shift in the zero level of the probe at the end of the wave record. This zero shift results in corrupted spectra near U=0 which in turn affects the accuracy of the C_w calculations. The magnitude of this bias-type error will be shown and discussed in a later section of the text. Towards the end of the experiment it was found that this contamination problem could be minimized by systematic probe cleaning and by recirculating the water around the probe at all times except when wavecut data were actually being collected. This contamination problem should be carefully monitored by those performing wavecut experiments.

LASER SLOPE DATA ANALYSIS

The laser slope data were analyzed on the Microvax II using a subroutine added to the same program which was used to analyze the wavecut data. The subroutine converts voltage from the optical tracker into longitudinal and transverse wave slope using a calibration of the wave slope meter apparatus obtained in the laboratory. The resulting wave slope information is processed in a similar manner to the wave height data, in order to obtain the free wave spectra and wave resistance coefficients. Details of the wave slope subroutine, data analysis procedures, accuracy and results will be documented in a forthcoming report.

PHOTOGRAMMETRIC DATA ANALYSIS

The photographs are developed by DTRC and then delivered to the National Ocean Survey (NOS) for analysis. NOS cartographers, using state-of-the-art "analytical plotters", measure wave elevations from the photographs over a grid of x-y- locations. Each stereopair covers an area in the towing basin of 35 X 20 ft (10.66 X 6.1 m). Typically 9000 data points are analyzed in a grid with 3-inch spacing. This process, including the instrument set-up, takes approximately 12 hours. The tabularized data is then stored on magnetic tape and returned to DTRC for plotting and analysis.

Data Accuracy

The accuracy of the photogrammetric data has been evaluated in three different ways. A "flat water" model was measured to determine the error (standard deviation) about the mean for the undisturbed water surface. This error was found to be 0.05 in.(1.37 mm) over the 35 X 20 ft (10.66 X 6.1 m) area. Next, a comparison was made between the capacitance wave probe and a photogrammetric profile. The profile chosen from the photogrammetric data was at the same distance from the centerline of the ship model as the capacitance probe was located, but on the opposite side

of the model. This choice was made because seeding was best on that side of the model, whereas it was avoided near the wave probe due to contamination problems. Assuming symmetry of the wave pattern, measurements obtained at equal distances from the centerline of the ship model should yield similar wave profiles. The comparison between the wire wave probe trace and the profile from a representative measured stereopair is shown in Figure 11. The agreement is quite good except in the locations of the highest crest and trough, where there are discrepancies of about 0.5 in. (12.7 mm). The cause of this discrepancy could be due to one of the following: lack of symmetry in the wave pattern, filtering techniques used in the collection of data with the wire probe, or lack of response of the probe to "high" frequency components of the wave system.

The third comparison which has been made is between two sequential stereopairs. Since there is some overlap between the two sets of data, two profiles can be overlaid on top of one another with a longitudinal offset. The result is shown in Figure 12. The two agree well over the first part of the profile and not quite as well over the remainder. The mean average difference between the two sets of vertical measurements is 0.26 in. (6.68 mm). The RMS variation about this mean difference is 0.15 in. (3.91 mm).

PRESENTATION AND DISCUSSION OF RESULTS

LONGITUDINAL WAVECUT DATA

One of the most interesting comparisons resulting from these experiments is that of the wavecuts and spectra for all five models operating at a Froude number of 0.25. These plots are presented in Figures 13 and 14. The wavecuts are plotted with respect to non-dimensionalized distance from the origin (model FP) which results in the longitudinal separation of bow and stern waves being almost identical. Results from only one of the four wave probes are presented in this report for brevity sake. The data presented here are from the probe located 6.1 feet (1.86 meters) from the model centerline.

The first comparison between wavecuts has been made initially on the basis of the ratio of the non-dimensionalized bow wave-to-stern wave peak-to-trough height. The two portions of the wave record used for these calculations were chosen to be the largest bow wave peak-to-trough height, centered about $xk_0 = 15$, and the largest stern wave peak-to-trough height, centered about $xk_0 = 30$. The first two wavecuts on Figure 13, obtained from Model 4645 and 5063 have bow-to-stern wave height ratios of 1.7 and 1.45 respectfully. The remaining 3 wavecuts, obtained from Models 5201, 5359 and 5415, have substantially smaller height ratios of 1.16, 0.966 and 0.911, respectively. A study of the respective sectional area curves reveals that the models with smaller bow/stern wave height ratios all have bow domes. On the other hand, Model 5063 has no dome and Model 4645 has

two keel-mounted domes and their bow/stern wave height ratios are significantly higher. From these observations, it is apparent that the presence of the bow domes on these particular hulls results in a height reduction of the bow wave. This may be a result of the sonar dome design philosophy to insure smooth flow around the dome. Unlike bulbous bows, however, domes are not optimized for minimum wave resistance, and likewise, the reduction in bow wave does not necessarily imply improved wave resistance characteristics of the hull.

Another feature of interest in these wavecuts is the region between the bow and stern wave systems. Determined by hull geometry, this complex wave system is difficult to predict analytically (see Reference 1). Although this is a complex region, there are some similarities between the wave records. All except Model 5063 show a double peaked crest in this "along the hull" region whereas Model 5063 generates a double peaked trough. The subsequent part of the wave record in this region is also similar for all models except 5063. This comparison suggests that the presence of a bow dome affects not only the bow wave height but also the characteristics of the entire wave disturbance. The complex wave system in this region may be due to nonlinear wave superposition or diffraction effects along the length of the model.

In a similar manner, the spectra from all five models at F_n=0.25, as presented in Figure 14, can be compared. In all of the spectral plots presented in this report, both the sine and cosine components of the spectra (F and G), as well as the amplitude (E), are shown. Initially, they look to be very similar, one from another, but close scrutiny reveals some interesting characteristics. The spectral plots are composed of maxima and minima. Each plot in Figure 14 has the same number of maxima and minima because they represent data for the same Froude number. The minima, which will be referred to as nodes in the following discussion, can actually be "observed" in the fan-like sun glitter photographs of ship wakes as dark rays, due to the small wave heights in those areas of the wave pattern. The transverse wave number at which the nodes occur can be used to determine the angle relative to the direction of ship motion at which the dark rays would be observed (see the figure contained in the nomenclature section). Theoretically, no nodes would occur at a transverse wave number higher than 8.5 as this corresponds to the Kelvin angle of 19.47 degrees or a direction of wave propagation that is 70.53 degrees from the direction of ship motion. More careful observation reveals that for certain ship models the level of these spectral nodes is lower than for others. One may even observe a loose correlation between the ratio of the bow/stern wave height and the depth of the nodes; as the ratio increases the amplitude of the spectra at the nodes become increasingly large. A hypothesis might be that in the cases where the bow and stern wave heights are similar, a more "balanced" or "pure" interference system results with low magnitude nodes. In Figure 15 a composite plot of spectral node location is presented for Models 5359, 5415, and 4645.

The location of the nodes are shown plotted for each Froude number at their respective tranverse wave number. The full scale implication of this information is that since all the nodal information falls along very distinct and common lines much could be inferred about the Froude number of a ship from the spectra of its wave pattern.

The next figures contain wavecuts and spectra obtained from each model. In Figure 16 the wavecuts for Model 5063 are presented both non-dimensionally and dimensionally for the two Froude numbers tested. F_n=0.185 and 0.25. The non-dimensional presentation affords a view of similar wave length scales whereas in the dimensional case the distance scales (i.e., bow to stern wave location) are the same. The large bow/stern wave height ratio as discussed previously for this model is present at both Froude numbers but the region between the bow and stern waves is clearly different at the two speeds. Figure 17 shows the spectral representation of the wavecuts for both Froude numbers. The large number of nodes in the first plot is consistent with the low Froude number.

Six sets of data were obtained for Model 4645 from Froude number 0.25 to 0.31. The wavecuts are presented in Figures 18 and 19 and the spectra in Figures 20 and 21. As speed increases, gradual changes in amplitude and phase are observed in the region of the wave record between the bow and stern waves. This pictorial evolution sheds light on the orderly progression of changes in the wave system as Froude number increases. Interestingly enough, the largest transverse wave heights and the largest spectral amplitudes are both observed at F_n=0.29 and not at F_n=0.31. Also, between F_n=0.29 and F_n=0.30 there is a change in the number of nodes in the amplitude spectra, from five to four.

The next set of plots, Figures 22 and 23, are for Model 5201 tested at three trim conditions non-propelled, and two trim conditions propelled. One striking comparison is that the height of the transverse waves downstream of the stern as seen in Figure 22 is much larger for the propelled model case than for the non-propelled model in both the bow down and design trim condition. This is also evident in the amplitude spectra of Figure 23 by examining the region of transverse wave numbers from 0 to 1. In studying the wavecuts again, the bow-down condition clearly has a large bow diverging wave and very small transverse waves. For this trim, the complex region between the bow and stern wave is very different from both the design trim condition and the stern-down case.

In the case of Model 5359, data at nineteen Froude numbers were obtained. The data are presented in Figures 24 through 30 for the wavecuts and Figures 31 through 37 for the spectra. By observing the wave records for the increased amplitude of the stern wave, the emergence of the transom can be seen to occur at F_n=0.28. With increasing Froude number the stern wave remains higher than the bow wave. The spectra show a general transition from eight nodes to two as the Froude number increases.

Figure 38 shows an interesting contour plot of the spectral components from Model 5359 over the complete Froude number range. This contour plot fills in the spectral amplitudes between the nodes (local minima) in the plot of Figure 15. Thorough study of this "spectral map" and future ones to be generated could give insight into the wave superposition phenomena for differing hull forms. This concept of spectral maps could also be used to verify results of numerical models over a range of Froude numbers.

A plot of C_W derived from the integration of the spectra is shown in Figure 39. Both calculations, with and without the truncation correction are shown in this plot. As is seen on the plot, there are inaccuracies in the wave resistance values at three Froude numbers between 0.25 and 0.30. After careful study of these wave records it is concluded that the bias-type errors in C_W are due to probe contamination manifested as a shift in the zero level of the probe. This zero shift alters the spectra and thus influences the C_W calculations. In repeat runs, after probe cleaning, the zero shift was negligible and a reasonable value of C_W resulted.

In Figures 40 and 41 the data from Model 5415, tested at three Froude numbers, 0.25, 0.28 and 0.41 are presented. The transverse waves at F_n=0.41 are significantly larger than at either of the other two speeds. Following from this, the amplitude spectra at a transverse wave number of "0" is observed to be three times larger than at the other Froude numbers. There are only two spectral nodes at this high Froude number compared to five at the other two speeds.

STEREOPAIRS

Although analysis of the stereopairs result in contour maps which serve to quantify a large region of the model-generated wave pattern, the photographs themselves are enlightening regarding the significant features and regions of the Kelvin wake. Figures 42 through 58 show single photographs from each stereopair obtained during the experiment. Stereopairs were not obtained at all model conditions due to camera malfunctions and the finite amount of seeding material available.

Features of interest in these photographs include: the lines of concentrated computer punch chips (may be associated with a breaking or highly sloped bow wave), the stern diverging wave and its interaction with the wake generated by the flow along the length of the hull, and the small capillary waves often observed close to the hull or near the bow wave. Each of these phenomena suggest regions of non-linearities in the wave pattern. Another interesting feature in the photographs is the region at the stern of the model which is swept clear of the seeding. The width of this swath increases with speed and this phenenomena may provide additional information to correlate with wake images seen from aircraft or satellites.

CONTOUR PLOTS

Due to the cost of obtaining a contour plot from a stereopair, analysis was not done on all of the photographs. The results of the stereomodels which were analyzed are presented in Figures 59 through 69. The regions of missing data in the contour plots are due to the presence of the ship model and also to the absence of surface seeding at the stern of the model where the computer chips are submerged by wavebreaking and/or "plowed" to the side.

In the case of Model 5063 contour plots for both Froude numbers are presented in Figures 59 and 60. The contour plot for Model 4645 is from data obtained at F_n=0.25 and is presented in Figure 61. Contours of Model 5201 are presented in the next four figures. Figure 62 shows the bow-down drag body condition. Two sequential contour maps of the drag body wake for the design trim condition is shown in Figure 63 and 64. In Figure 65 a propelled contour plot is shown, also for the design trim condition of Model 5201. The contour plot for Model 5359 operating at F_n=0.258 is shown in Figure 66. In Figures 67-69 contour plots are shown for Model 5415 at three Froude numbers, F_n=0.25, 0.28 and 0.41, respectively.

In the case of Model 5201, the bow-down drag condition (Figure 62) clearly shows a larger bow wave and smaller stern wave than is seen in the design trim condition (Figure 63). In comparing the contour plots from the propelled and drag conditions (Figures 64 and 65, respectfully) it is difficult to see any differences. As observed in the wave profiles presented earlier, the major manifestation of propulsion in the Kelvin wake is seen in the transverse waves. Unfortunately the transverse waves are difficult to resolve in the contour maps due to the lack of seeding remaining behind the model.

CONCLUSIONS

This set of experiments represents the first time that such an extensive Kelvin wake data base has been obtained. This was accomplished in light of full-scale observations and with the hope of gaining a further understanding of fundamental wave pattern phenomena. The longitudinal wavecut data, stereopairs and contour maps together present a detailed account of ship model wave generation.

Based on the study of longitudinal wavecut measurements and derived free wave spectra at F_n=0.25, the models with the lowest bow-to-stern wave height ratio, Models 5201, 5359 and 5415, were found to be the hulls fitted with bow domes. The spectra from these models were observed to have very well-defined "nodes" or periodic minima of spectral amplitude. This phenomena is manifested visually as dark rays of low wave amplitude. This is hypothesized to be caused by cancellation effects between the bow and stern wave systems. The composite contour plots of spectral amplitude and sine and cosine components provide additional information to the nodal plots and show systematic variation with Froude number. These unusual contour plots may assist in the evaluation of Kelvin wake numerical modeling techniques.

Results of longitudinal wavecut measurements also show large effects of trim on the bow and stern wave systems. For Model 5201, propulsion accounts for a much larger amplitude of transverse waves than is generated in the drag body condition. This is important to note since wave resistance experiments are usually performed with unpropelled models. A complex region of wave generation and superposition is seen to occur between the bow and stern wave. In the case of Model 5359, for which longitudinal wavecuts were obtained over a finely spaced range of Froude numbers, an orderly change in this complex system can be observed with increasing speed.

Even the individual photographs which form the stereopairs provide thought-provoking insights into the overall Kelvin wake pattern. The computer punch chips, used in analyzing the stereopairs, show both fine detail and general wake features. The contour plots quantify the photographs and disclose even finer structure in the divergent wave system than is seen in the photos.

This set of wake measurements provides greater understanding of the model-generated Kelvin wave pattern and it is hoped that it will spawn future Kelvin wake studies, both experimental and computational.

ACKNOWLEDGEMENTS

The authors would like to thank Steve McGuigan for his time, effort and ingenuity in support of the wave-measuring instrumentation used for these experiments. In addition, appreciation is extended to Greg Snyder at NOS for his diligence in the analysis of the stereopairs.

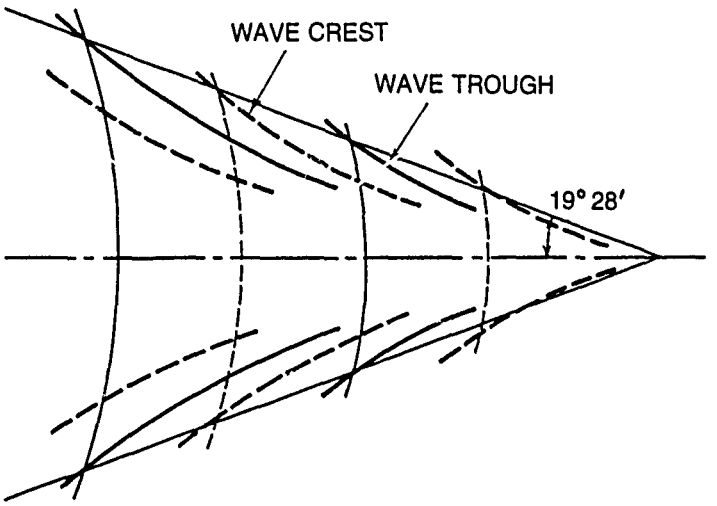

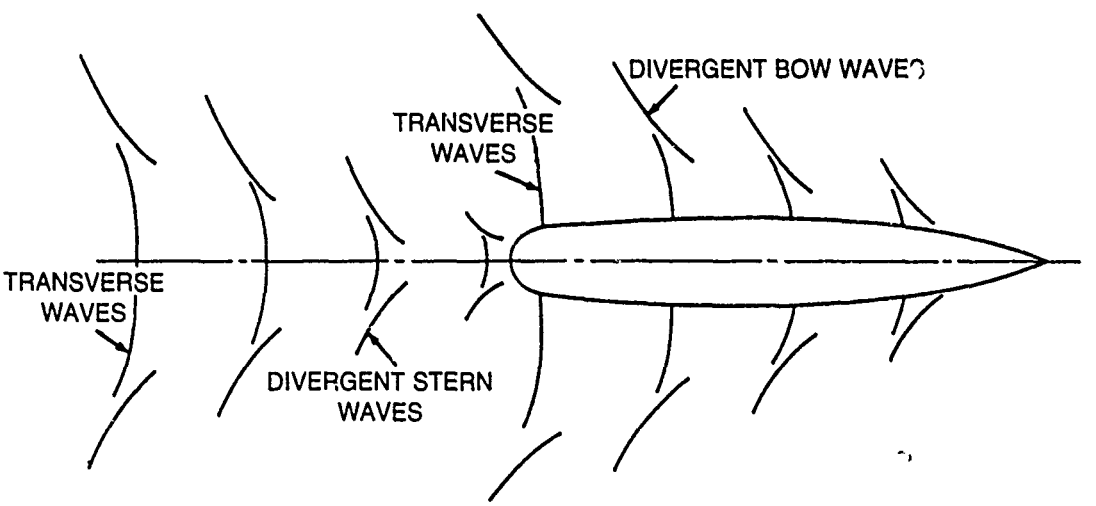

Fig. 1. Kelvin wake pattern.

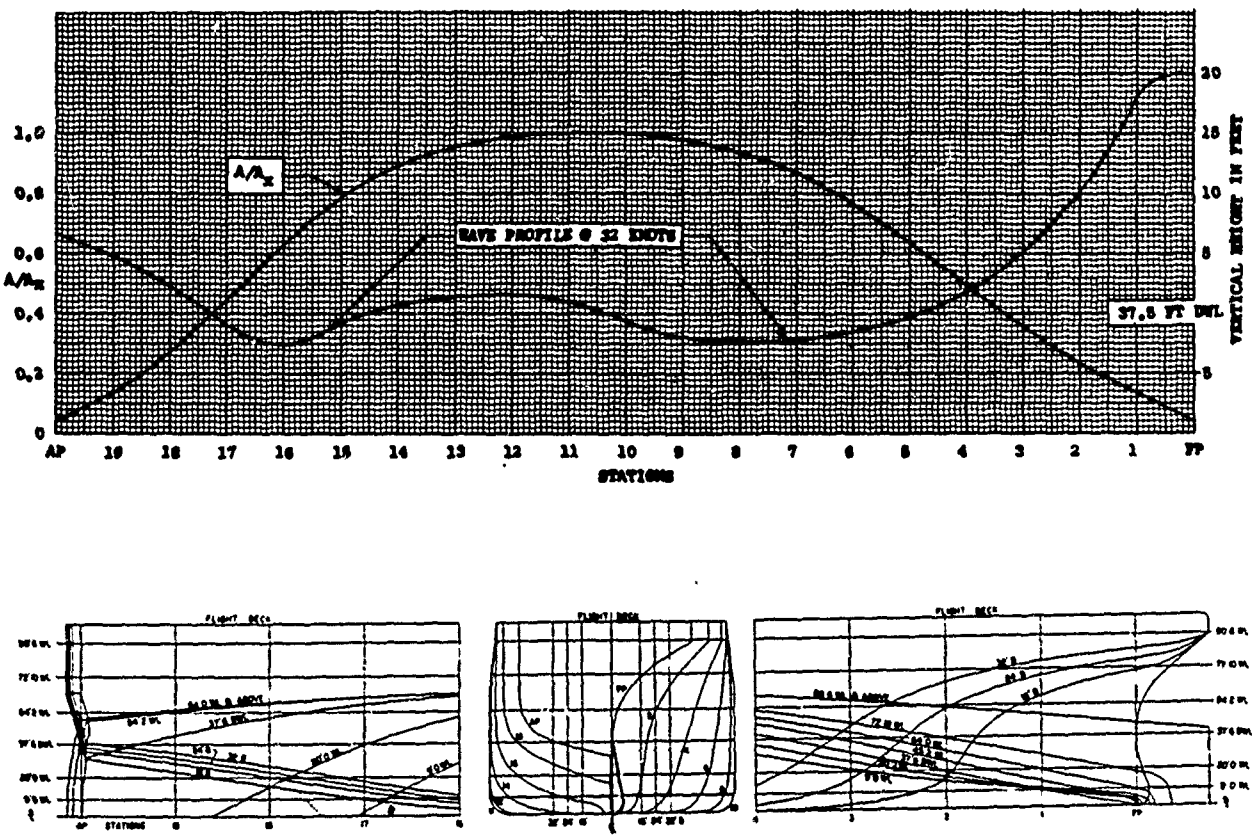

Fig. 2. Model 5063 sectional area curve and lines of form.

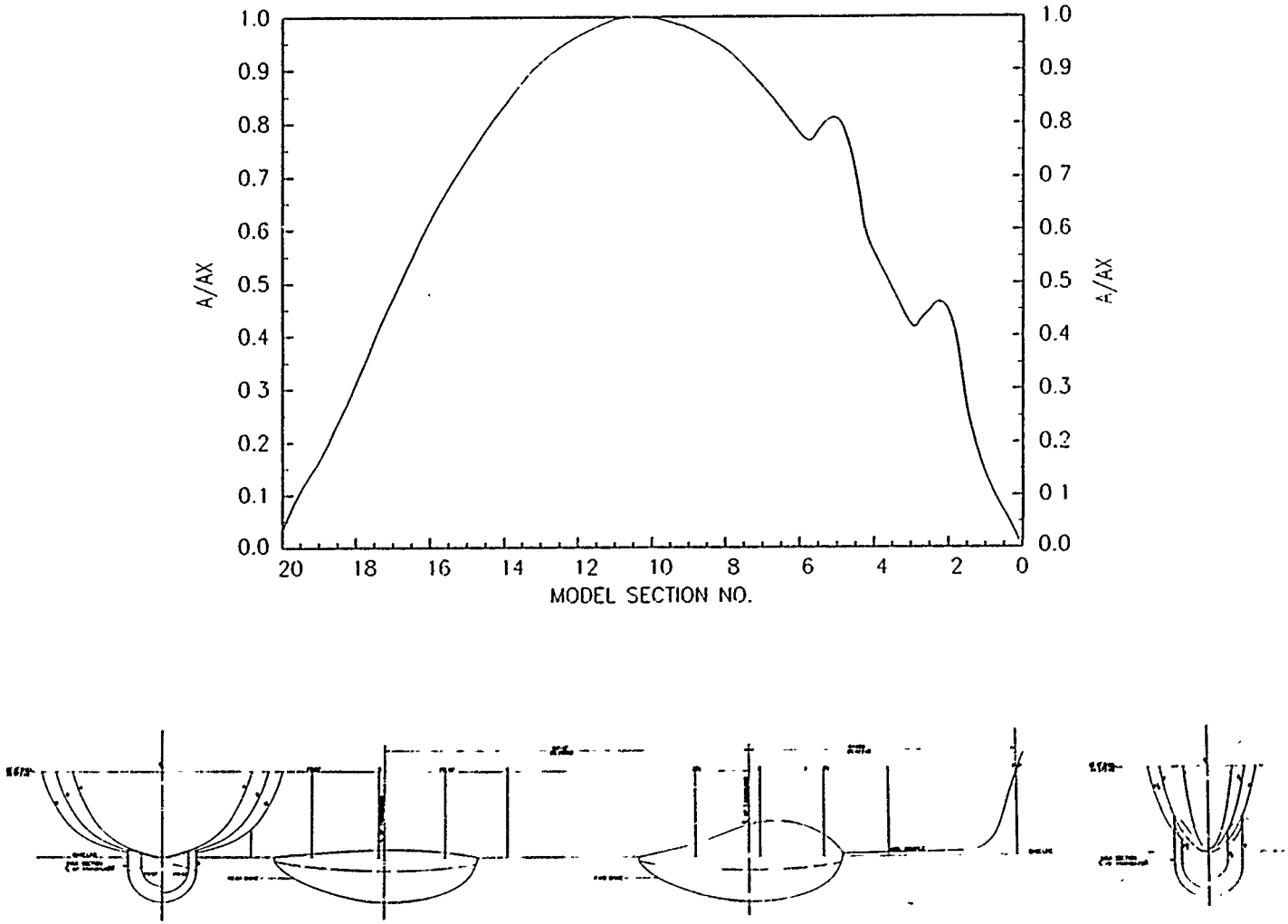

Fig. 3. Model 4645 sectional area curve and dome details.

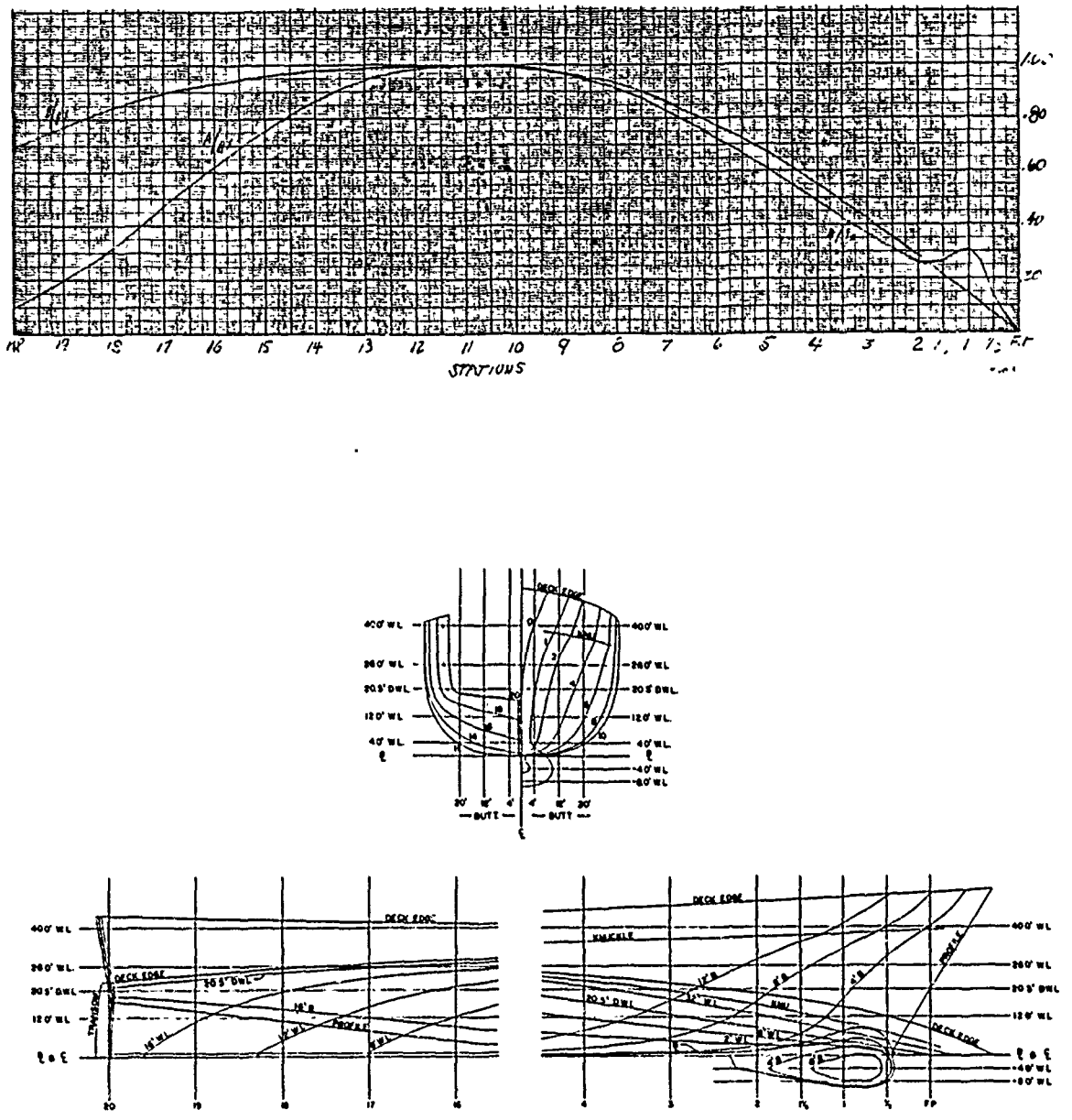

Fig. 4. Model 5201 sectional area curve and lines of form.

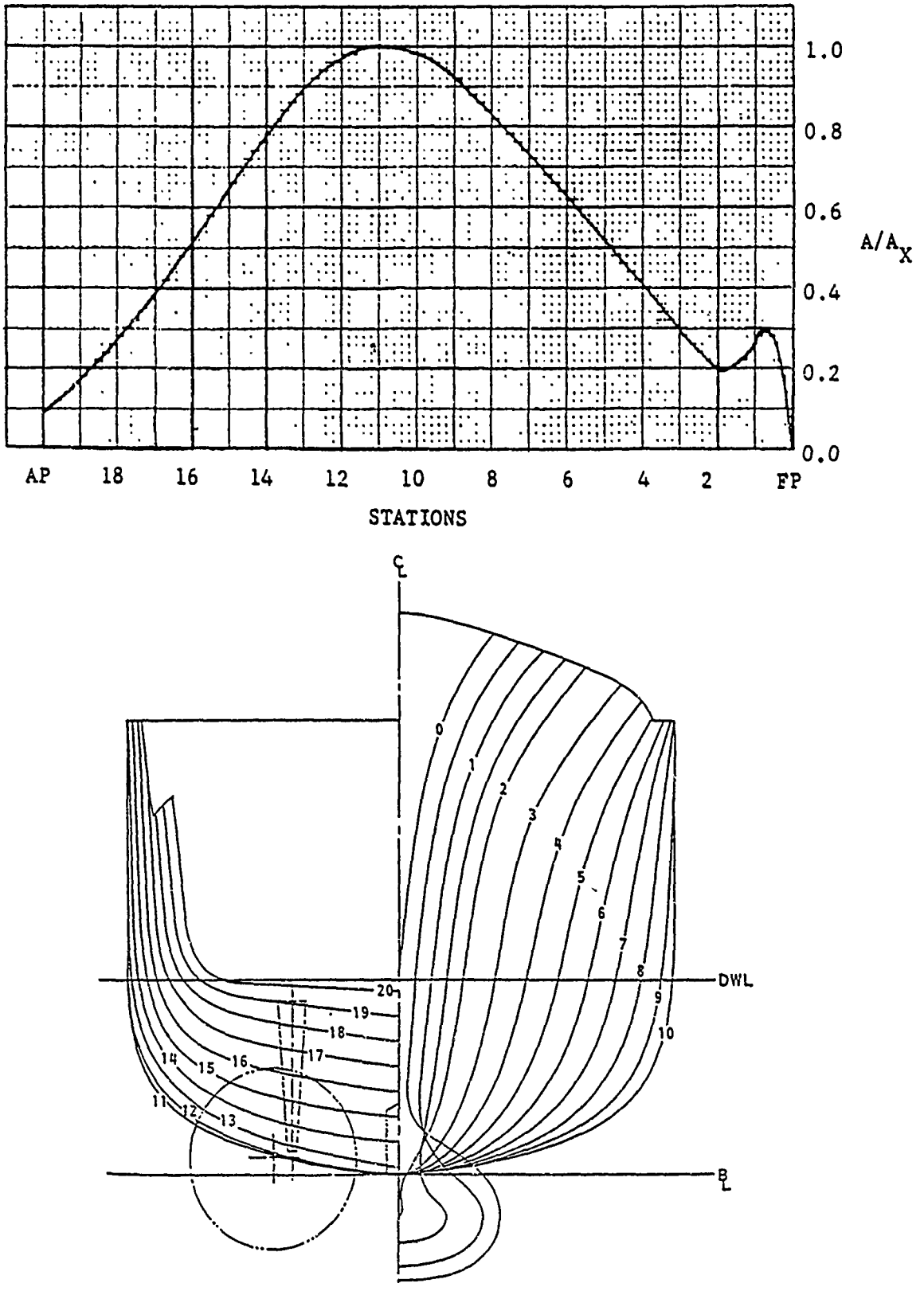

Fig. 5. Model 5359 sectional area curve and body plan.

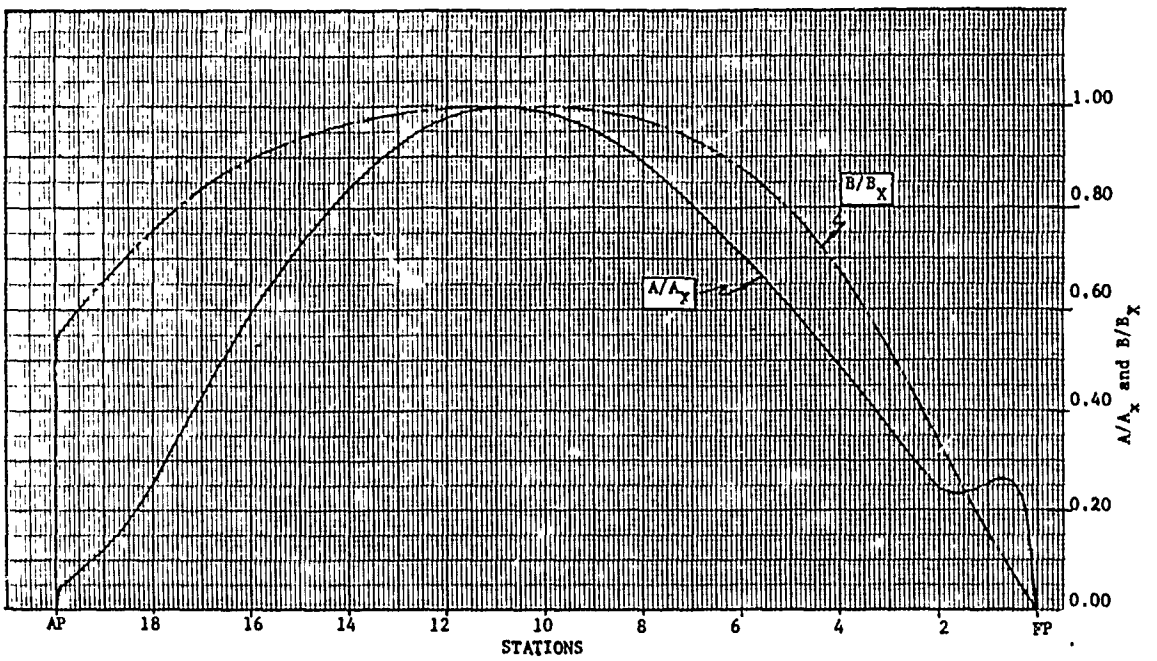

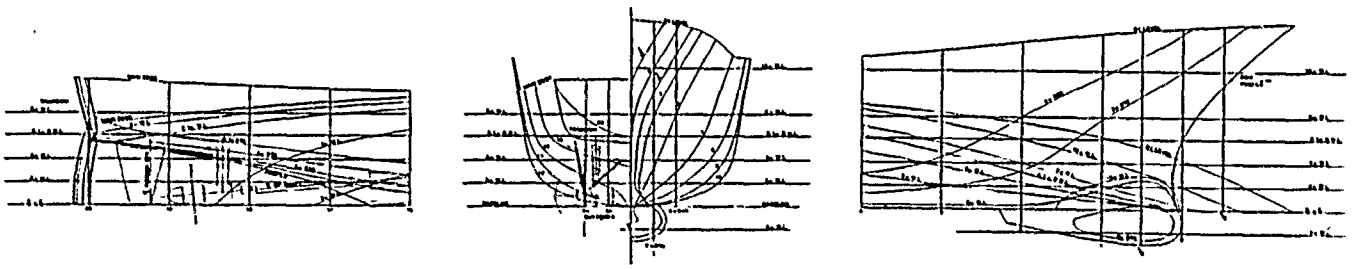

Fig. 6. Model 5415 sectional area curve and lines of form.

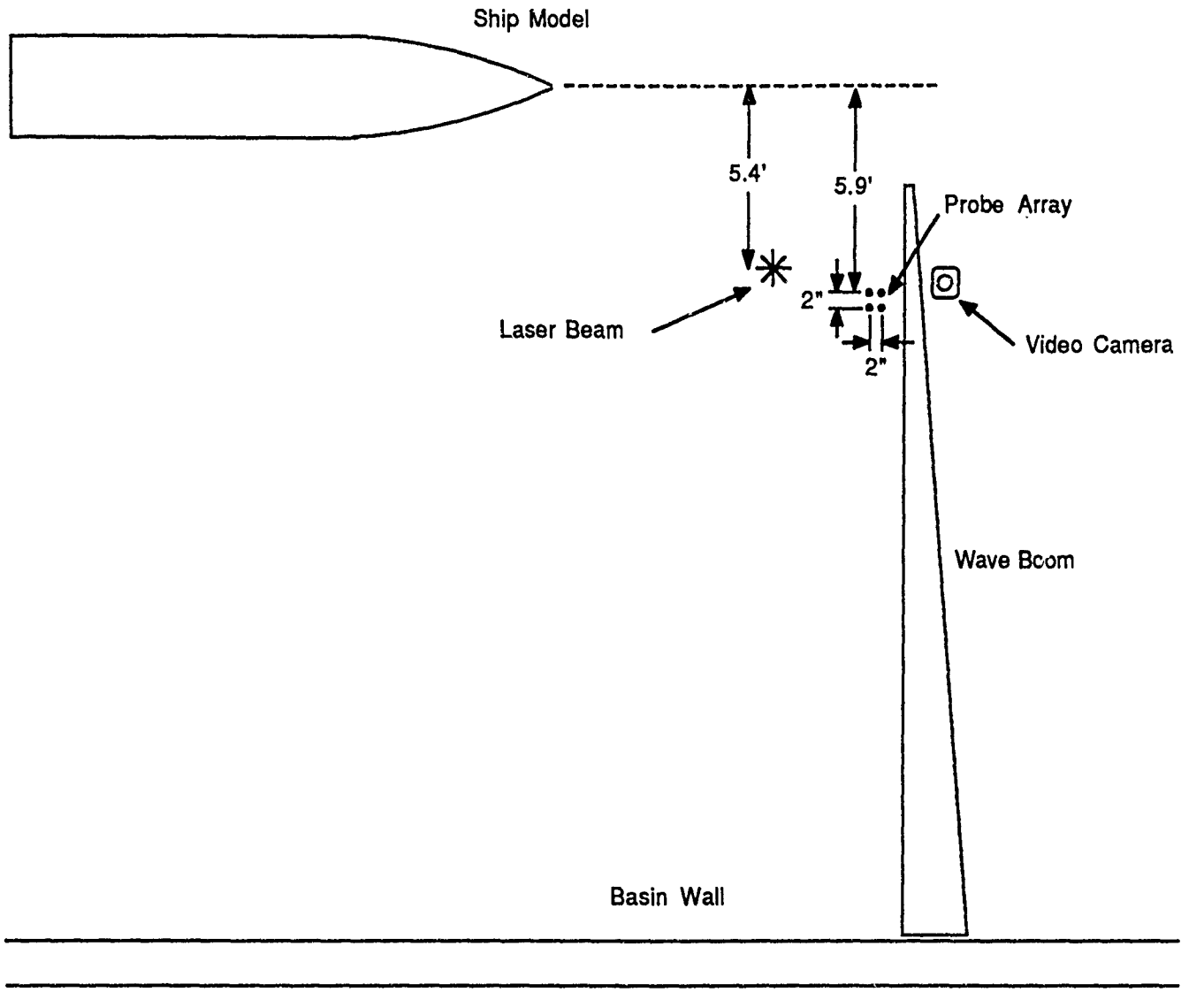

Fig. 7. Diagram of wave probe configuration in towing basin.

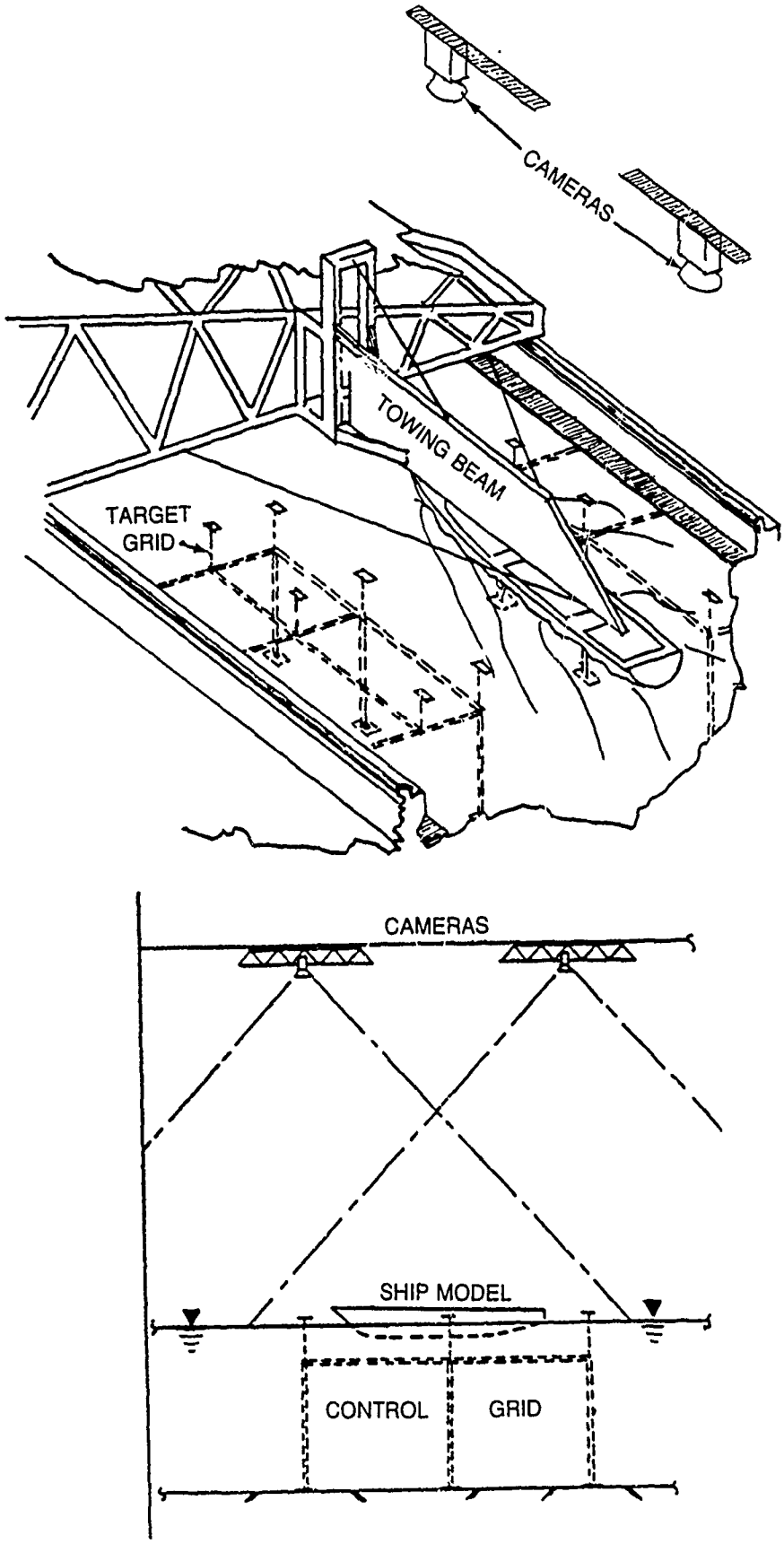

Fig. 8. Two views of photogrammetric system components.

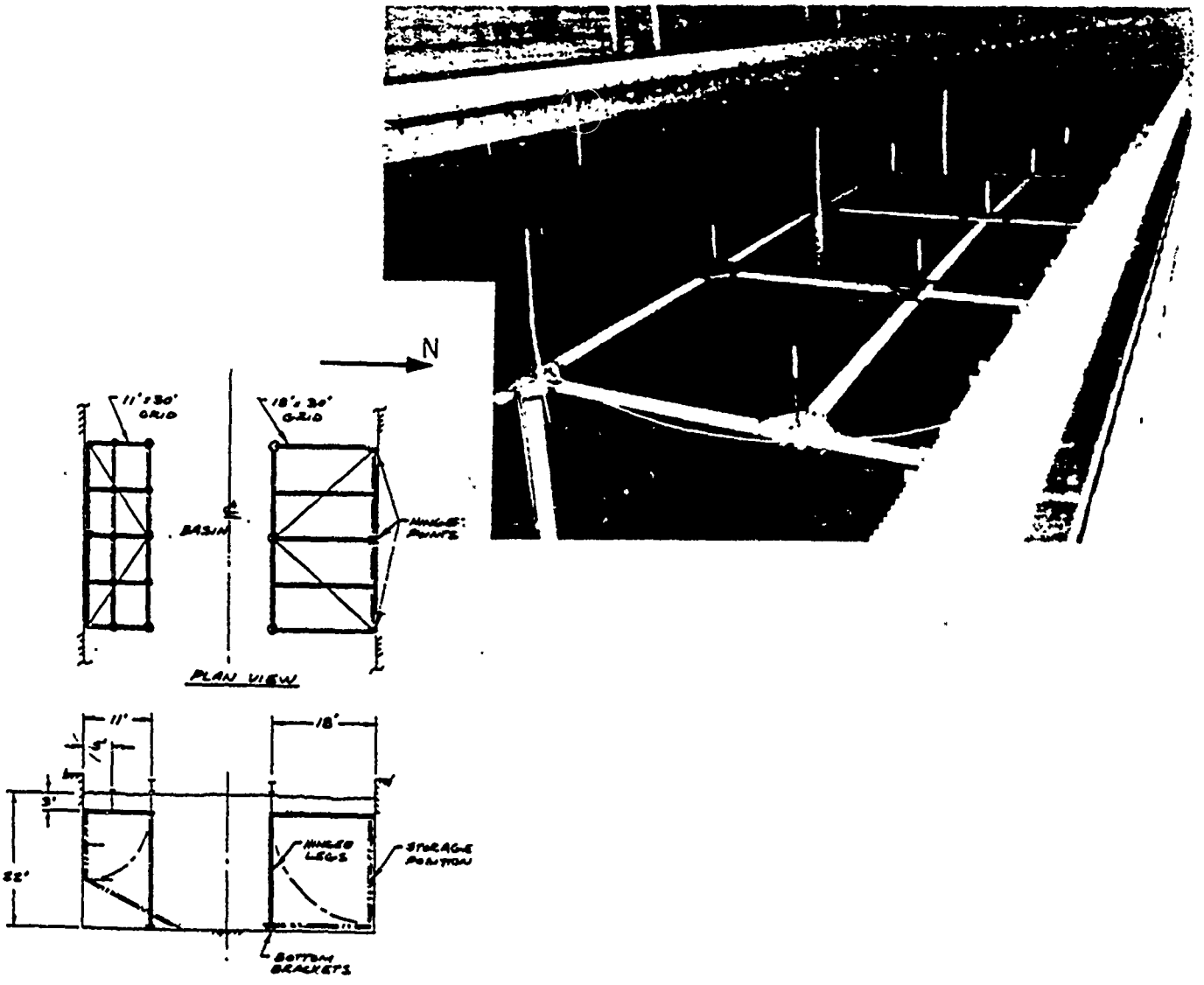

Fig. 9. Photograph and diagram of control target grid assembly.

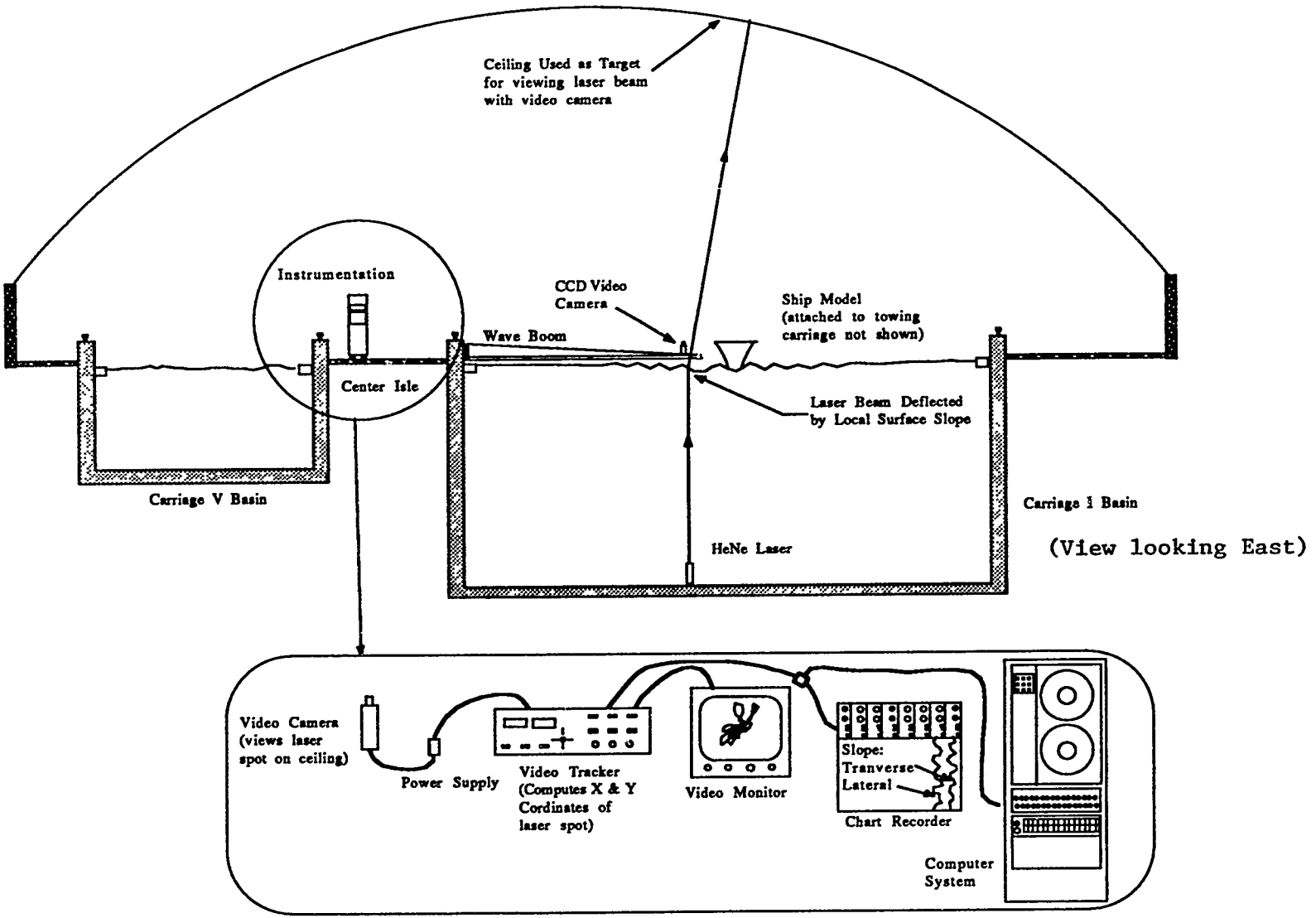

Fig. 10. Schematic of laser slope system.

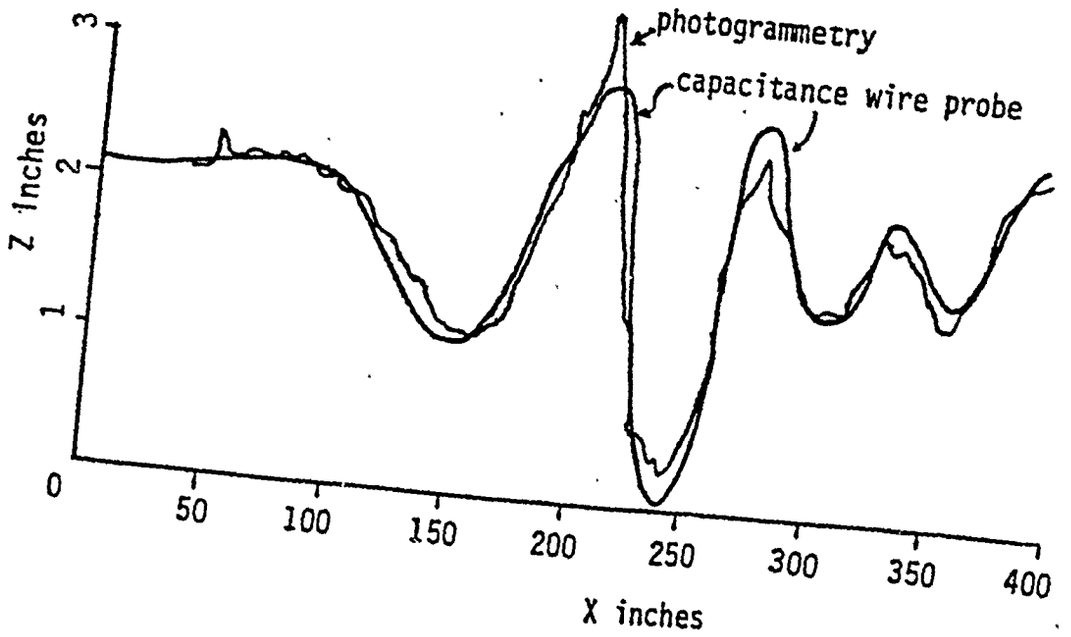

Fig. 11. Comparison of wave profiles from capacitance probe and stereopair.

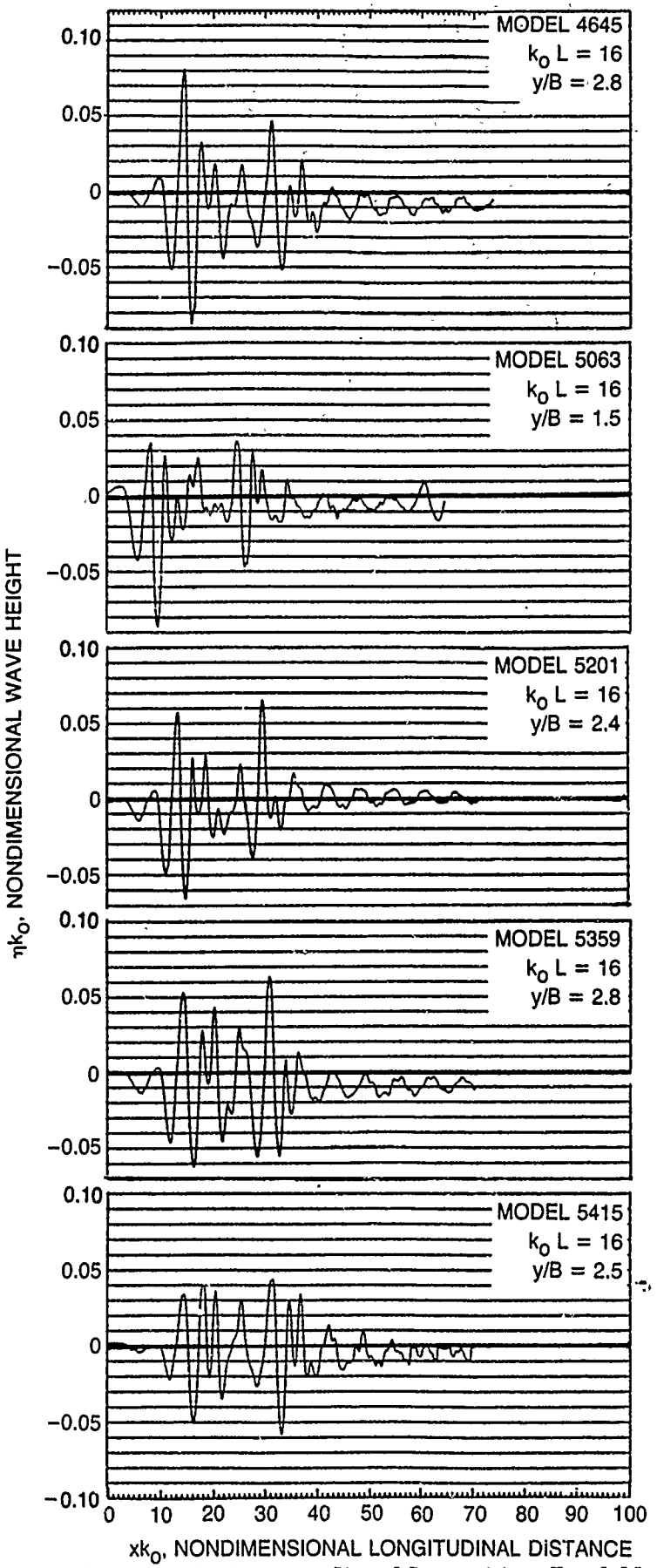

Fig. 13. Longitudinal wave profiles of five models at F_n=0.25.

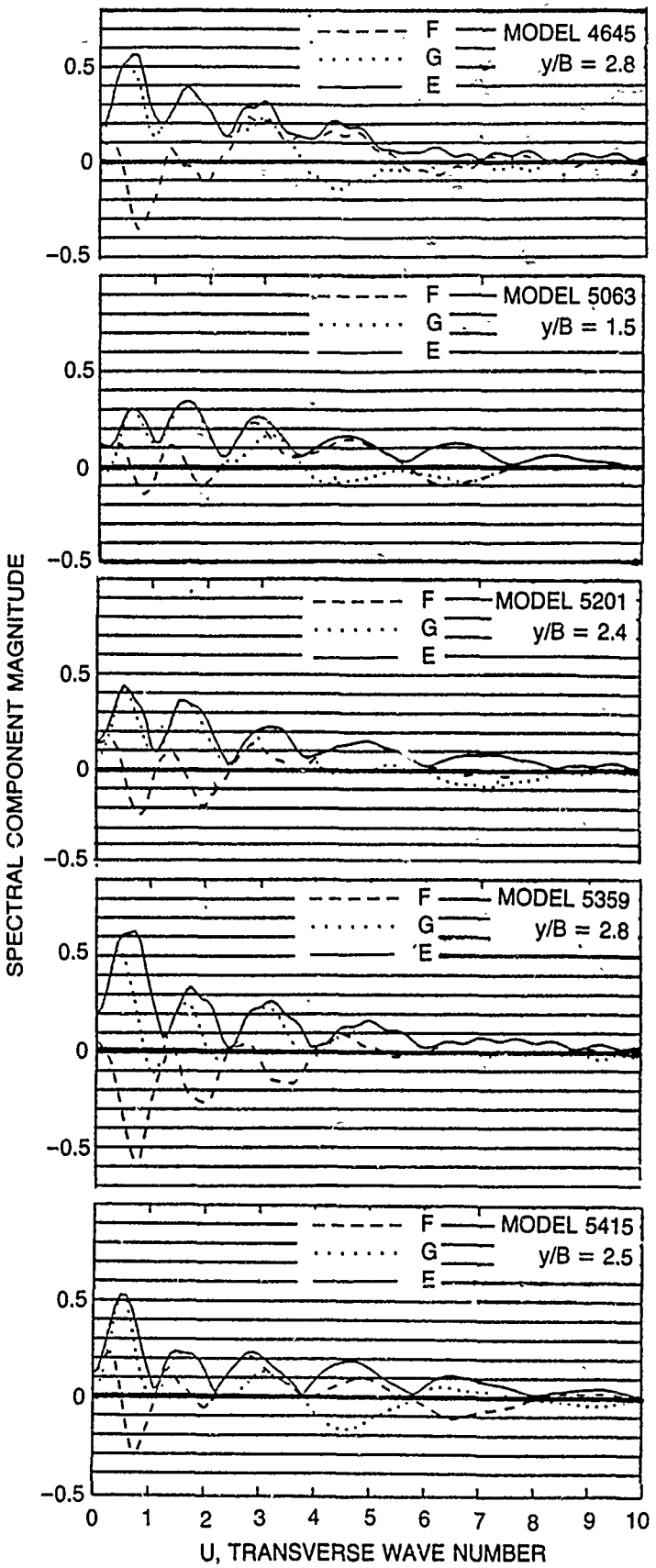

Fig. 14. Wave spectra of five models at $F_n = 0.25$.

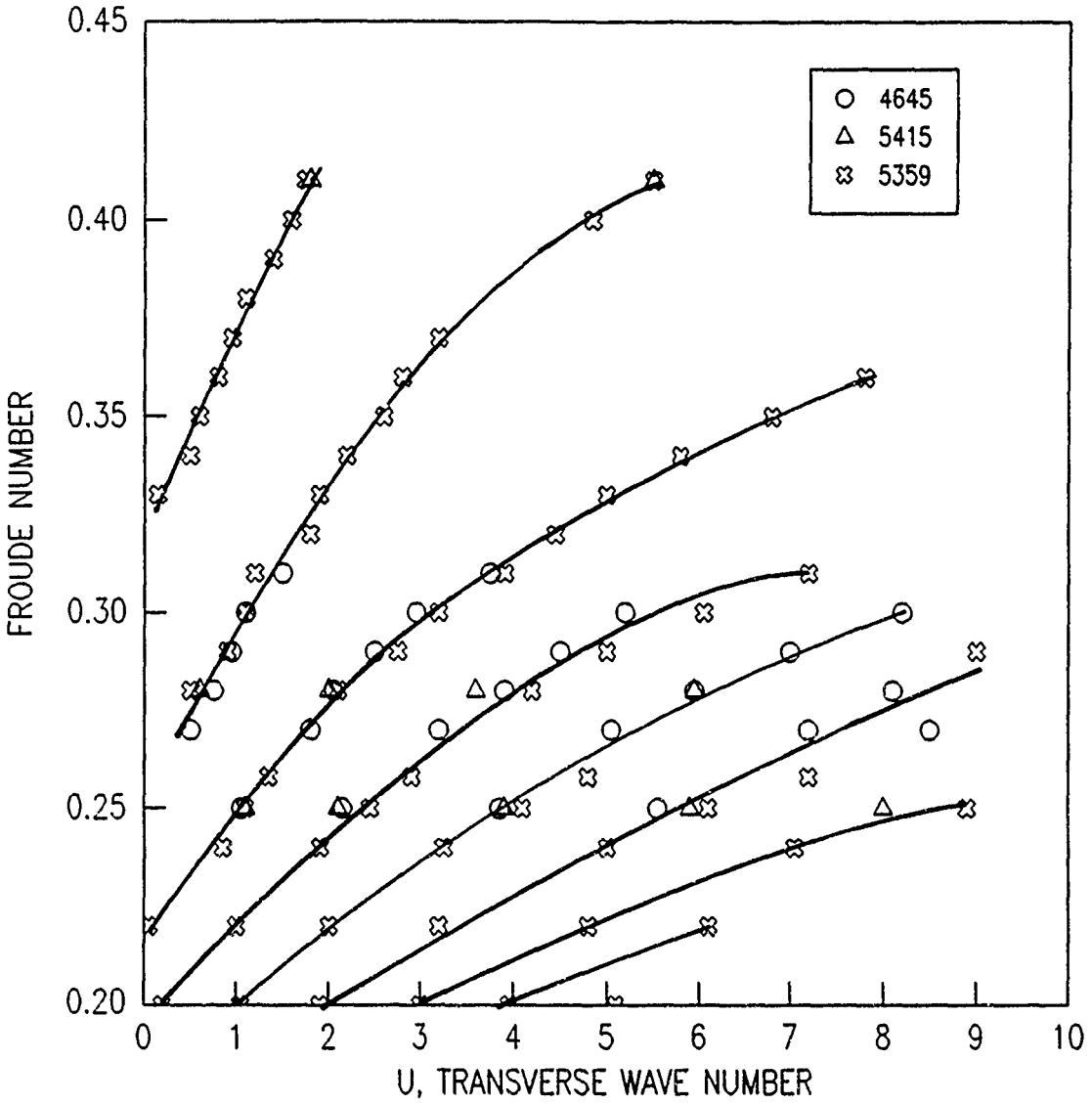

Fig. 15. Transverse wave number location of spectral nodes as a function of Froude number for Models 5359, 5415 and 4645.

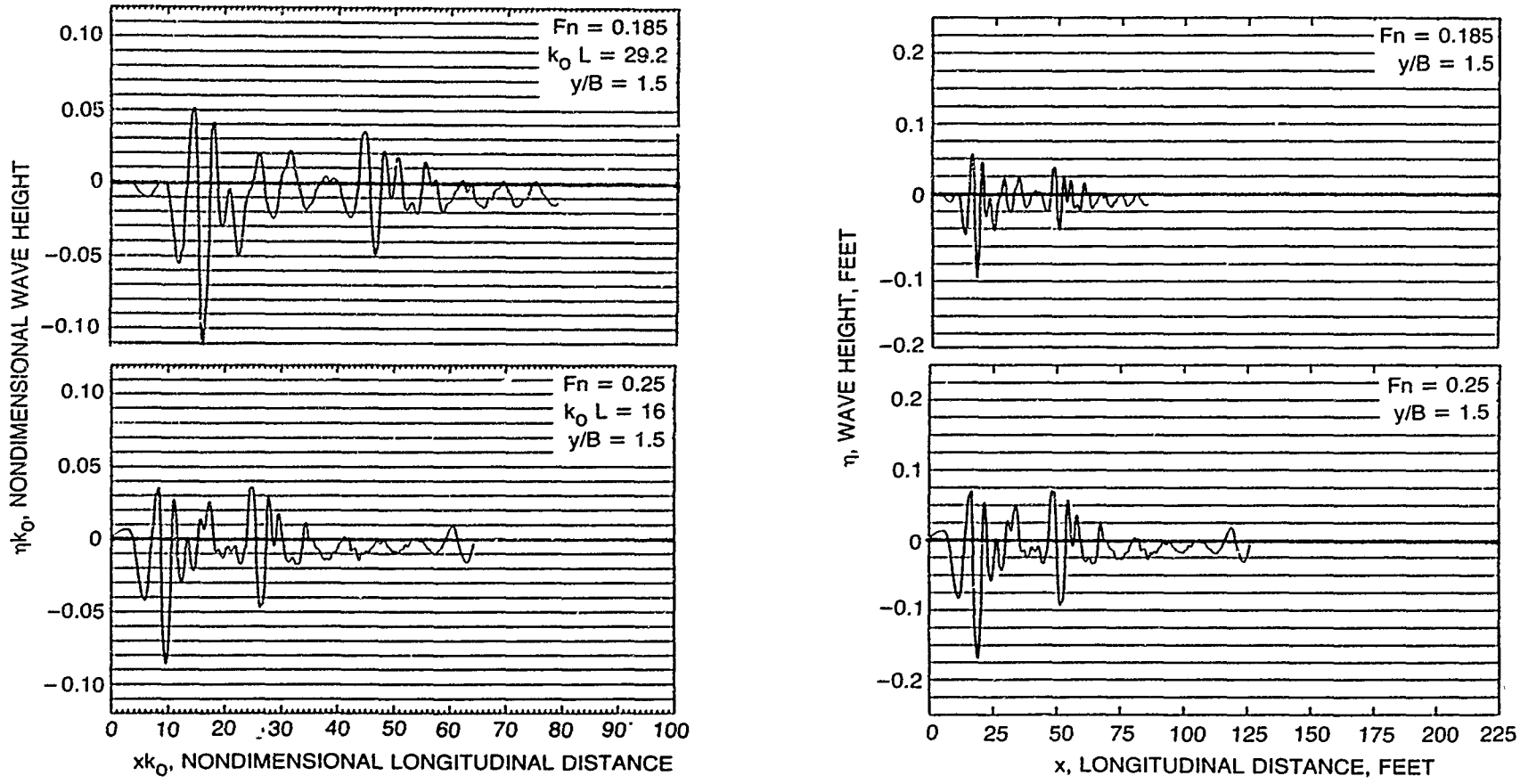

Fig. 16. Non-dimensional and dimensional longitudinal wave profiles of Model 5063 at $F_n = 0.185$ and $F_n = 0.25$.

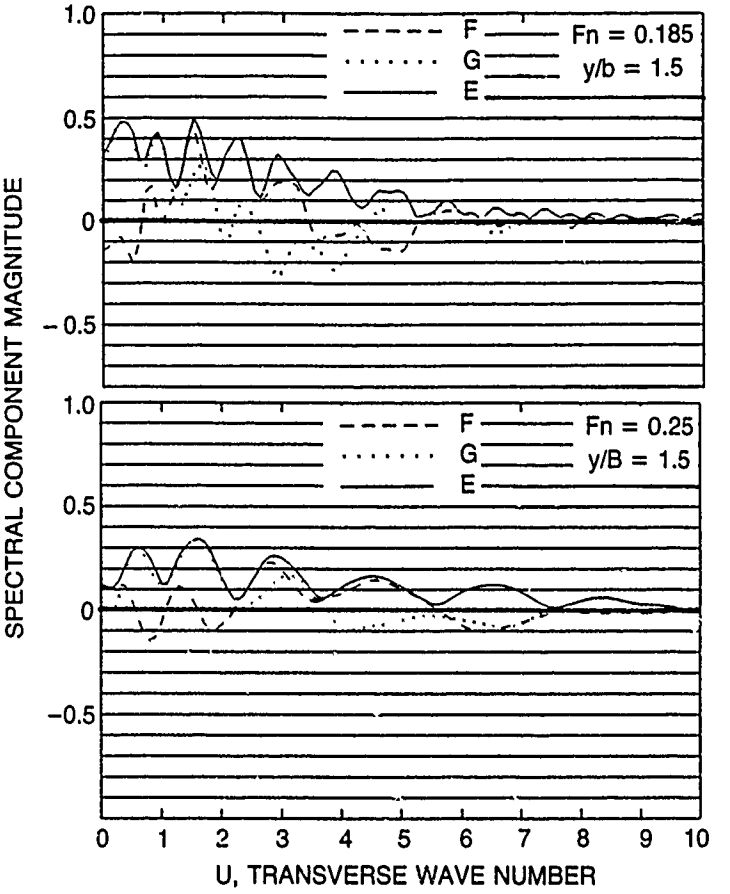

Fig. 17. Wave spectra of Model 5063 at F_n=0.185 and F_n=0.25.

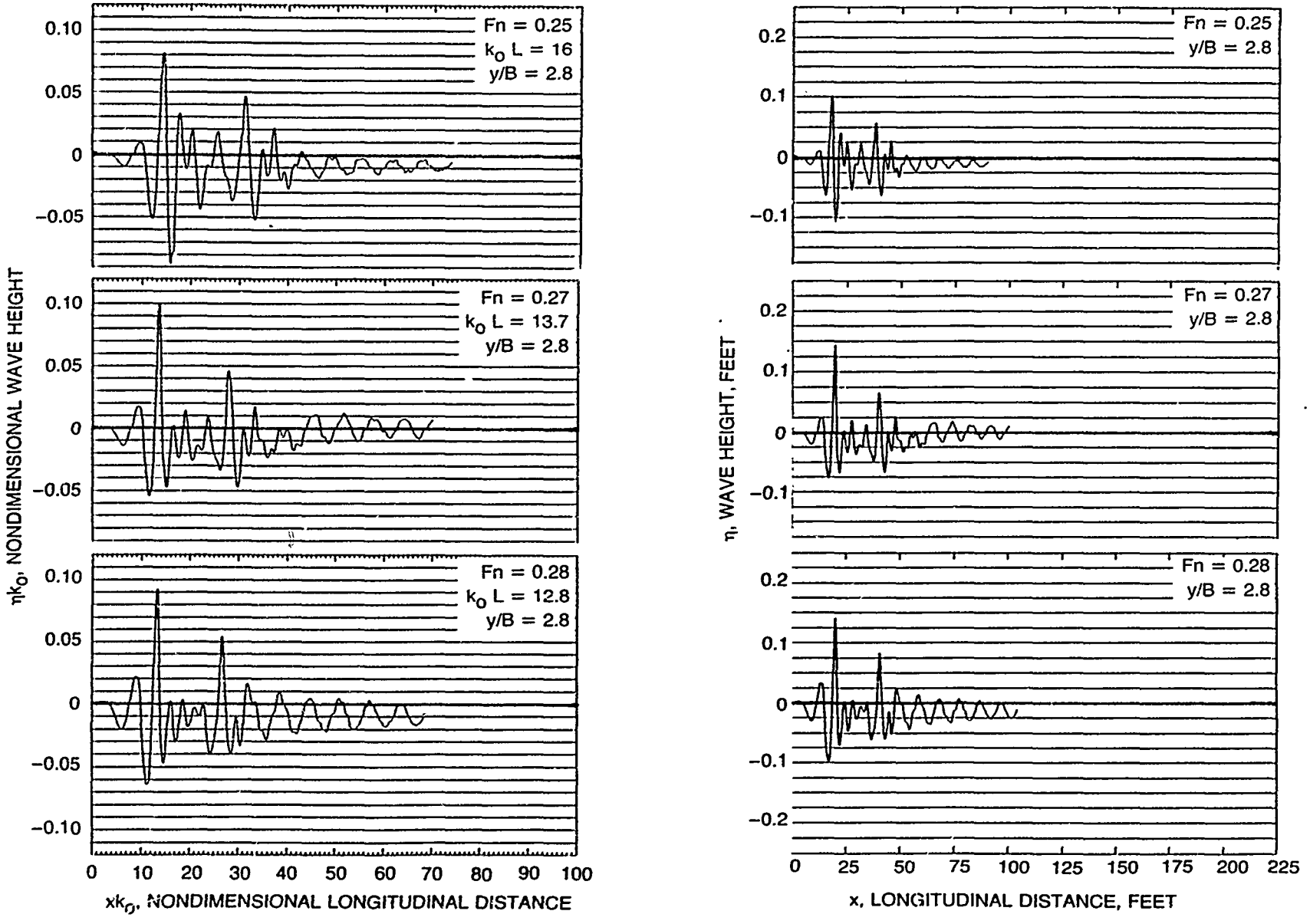

Fig. 18. Non-dimensional and dimensional longitudinal wave profiles of Model 4645 at F_n=0.25, F_n=0.27 and F_n=0.28.

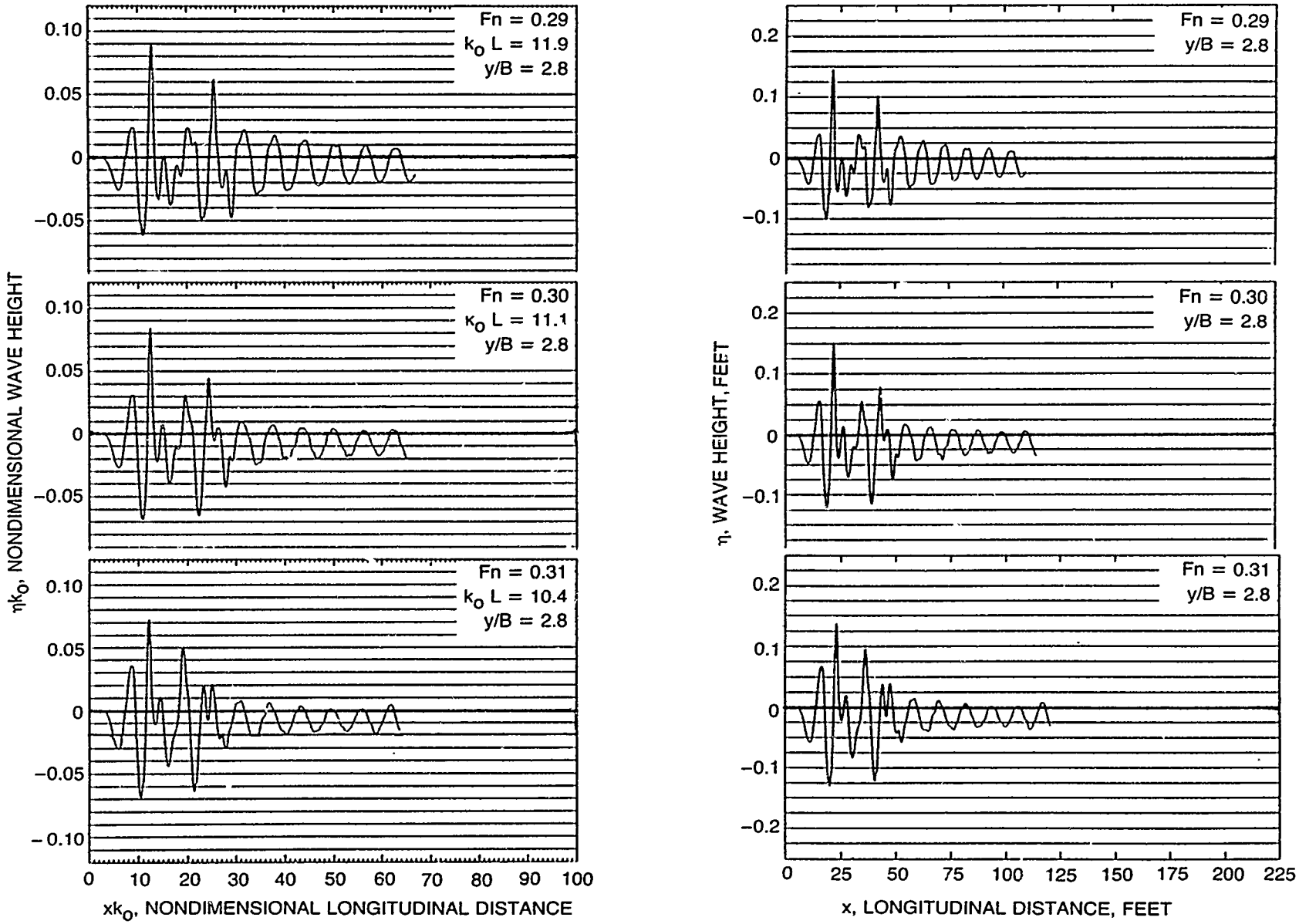

Fig. 19. Non-dimensional and dimensional longitudinal wave profiles of Model 4645 at F_n=0.29, F_n=0.30 and F_n=0.31.

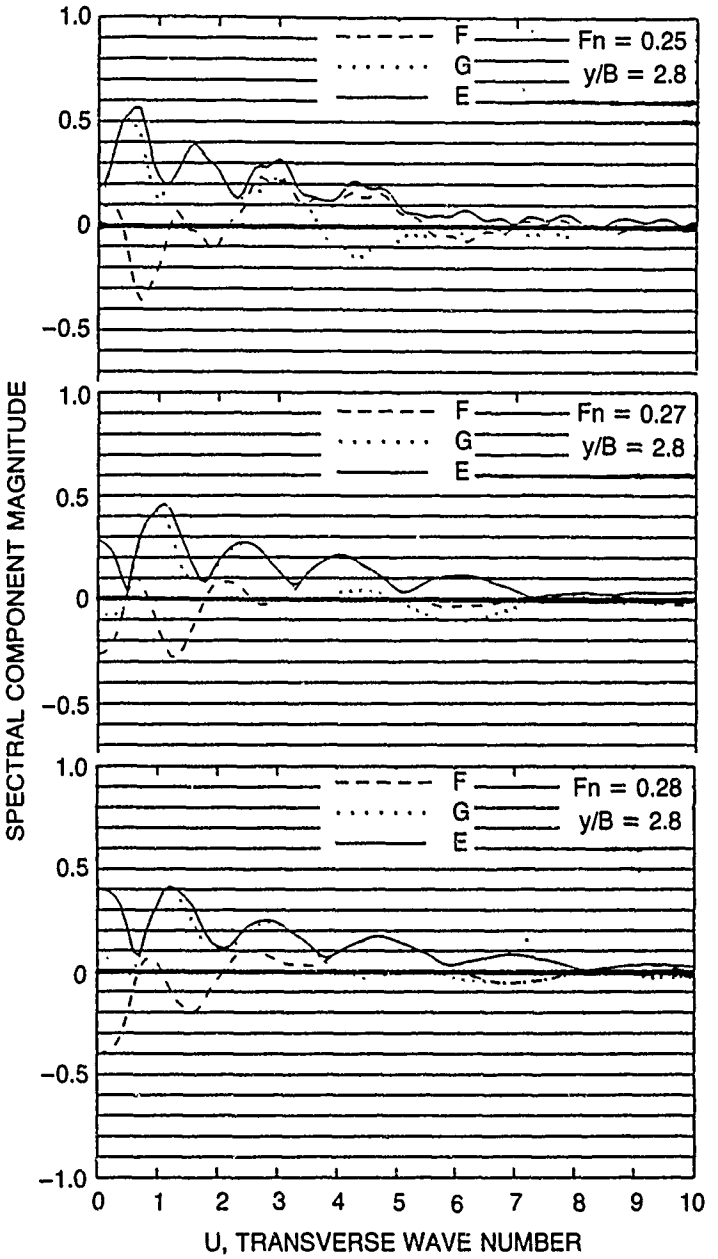

Fig. 20. Wave spectra of Model 4645 at F_n=0.25, F_n=0.27 and F_n=0.28.

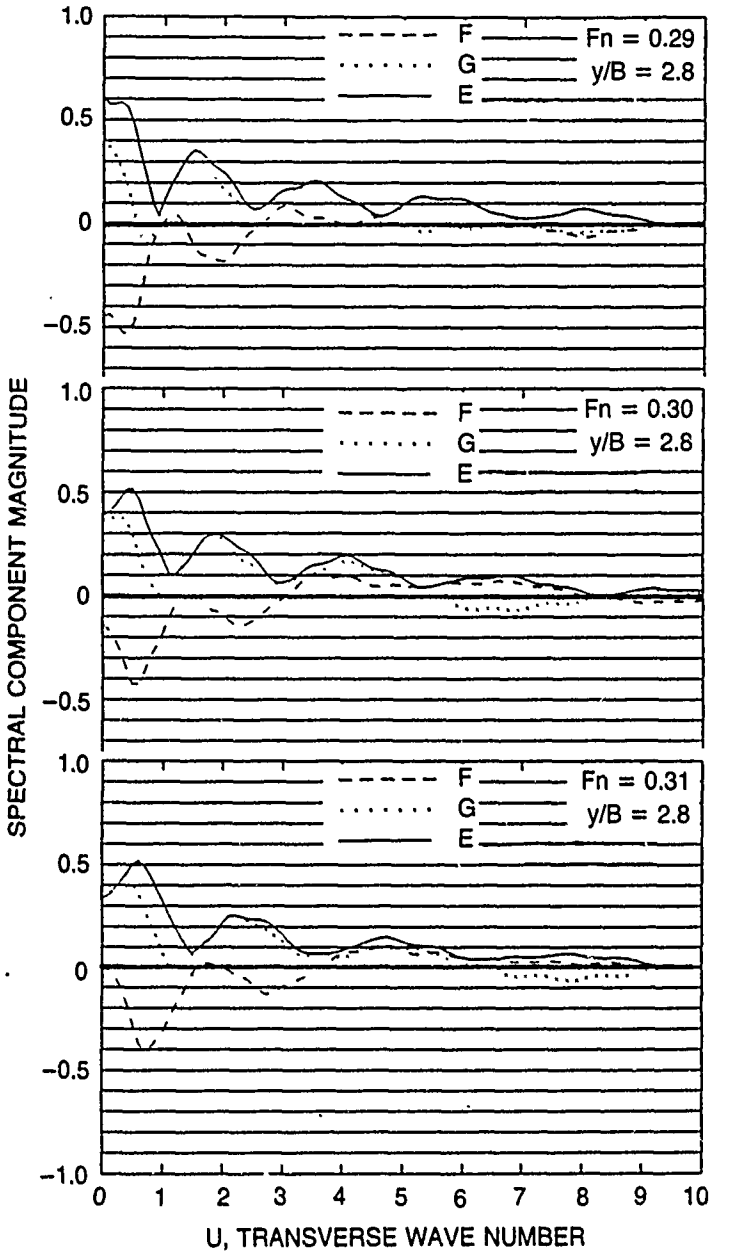

Fig. 21. Wave spectra of Model 4645 at F_n=0.29, F_n=0.30 and F_n=0.31.

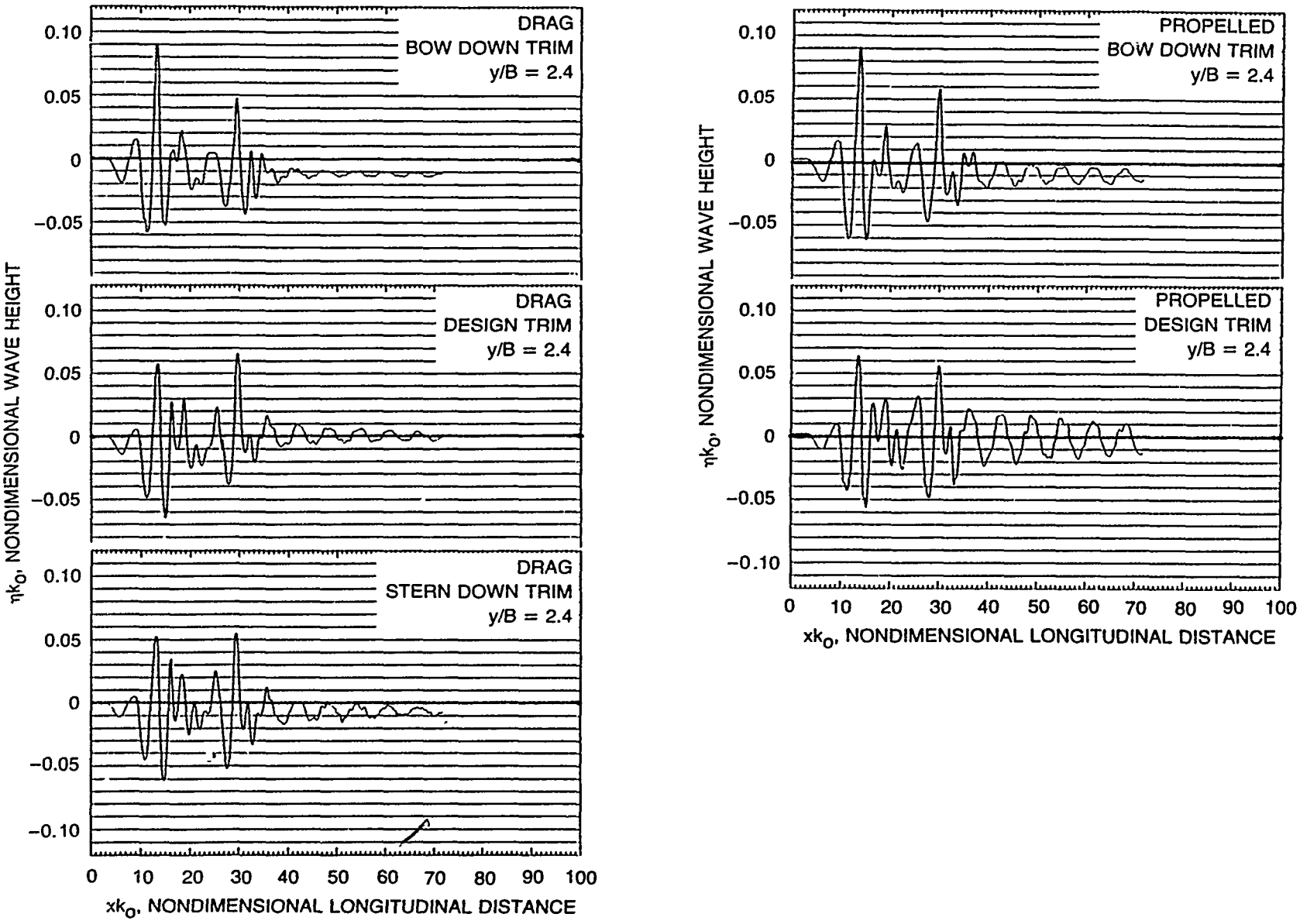

Fig. 22. Non-dimensional longitudinal wave profiles of the drag and propelled Model 5201 for three trim conditions at $F_n = 0.25$.

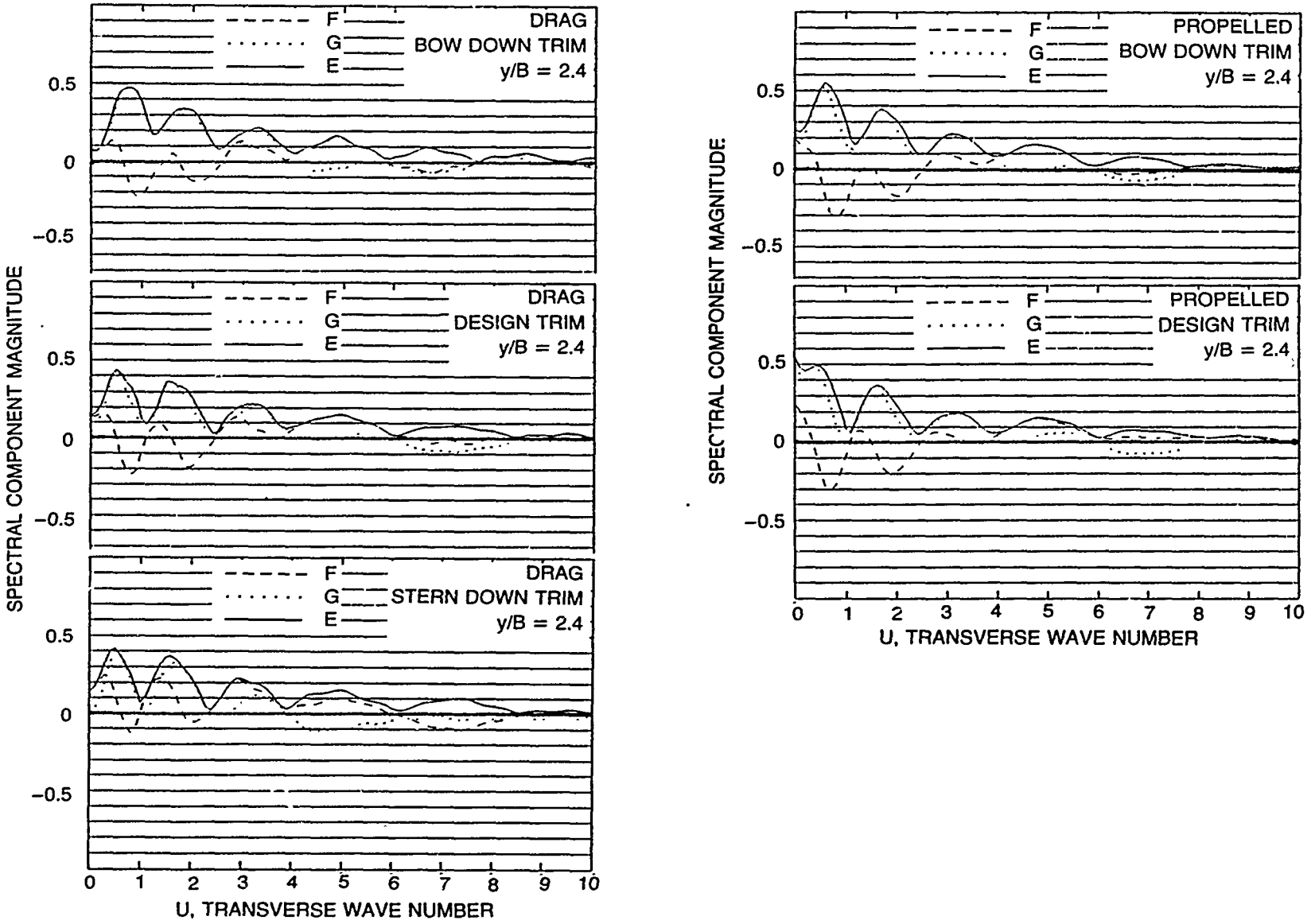

Fig. 23. Wave spectra of the drag and propelled Model 5201 for three trim conditions at $F_n = 0.25$.

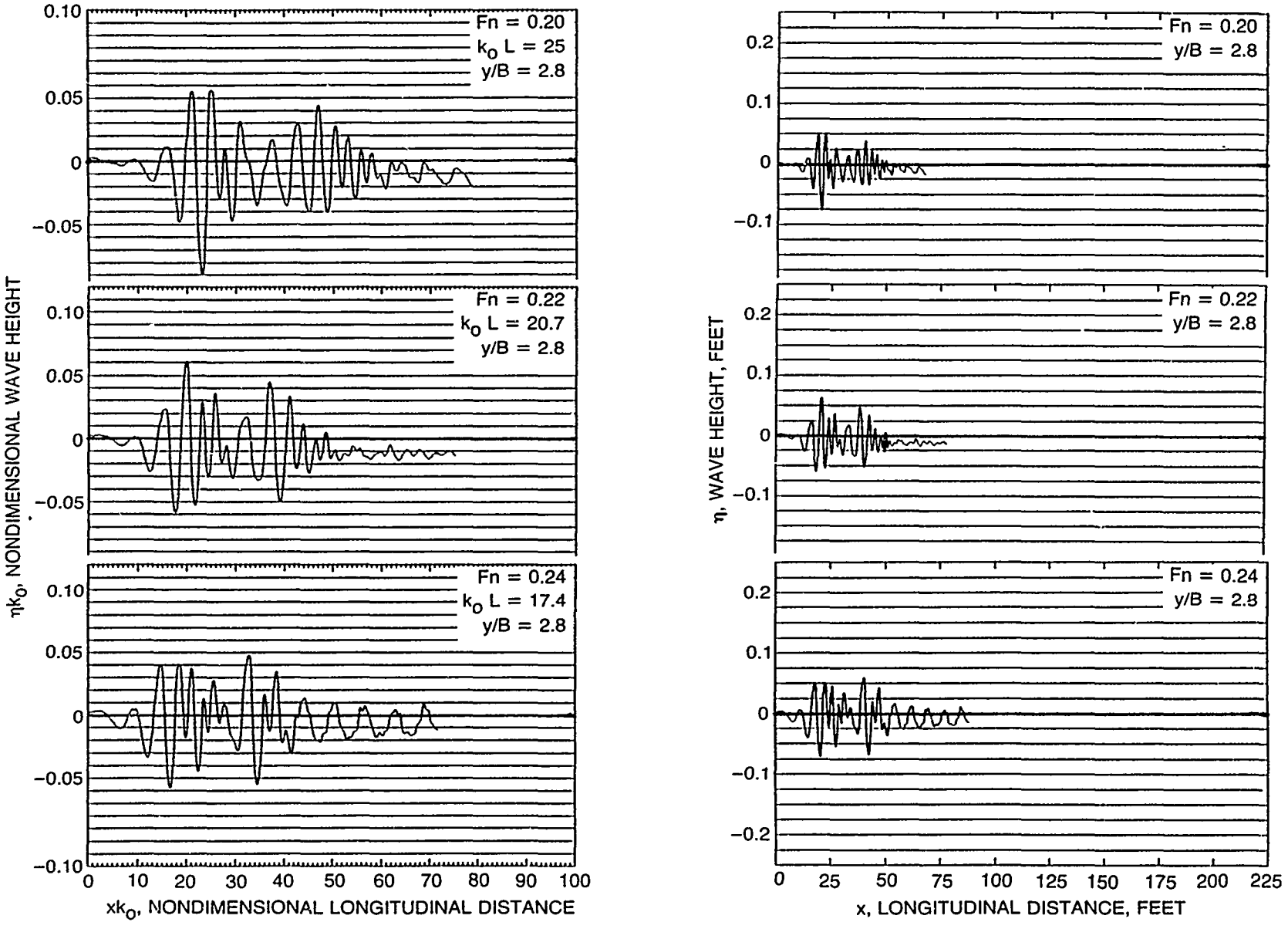

Fig. 24. Non-dimensional and dimensional longitudinal wave profiles of Model 5359 at F_n=0.20, F_n=0.22 and F_n=0.24.

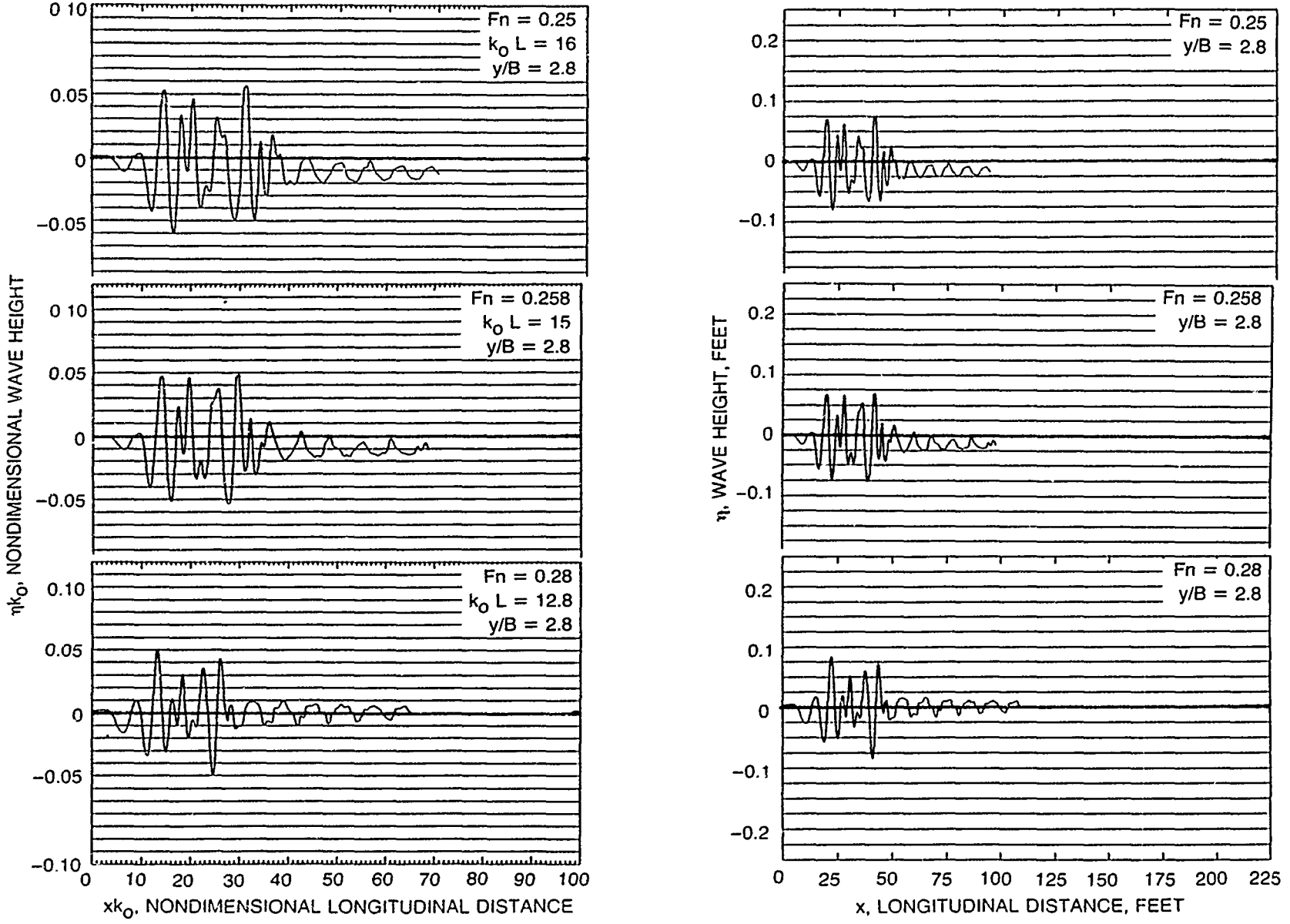

Fig. 25. Non-dimensional and dimensional longitudinal wave profiles of Model 5359 at F_n=0.25, F_n=0.258 and F_n=0.28.

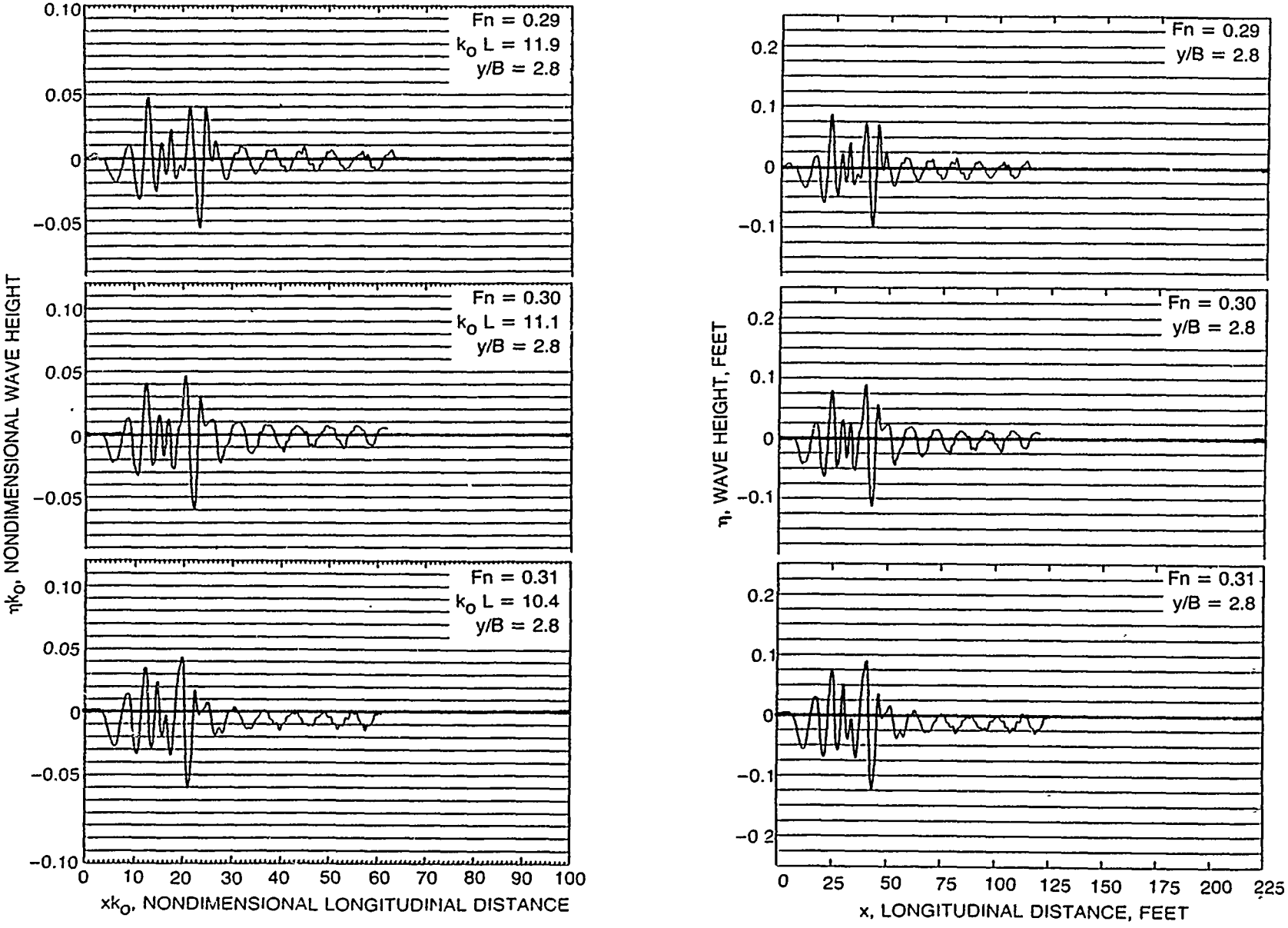

Fig. 26. Non-dimensional and dimensional longitudinal wave profiles of Model 5359 at F_n=0.29, F_n=0.30 and F_n=0.31.

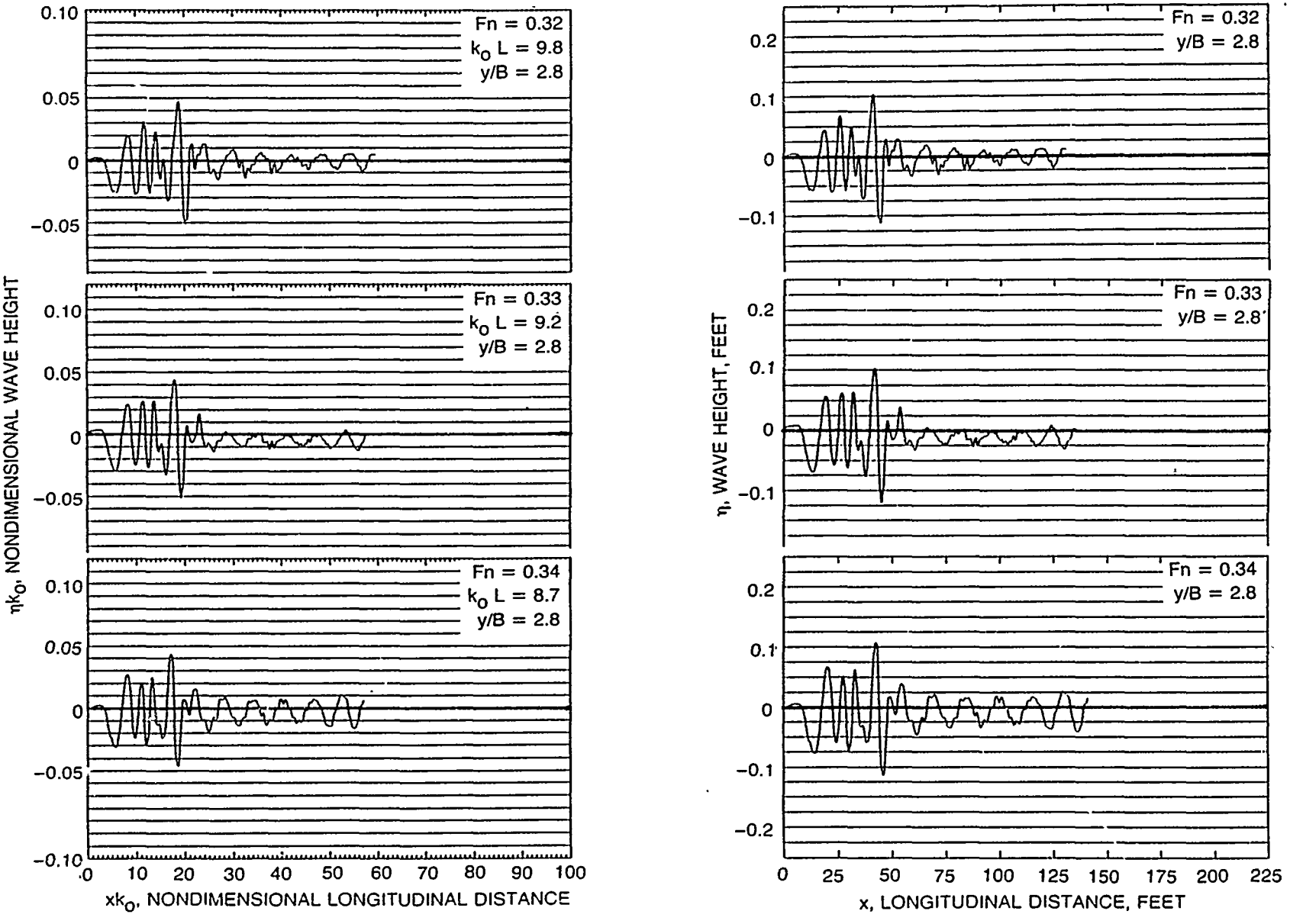

Fig. 27. Non-dimensional and dimensional longitudinal wave profiles of Model 5359 at F_n=0.32, F_n=0.33 and F_n=0.34.

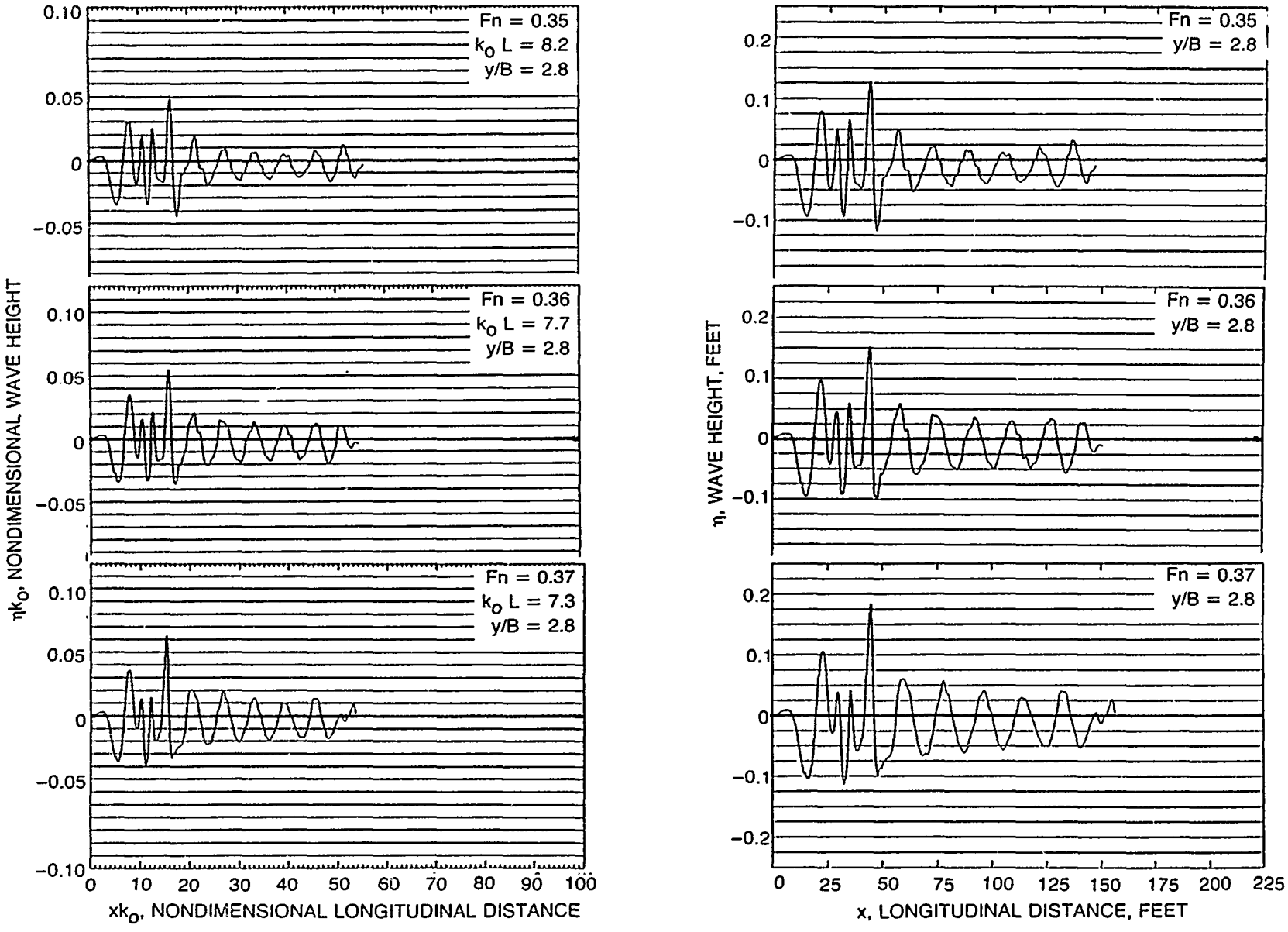

Fig. 28. Non-dimensional and dimensional longitudinal wave profiles of Model 5359 at F_n=0.35, F_n=0.36 and F_n=0.37.

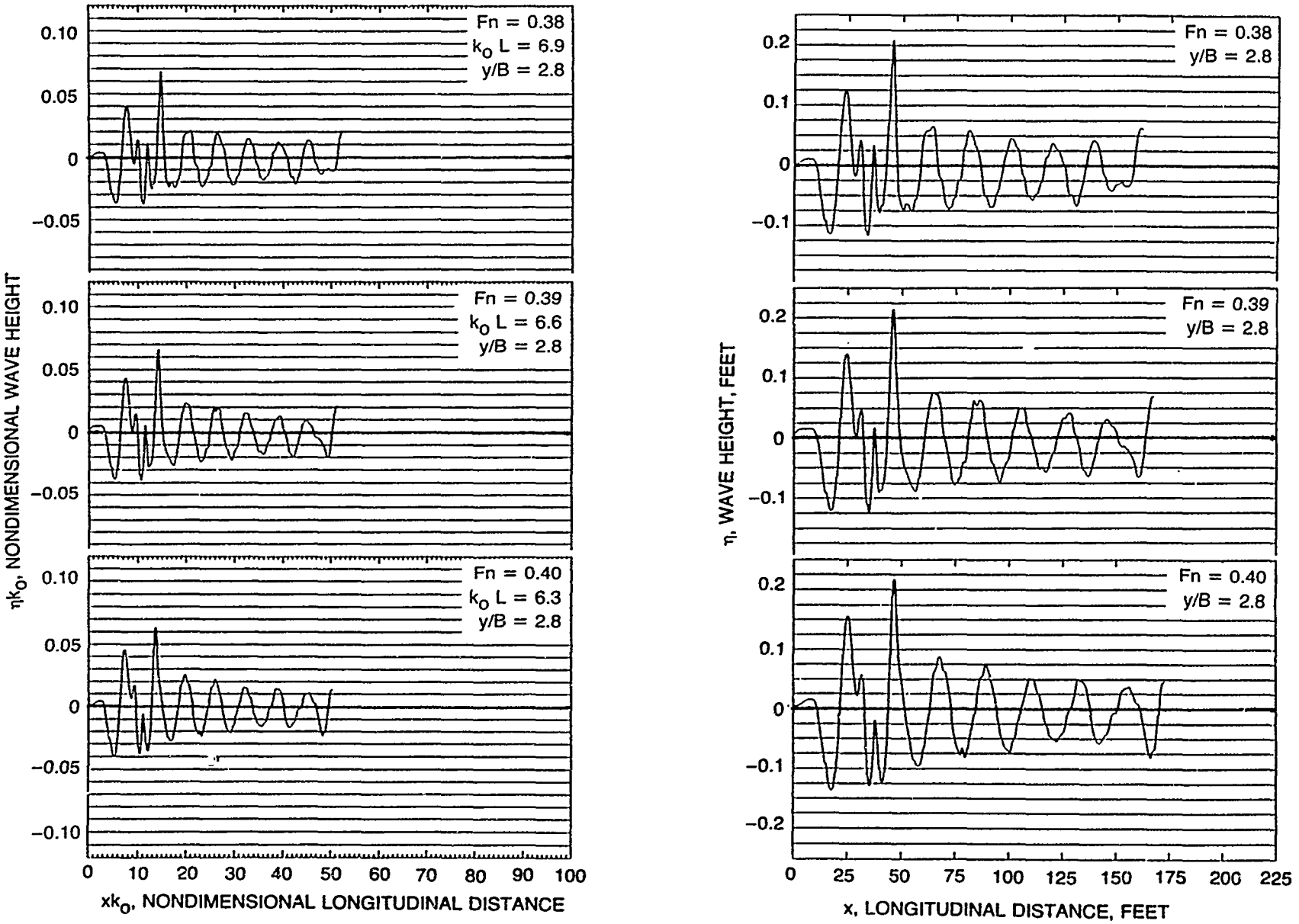

Fig. 29. Non-dimensional and dimensional longitudinal wave profiles of Model 5359 at F_n=0.38, F_n=0.39 and F_n=0.40.

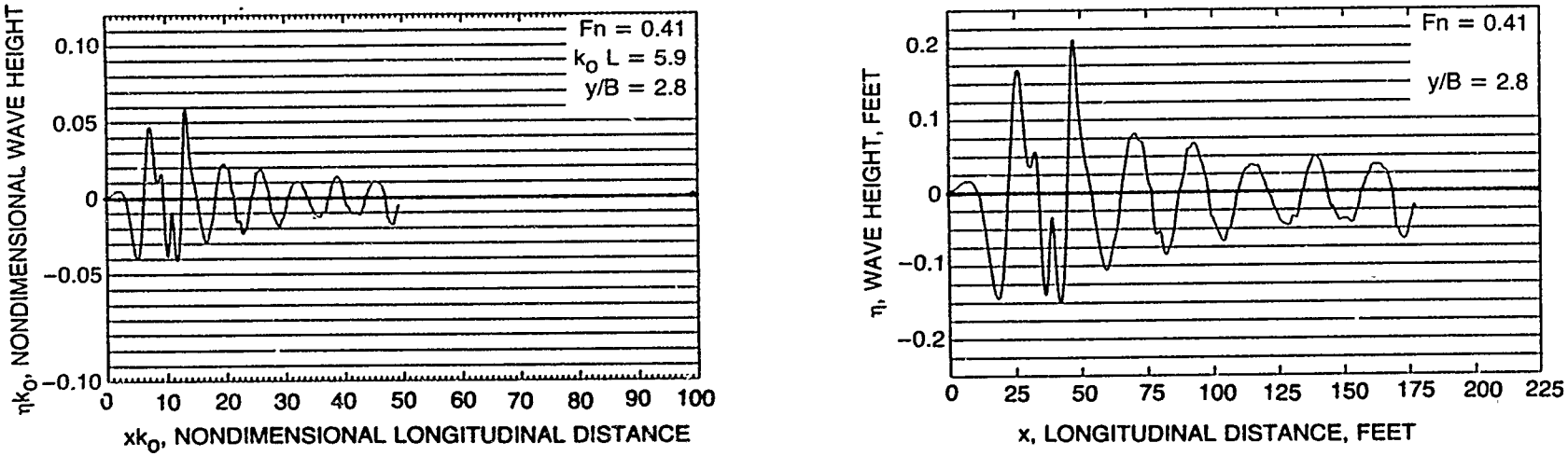

Fig. 30. Non-dimensional and dimensional longitudinal wave profiles of Model 5359 at $F_n = 0.41$.

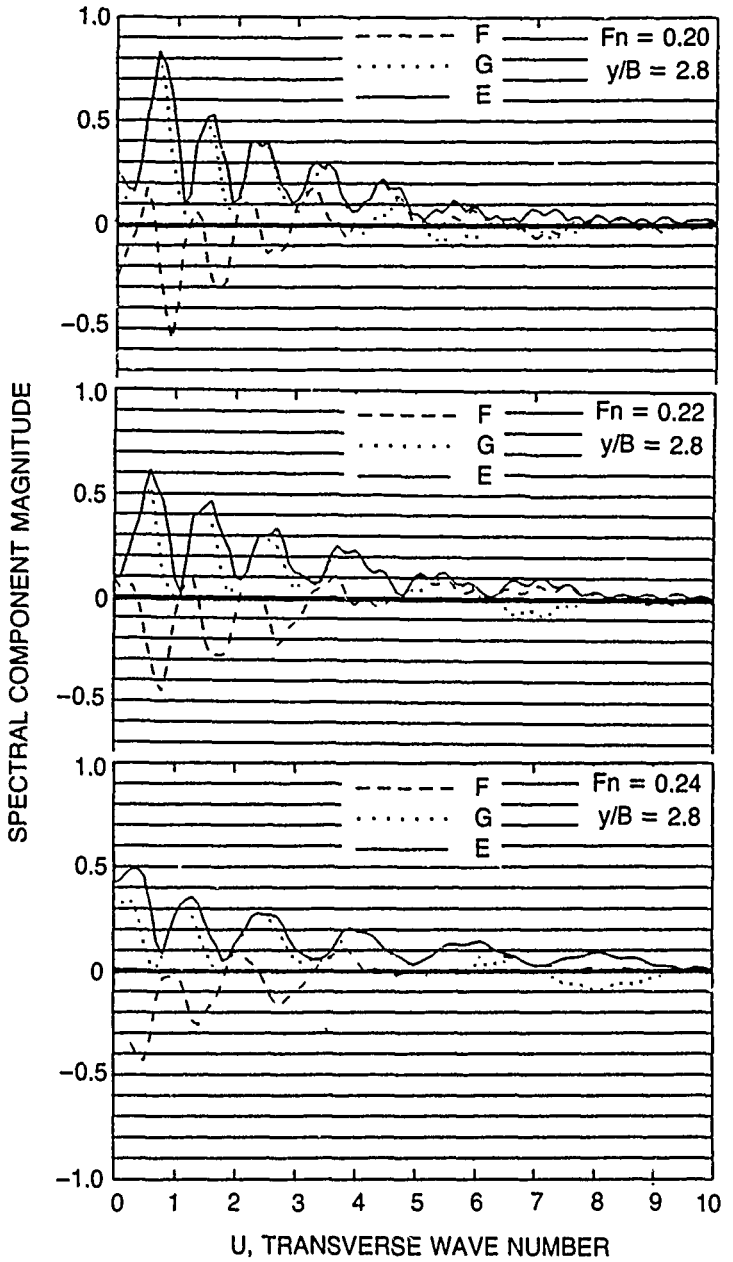

Fig. 31. Wave spectra of Model 5359 at F_n=0.20, F_n=0.22 and F_n=0.24.

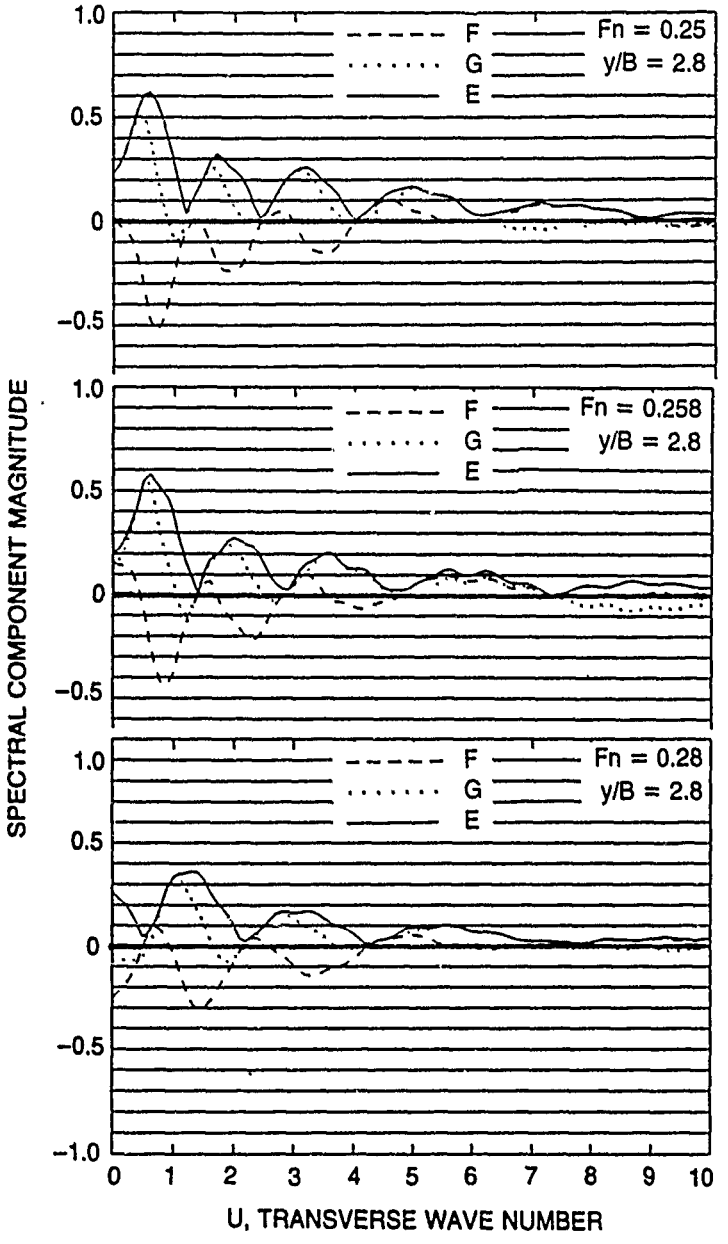

Fig. 32. Wave spectra of Model 5359 at F_n=0.25, F_n=0.258 and F_n=0.28.

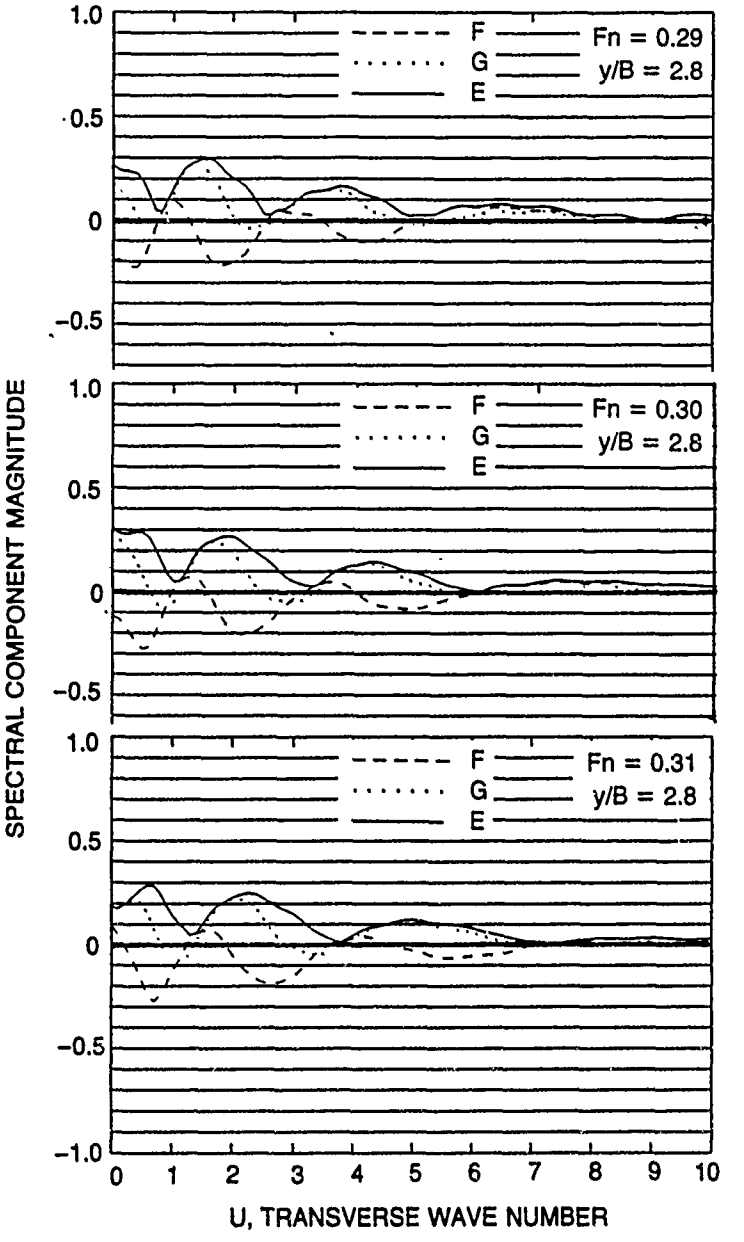

Fig. 33. Wave spectra of Model 5359 at F_n=0.29. F_n=0.30 and F_n=0.31.

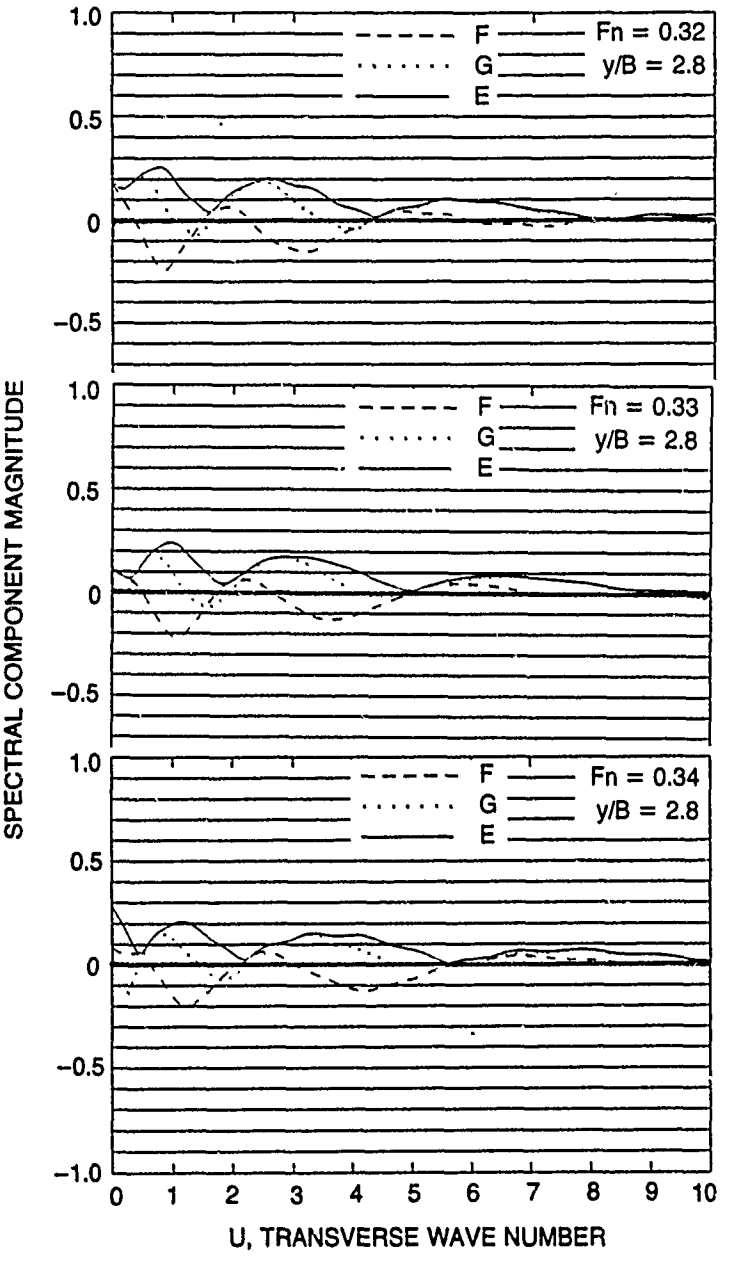

Fig. 34. Wave spectra of Model 5359 at F_n=0.32, F_n=0.33 and F_n=0.34.

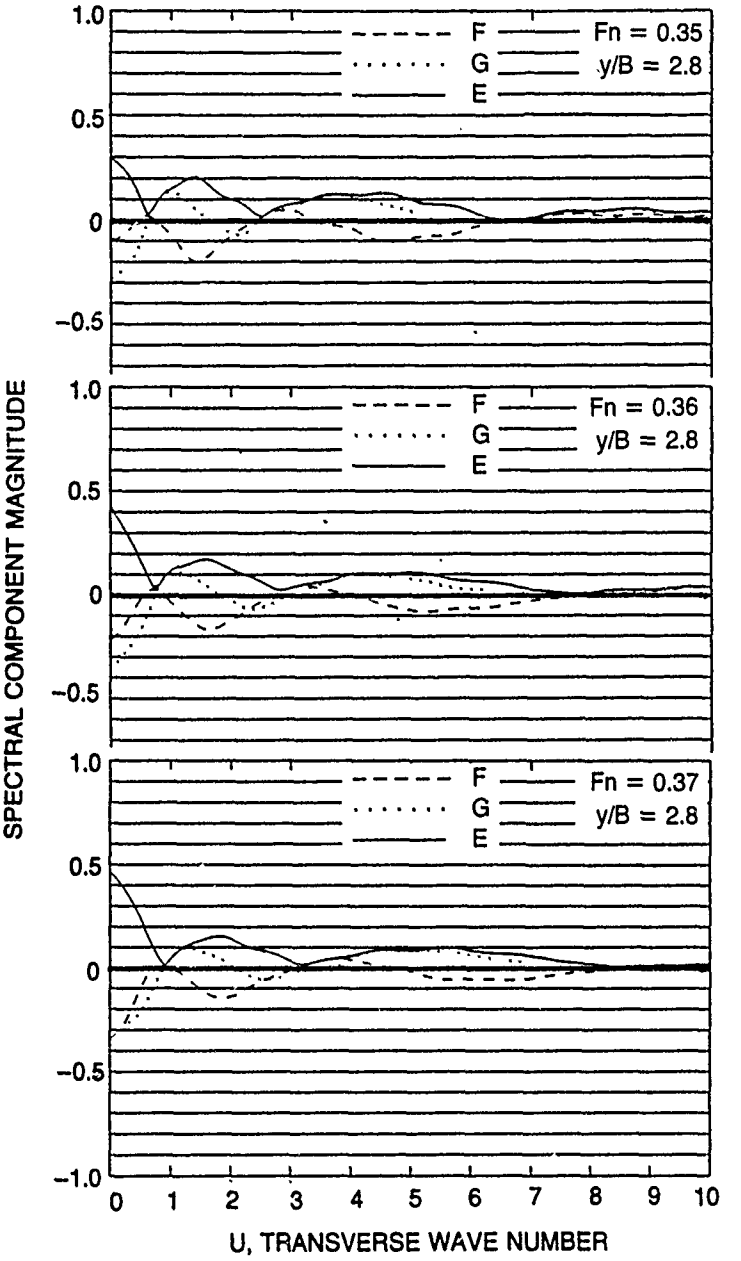

Fig. 35. Wave spectra of Model 5359 at F_n=0.35, F_n=0.36 and F_n=0.37.

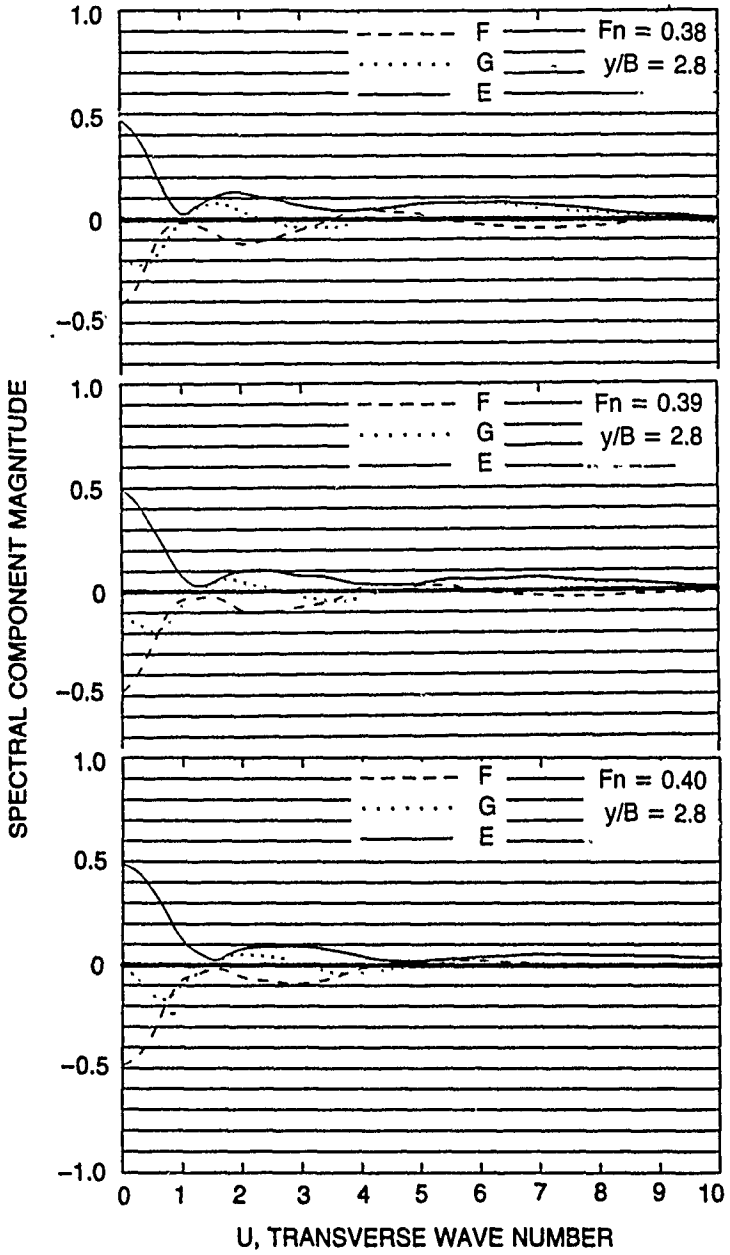

Fig. 36. Wave spectra of Model 5359 at F_n=0.38, F_n=0.39 and F_n=0.40.

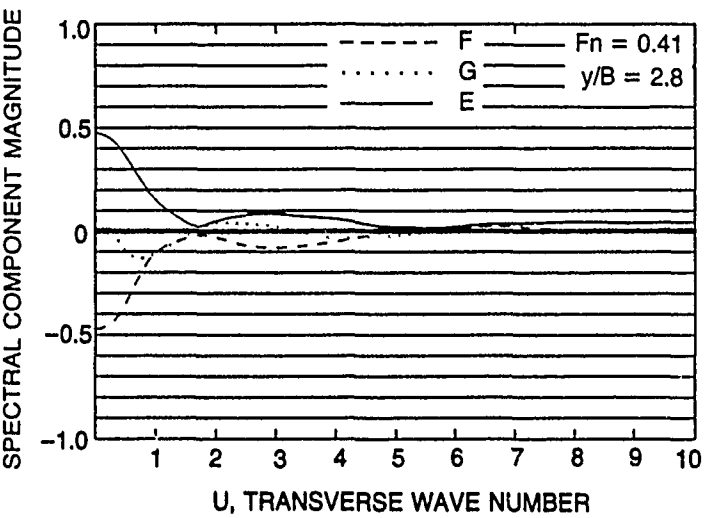

Fig. 37. Wave spectra of Model 5359 at $F_n = 0.41$.

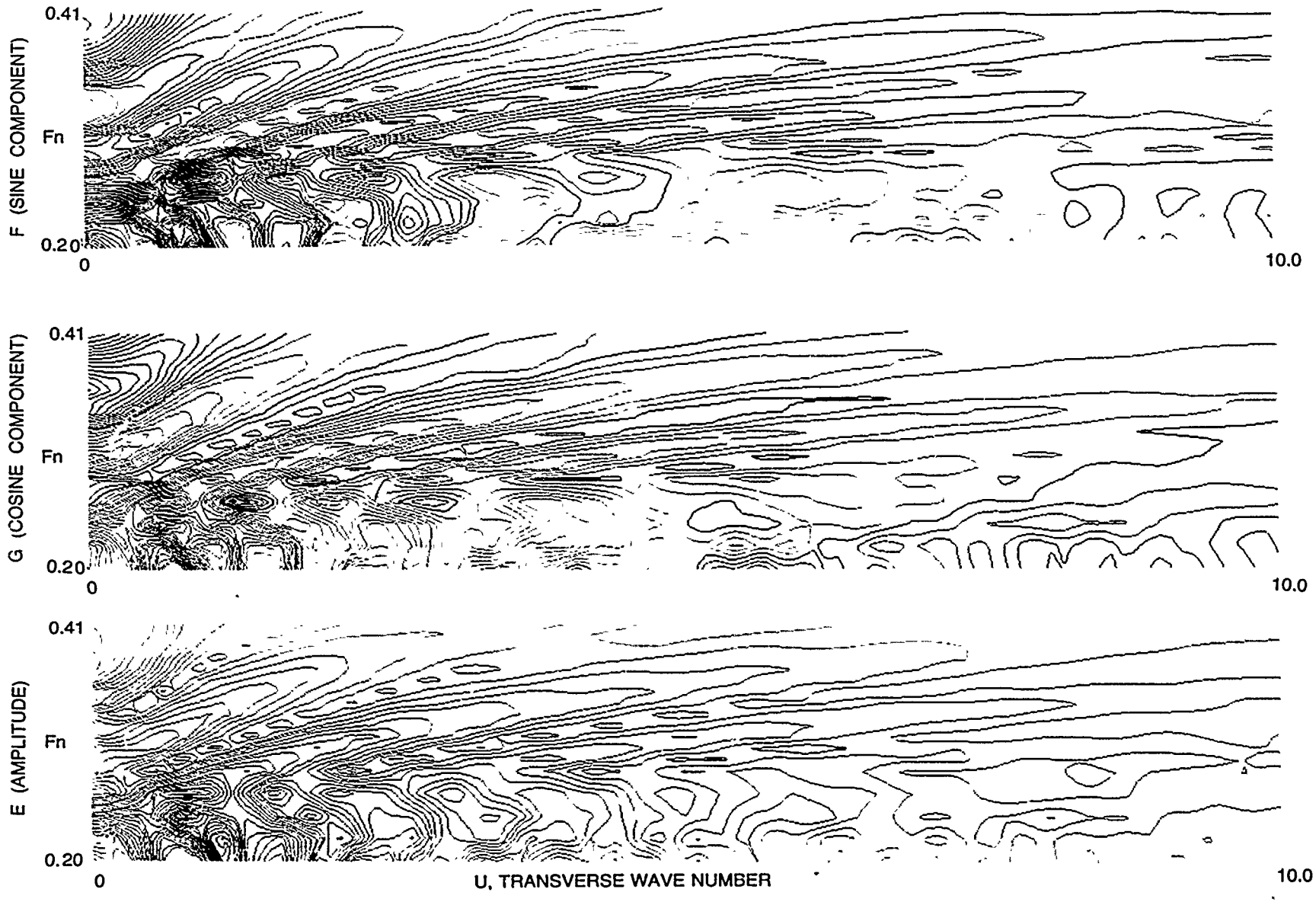

Fig. 38. Contour plots of the sine component, cosine component and amplitude of the wave spectra from Model 5359.

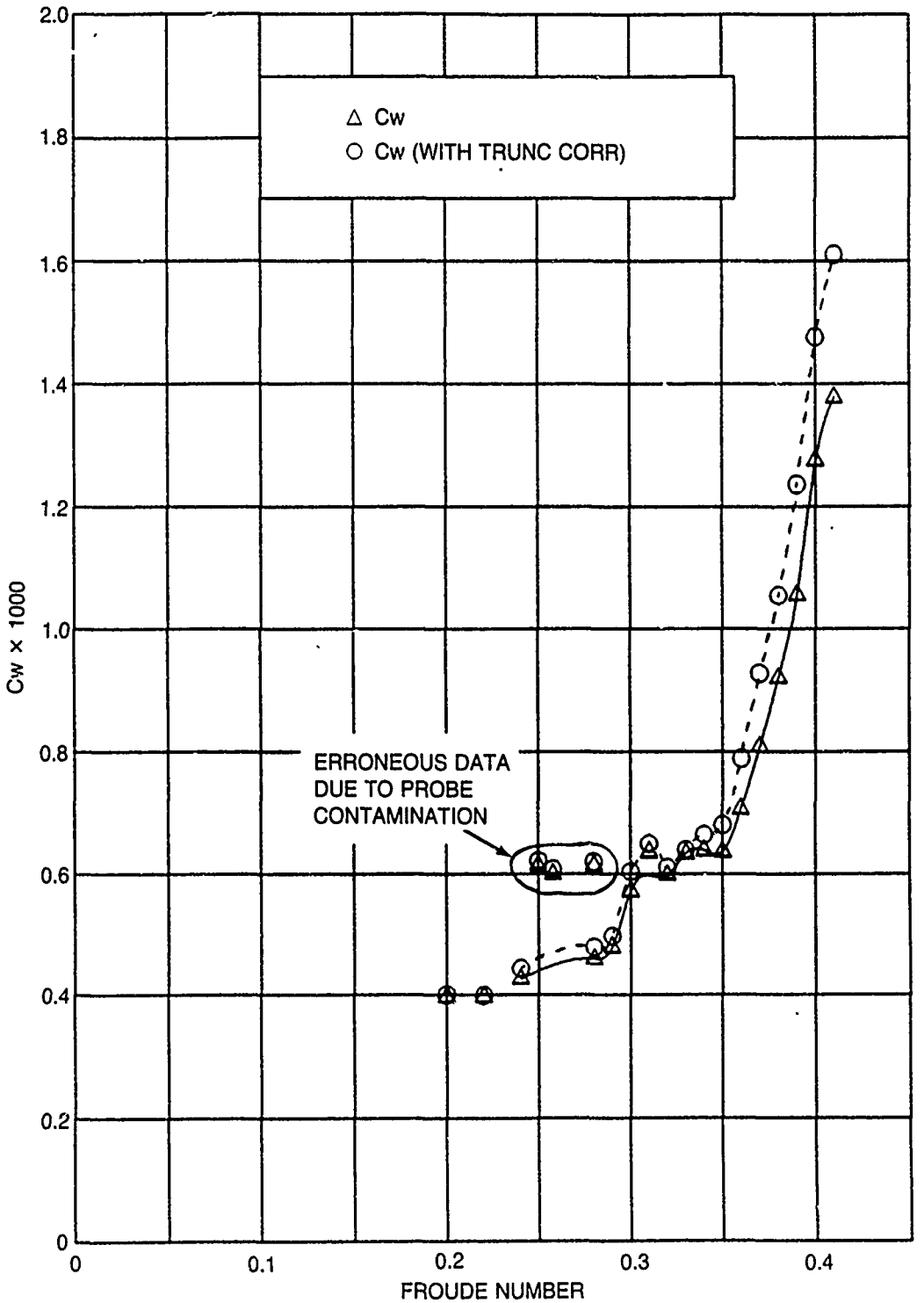

Fig. 39. Plot of C_w for Model 5359.

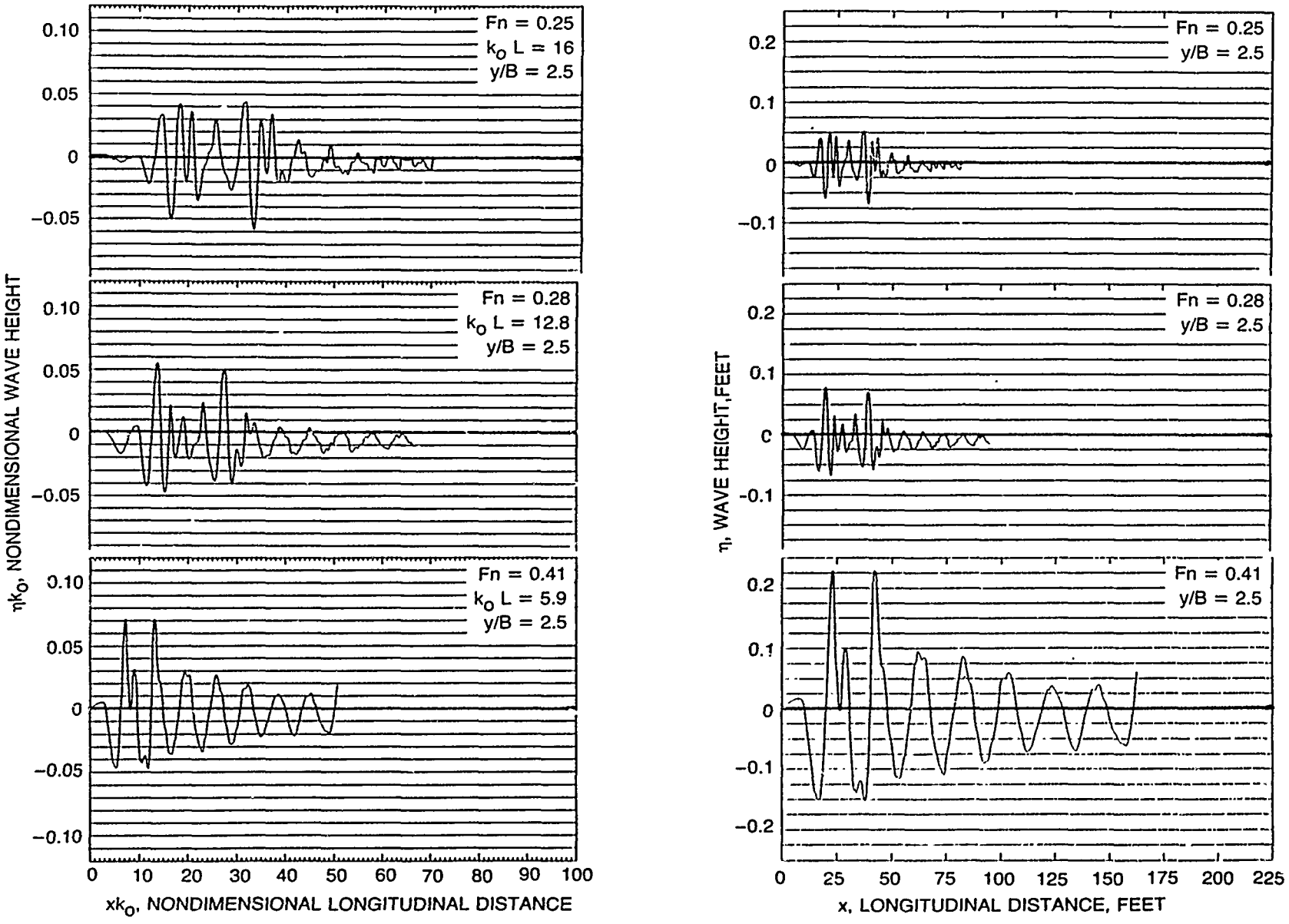

Fig. 40. Non-dimensional and dimensional longitudinal wave profiles of Model 5415 at $F_n = 0.25$, $F_n = 0.28$ and $F_n = 0.41$.

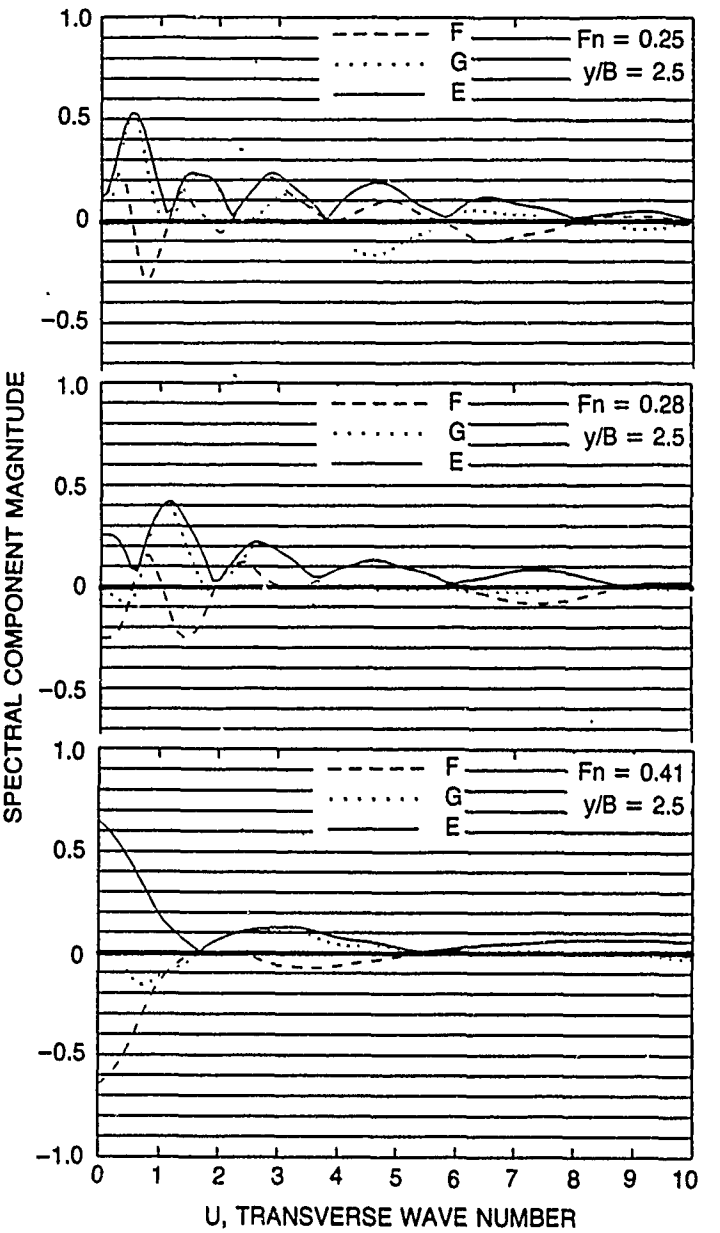

Fig. 41. Wave spectra of Model 5415 at F_n=0.25, F_n=0.28 and F_n=0.41.

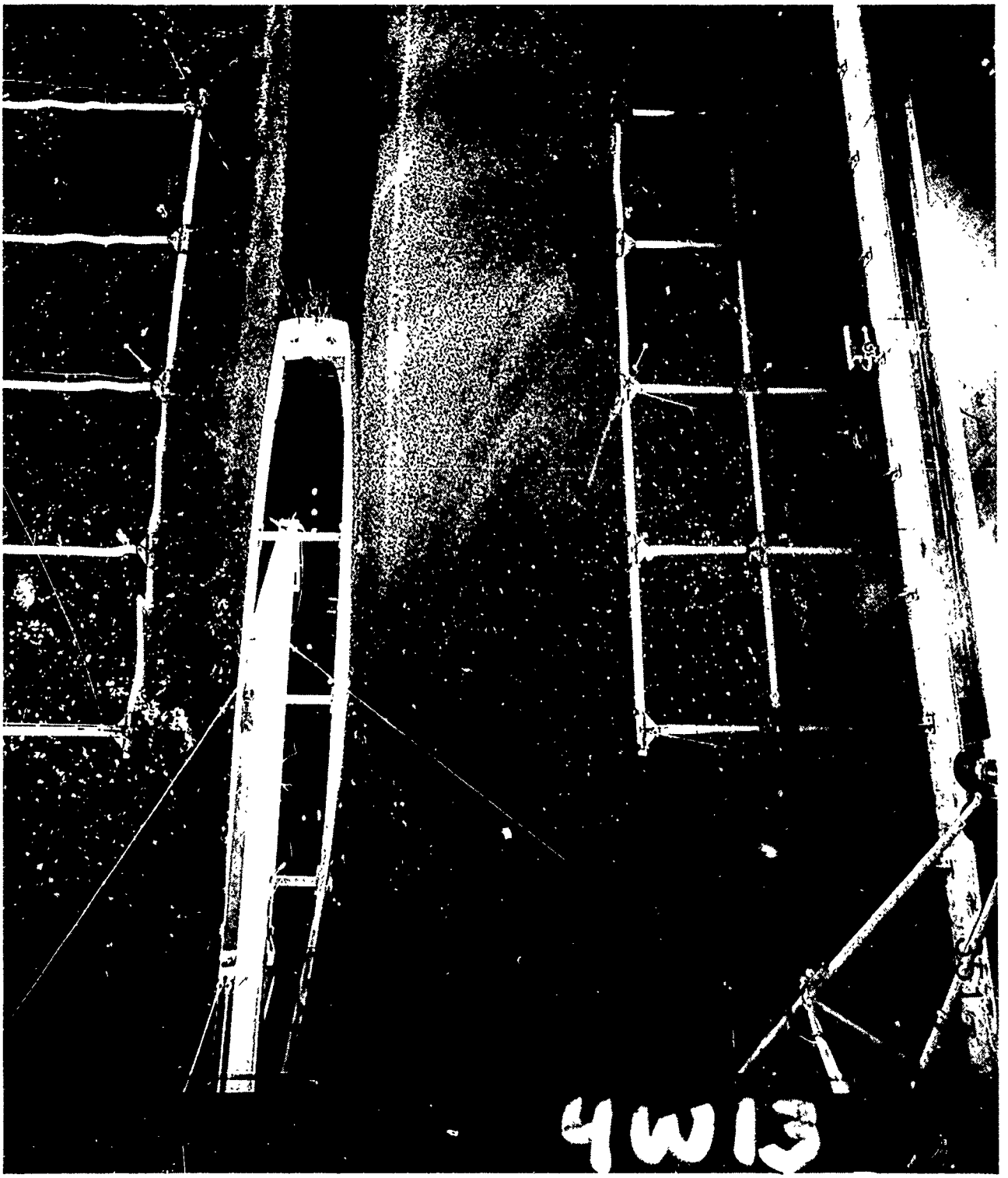

Fig. 42. Photograph of the Kelvin wake generated by Model 5063 at $F_n = 0.185$.

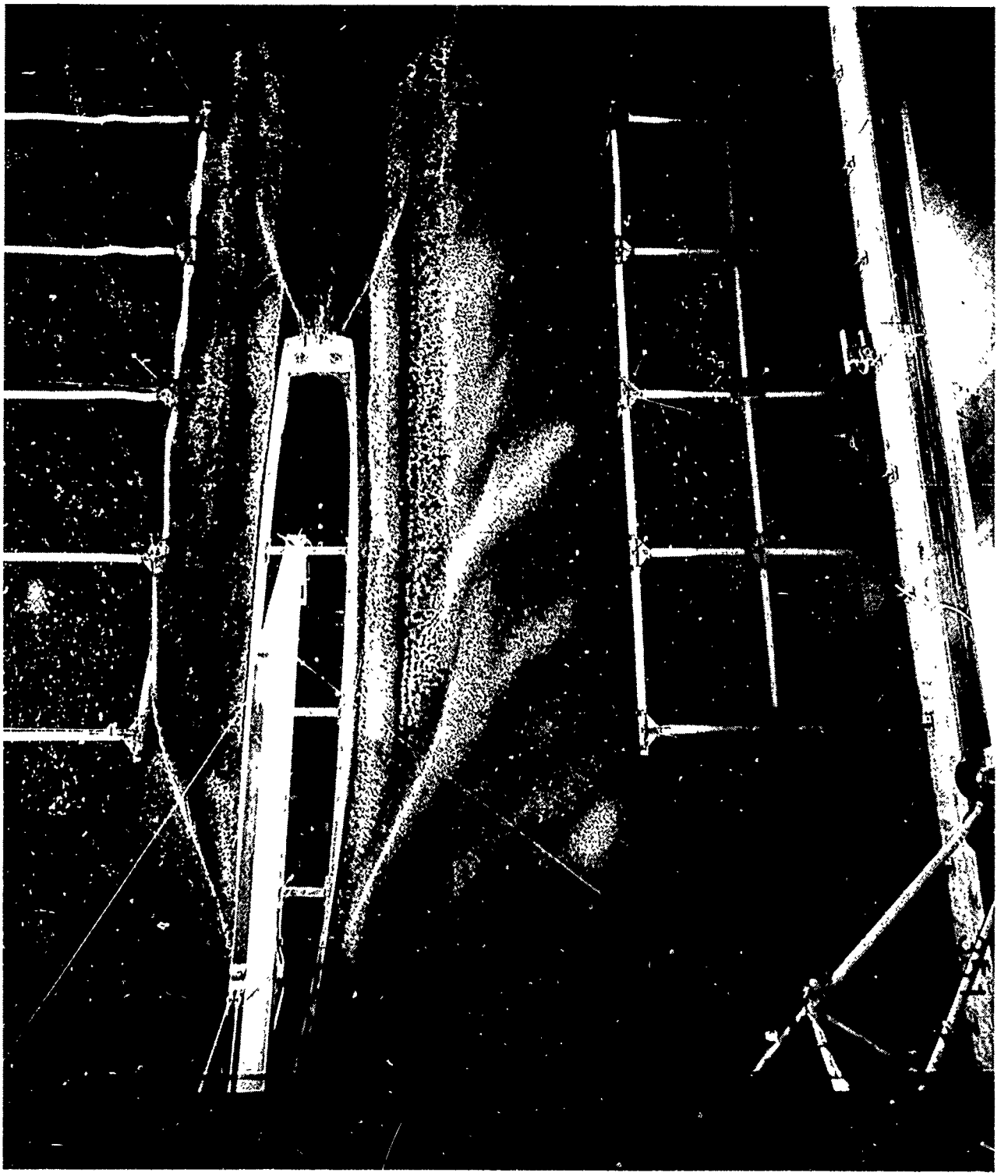

Fig. 43. Photograph of the Kelvin wake generated by Model 5063 at $F_n = 0.25$.

Fig. 44. Photograph of the Kelvin wake generated by Model 4645 at $F_n = 0.25$.

Fig. 45. Photograph of the Kelvin wake generated by Model 4645 at $F_n = 0.268$.

Fig. 46. Photograph of the Kelvin wake generated by Model 4645 at $F_n = 0.29$.

Fig. 47. Photograph of the Kelvin wake generated by Model 4645 at $F_{II}=0.30$.

Fig. 48. Photograph of the Kelvin wake generated by Model 4645 at $F_n = 0.31$.

Fig. 49. Photograph of the Kelvin wake generated by the drag Model 5201 with bow down trim at $F_n = 0.25$.

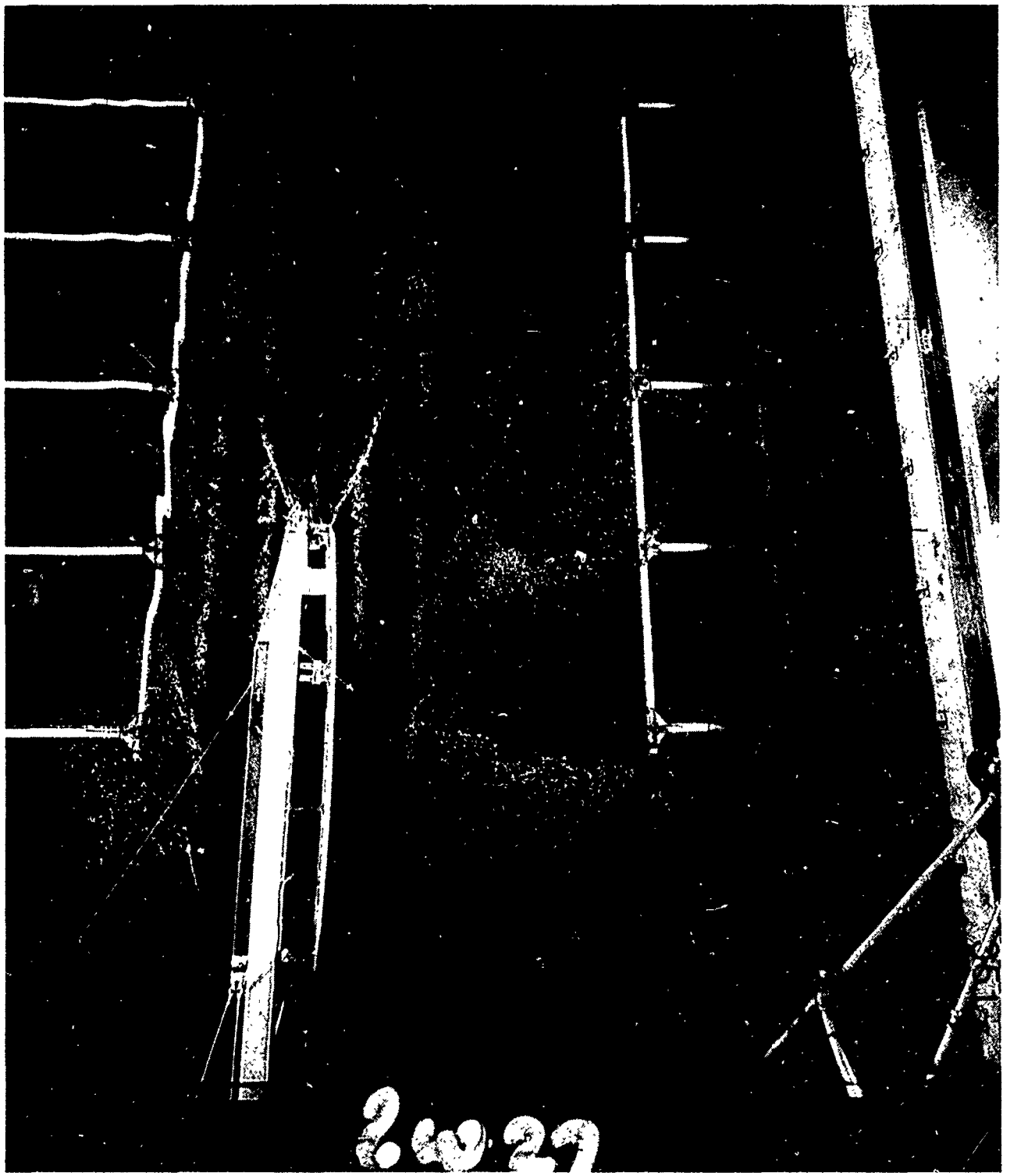

Fig. 50. Photograph of the Kelvin wake generated by the drag Model 5201 with design trim at $F_n = 0.25$.

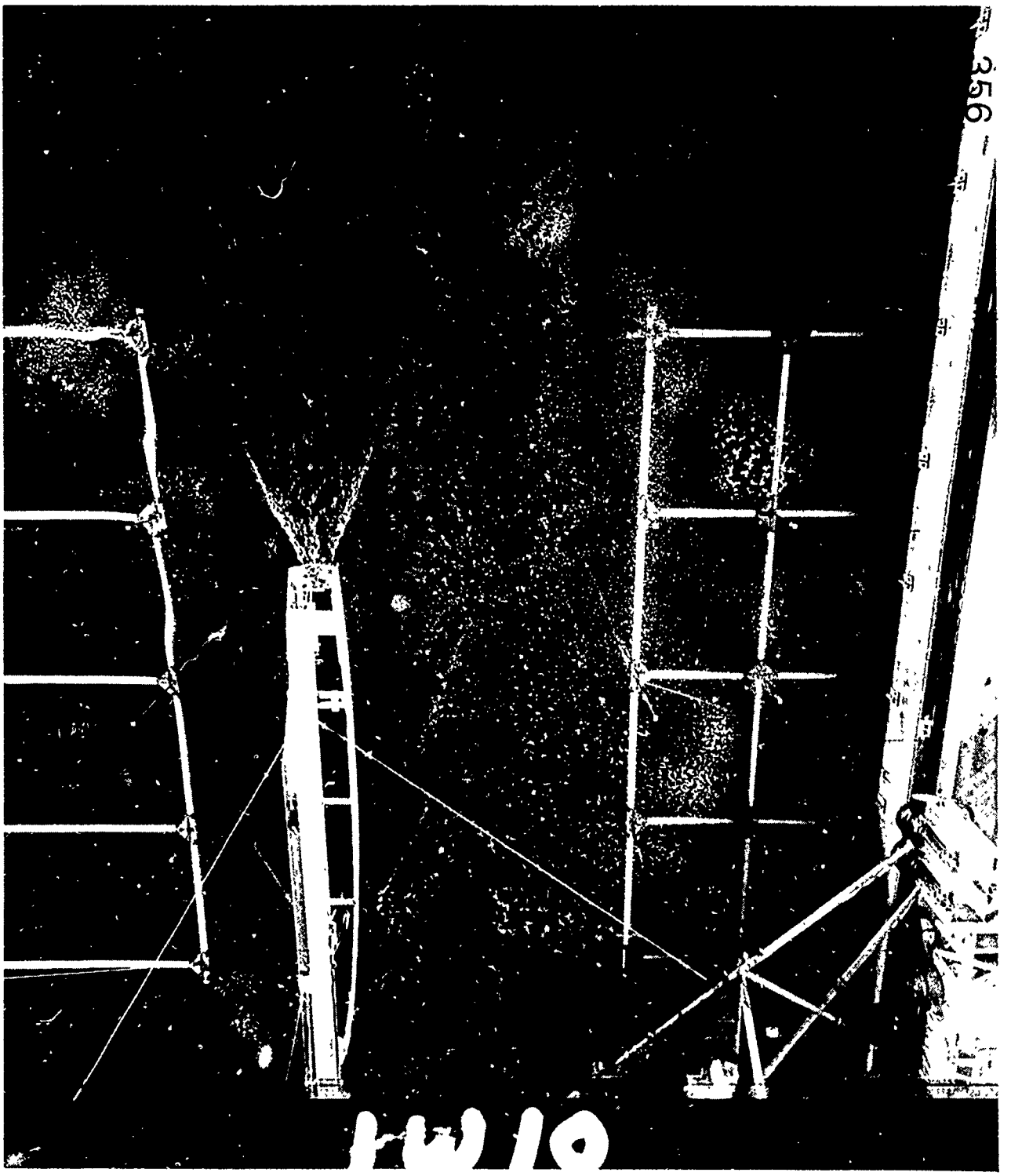

Fig. 51. Photograph of the Kelvin wake generated by the propelled Model 5201 with design trim at $F_n = 0.25$.

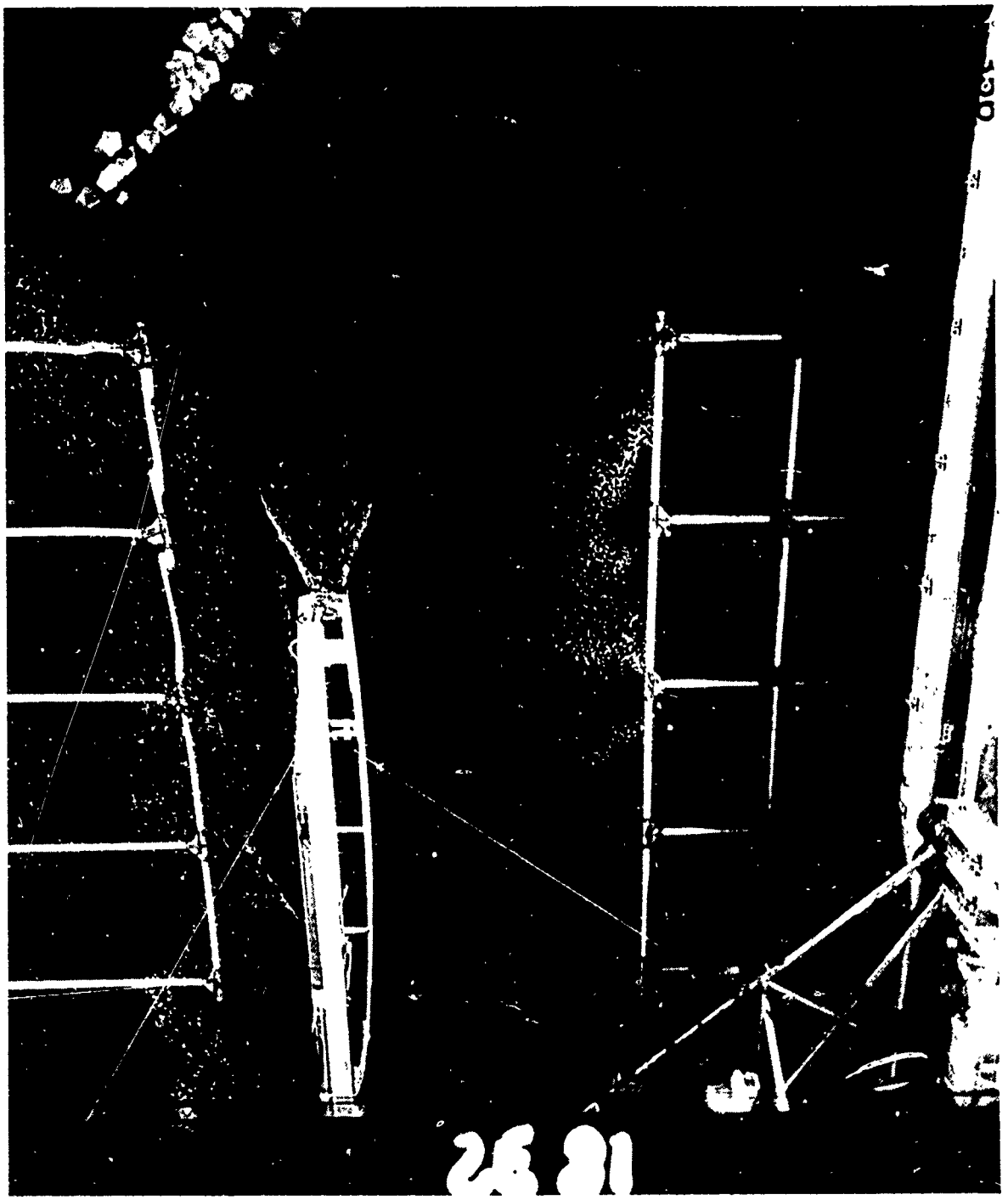

Fig. 52. Photograph of the Kelvin wake generated by the drag Model 5201 with stern down trim at $F_n = 0.25$.

Fig. 53. Photograph of the Kelvin wake generated by Model 5359 at $F_n = 0.25$.

Fig. 54. Photograph of the Kelvin wake generated by Model 5359 at $F_n = 0.258$.

Fig. 55. Photograph of the Kelvin wake generated by Model 5359 at $F_n = 0.41$.

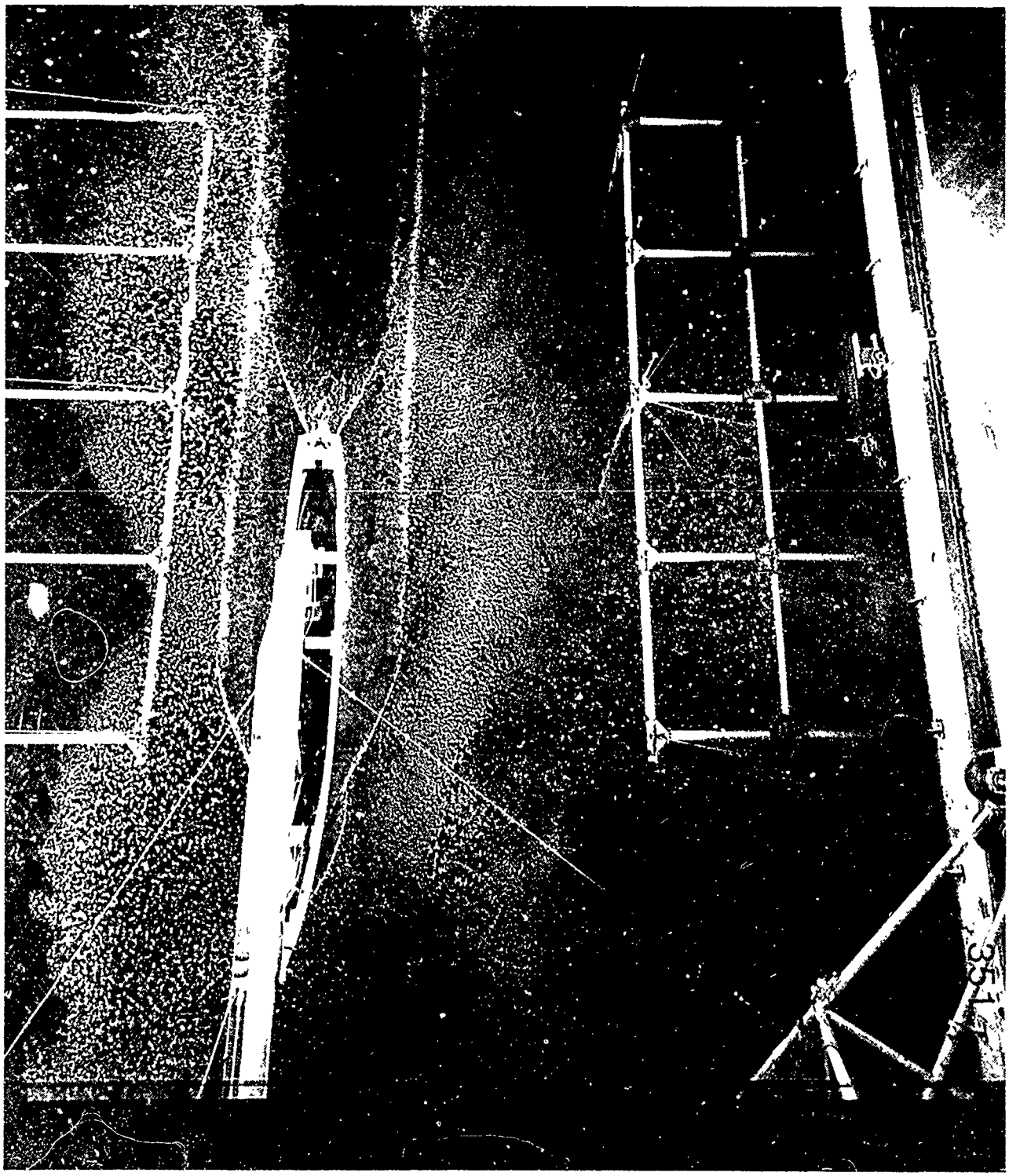

Fig. 56. Photograph of the Kelvin wake generated by Model 5415 at $F_n = 0.25$

Fig. 57. Photograph of the Kelvin wake generated by Model 5415 at $F_n = 0.28$.

Fig. 58. Photograph of the Kelvin wake generated by Model 5415 at $F_n = 0.41$.

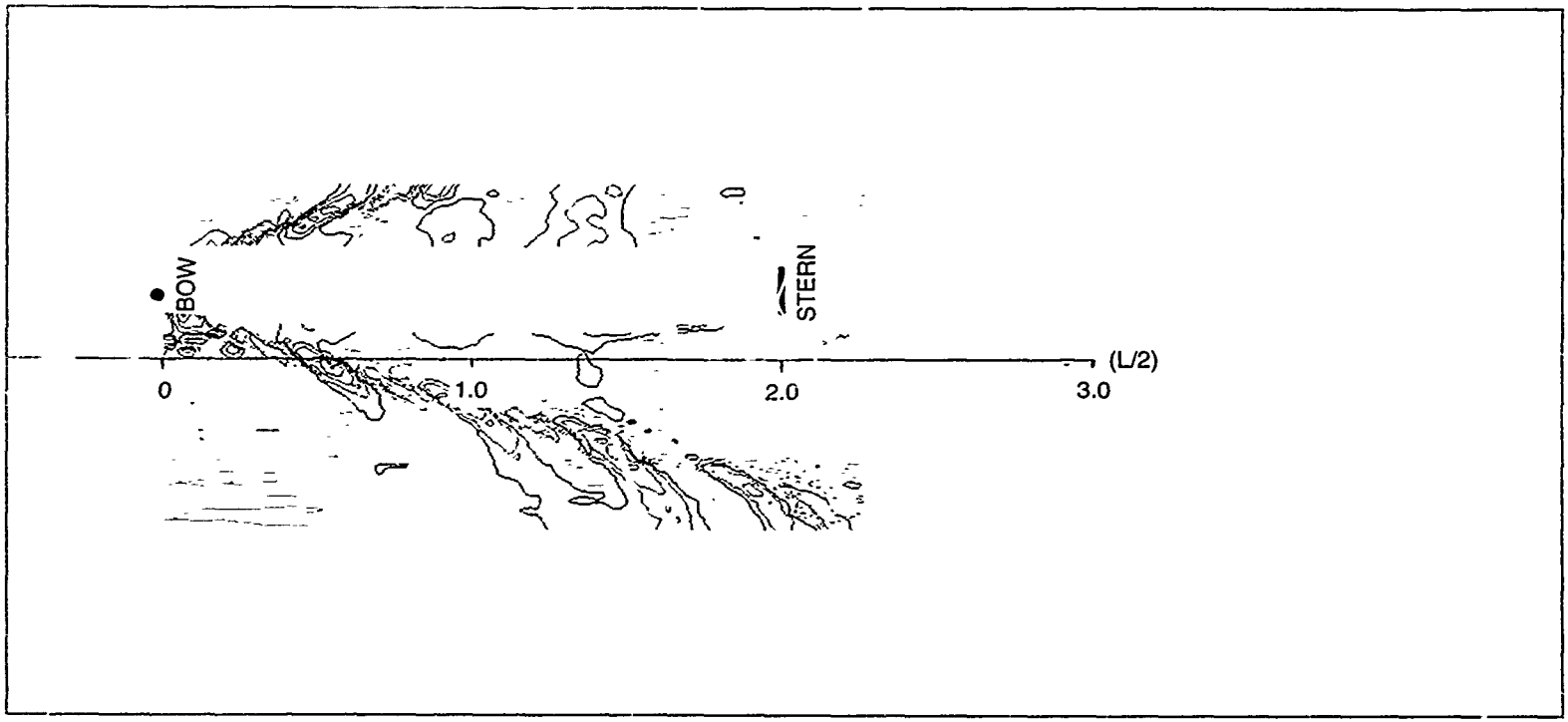

Fig. 59. Contour plot of Kelvin wake generated by Model 5063 at F_n=0.185.

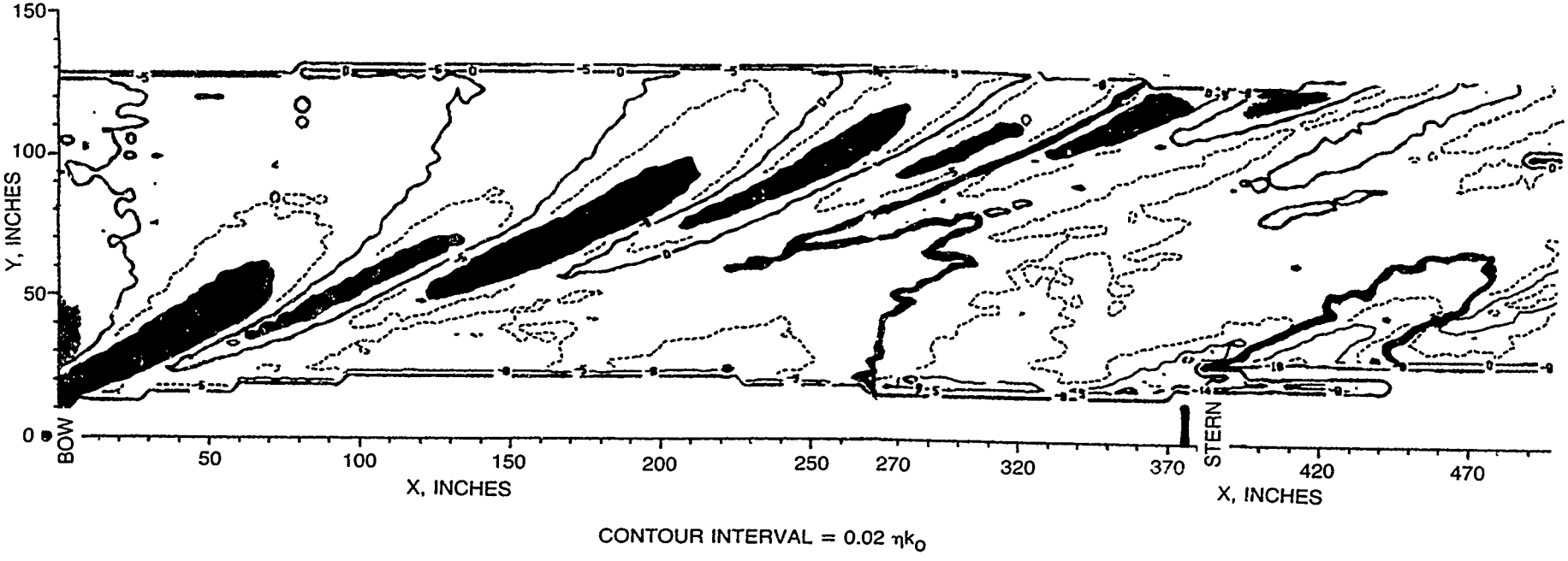

Fig. 60. Contour plot of Kelvin wake generated by Model 5063 at $F_n = 0.25$.

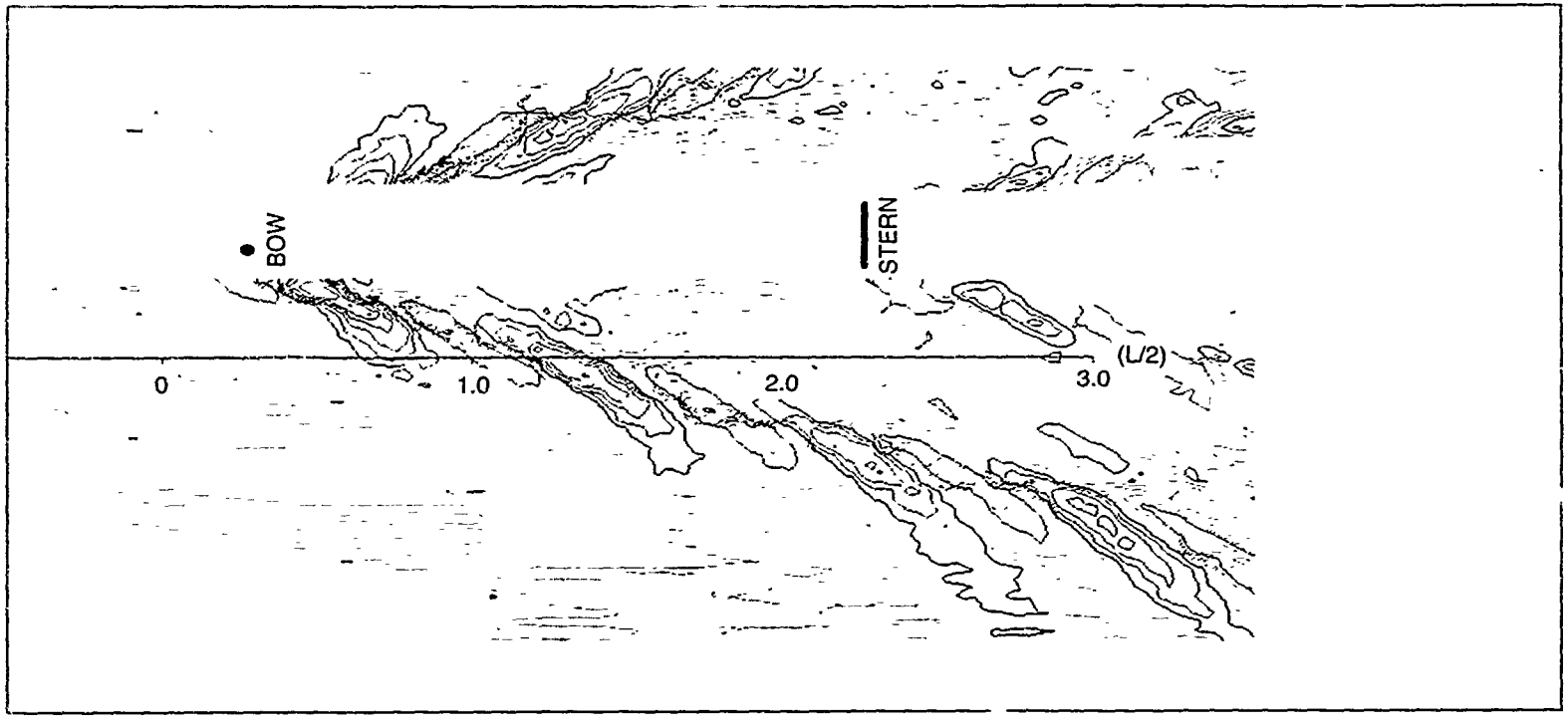

Fig. 61. Contour plot of Kelvin wake generated by Model 4645 at F_n=0.25.

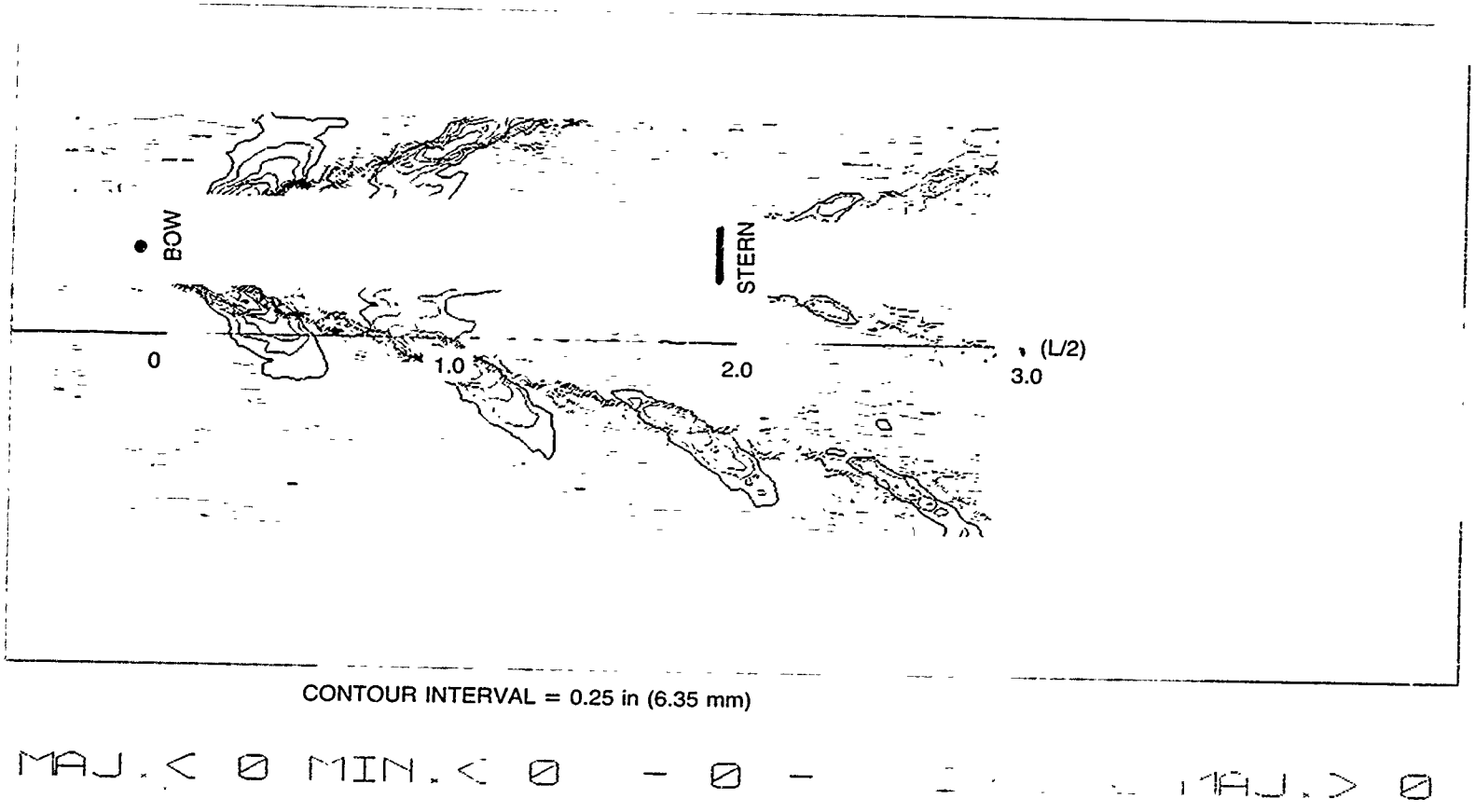

Fig. 62. Contour plot of Kelvin wake generated by drag Model 5201 with bow down trim at $F_n = 0.25$.

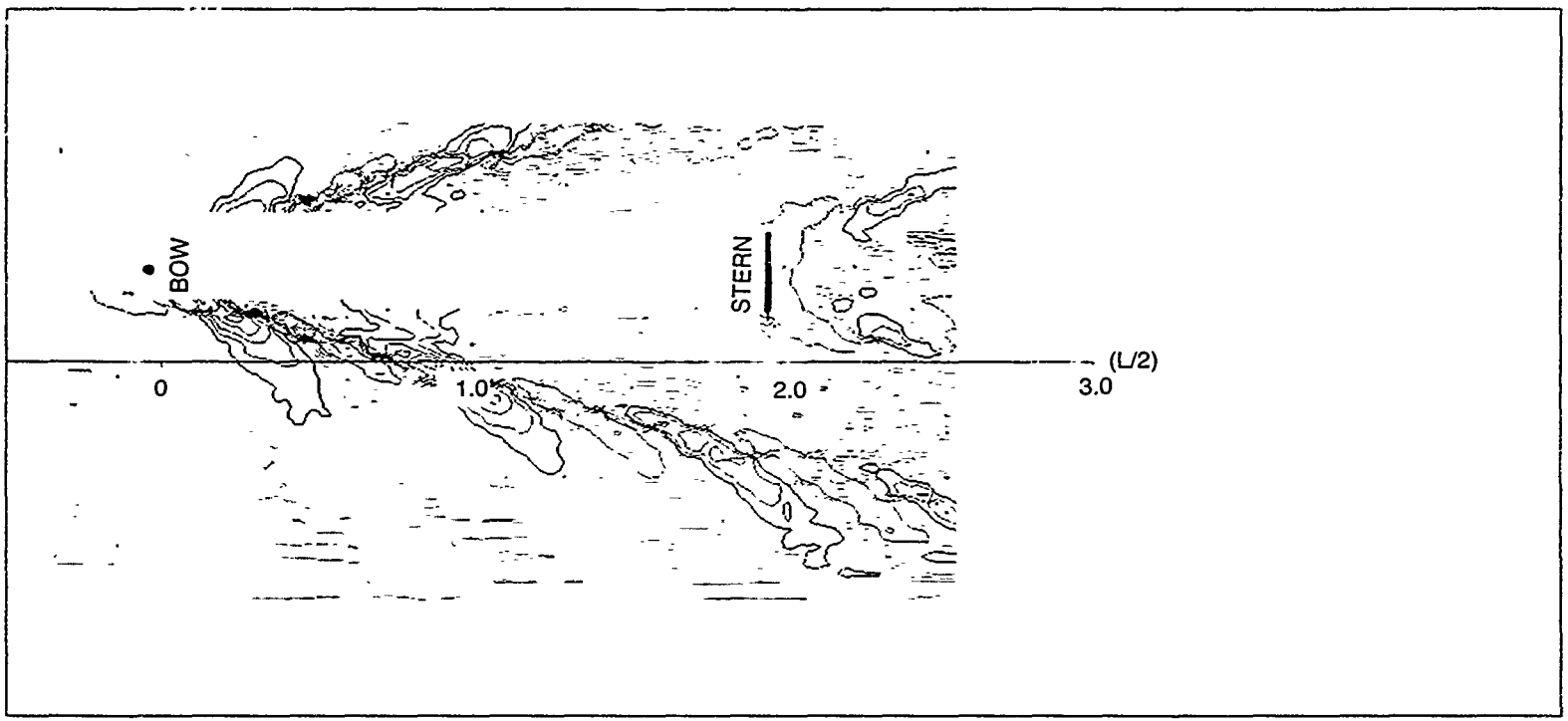

Fig. 63. Contour plot of Kelvin wake generated by drag Model 5201 with design trim at F_n=0.25, from first stereopair.

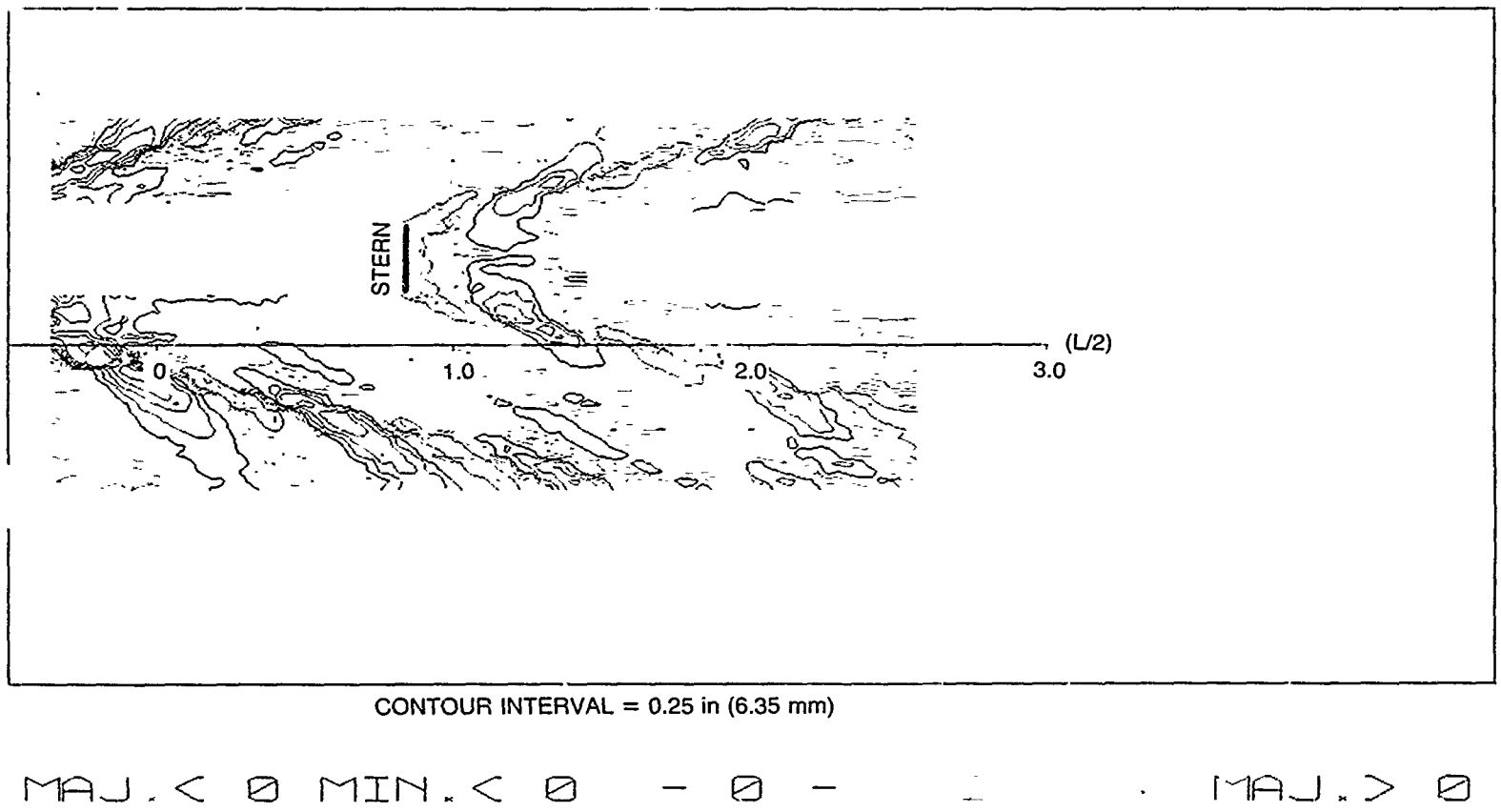

Fig. 64. Contour plot of Kelvin wake generated by drag Model 5201 with design trim at F_n=0.25, from second stercopair.

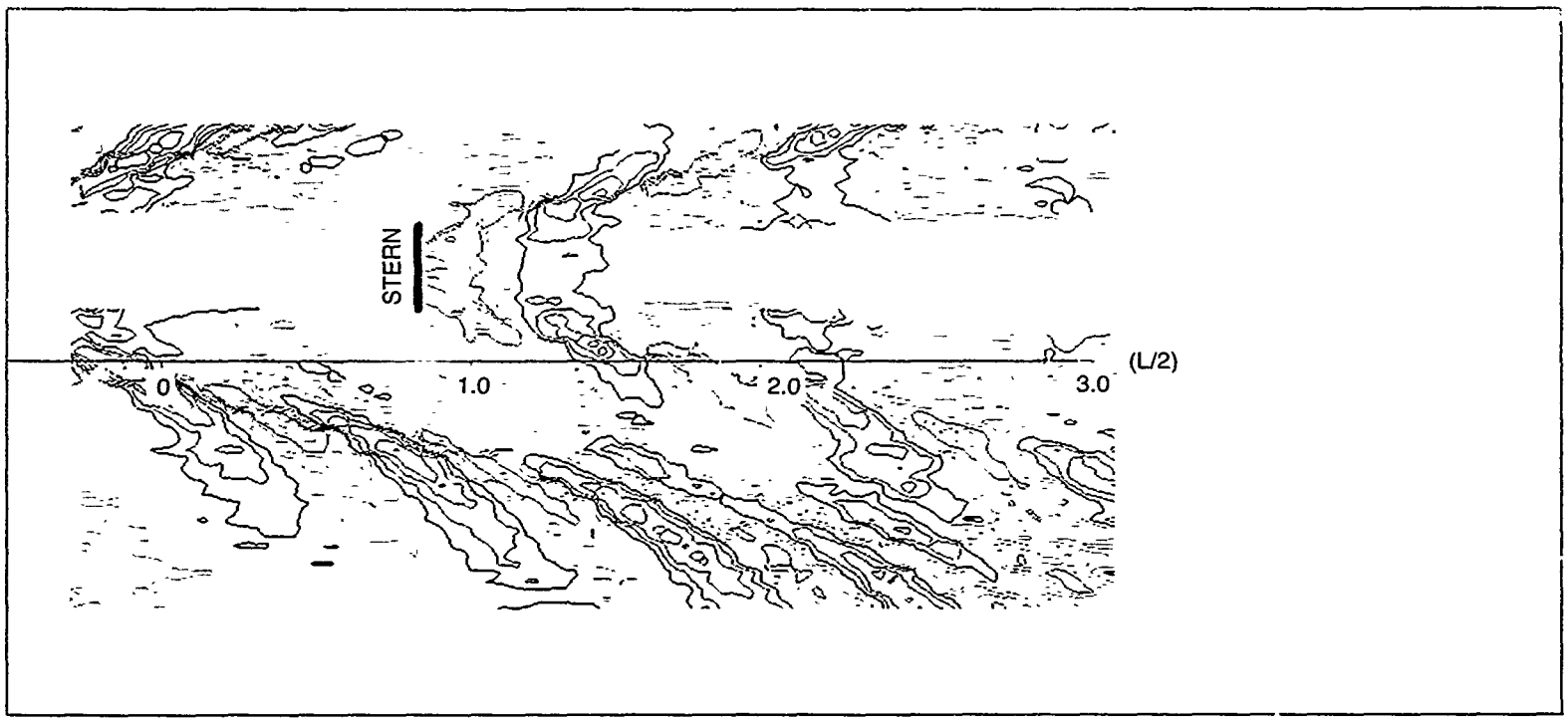

Fig. 65. Contour plot of Kelvin wake generated by propelled Model 5201 with design trim at F_n=0.25, from second stereopair.

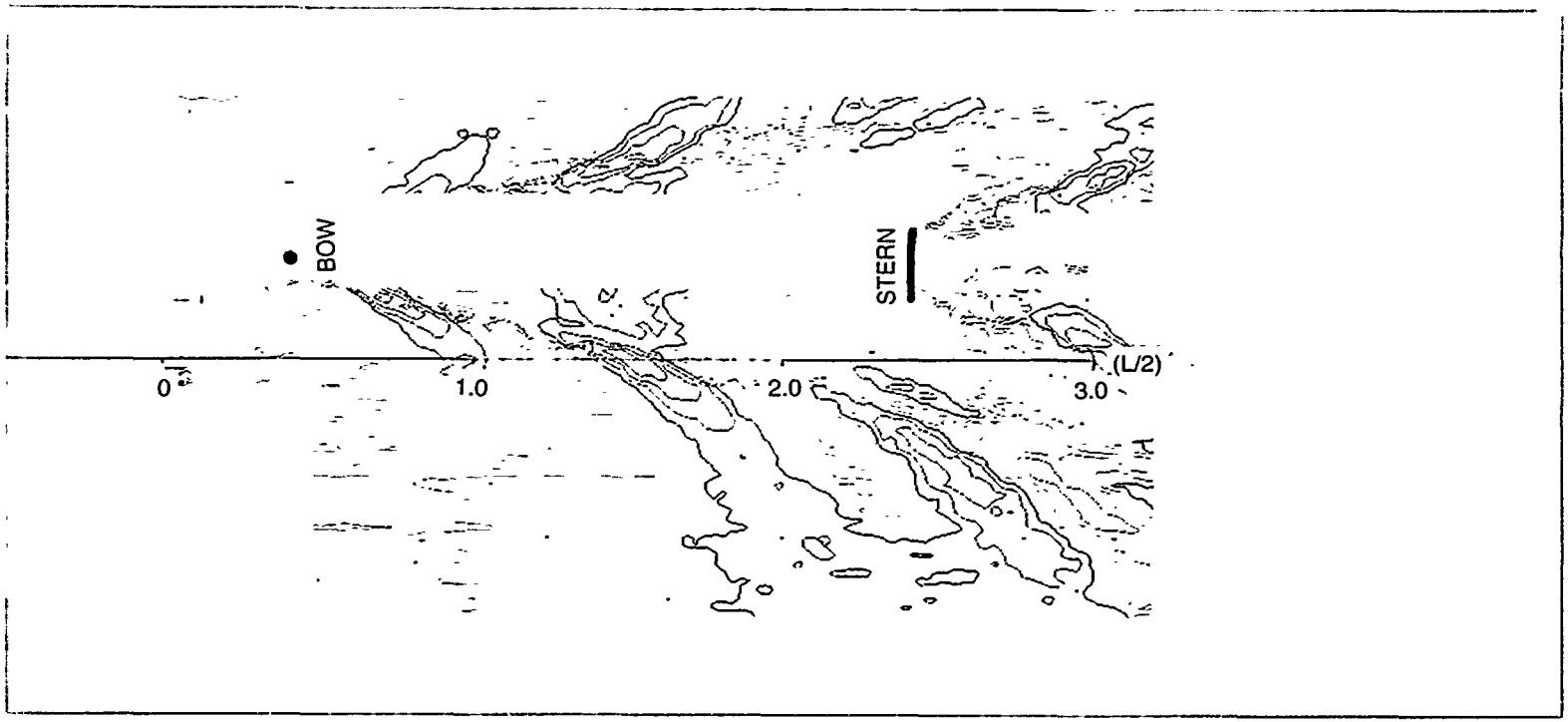

Fig. 66. Contour plot of Kelvin wake generated by Model 5359 at F_n=0.258.

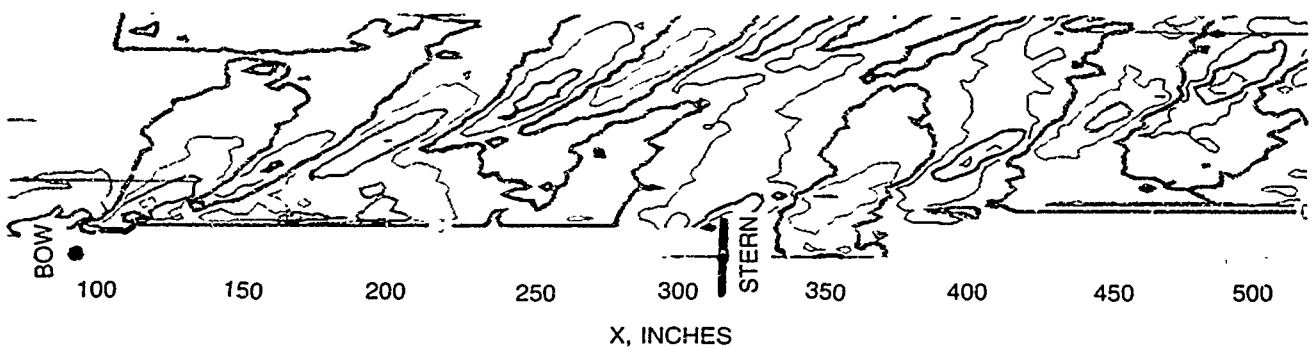

Fig. 67. Contour plot of Kelvin wake generated by Model 5415 at $F_n = 0.25$.

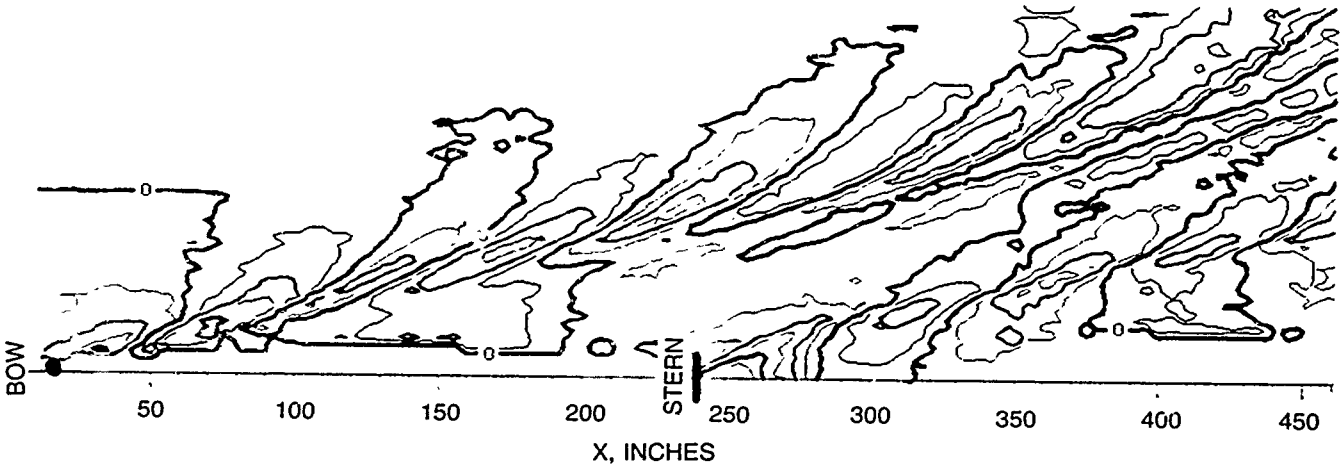

Fig. 68. Contour plot of Kelvin wake generated by Model 5415 at $F_n = 0.28$.

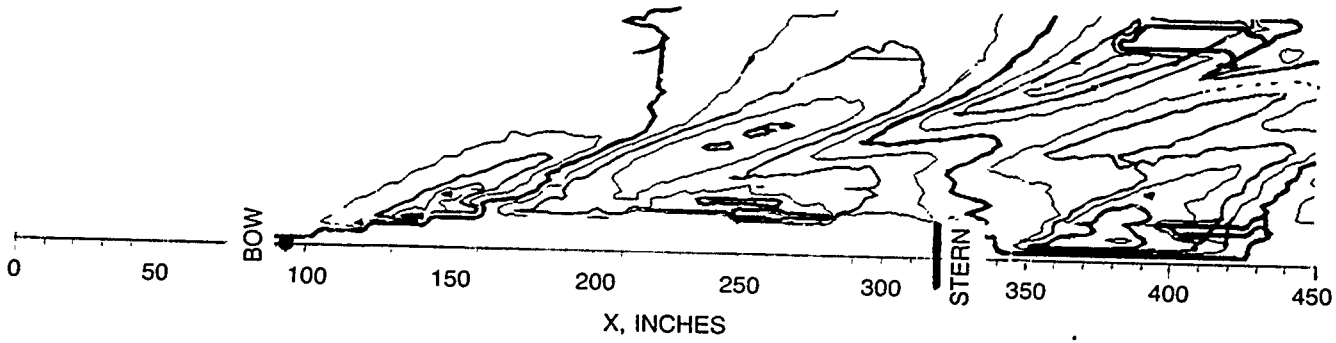

Fig. 69. Contour plot of Kelvin wake generated by Model 5415 at $F_n = 0.41$.

Table 1. Table of hull form coefficients.

	Model 4645	Model 5063	Model 5201	Model 5359	Model 5415
C_B	0.531	0.623	0.511	0.503	0.506
C_P	0.636	0.629	0.633	0.592	0.613
C_X	0.835	0.990	0.808	0.850	0.825
C_{WP}	0.765	0.768	0.767	0.746	0.778
L/B	8.930	7.764	9.055	9.668	7.527
B_X/T	3.135	3.573	3.017	2.570	3.092
L_E/L	0.518	0.528	0.550	0.551	0.550
L_R/L	0.482	0.472	0.450	0.449	0.450
$1/2\alpha_E$	10.75	9.50	9.00	7.00	11.00
$\frac{\Delta}{(0.01L)^3}$	60.67	82.70	59.08	59.86	82.55

Table 2. Summary of kelvin wake experimental data.

Ship	Model	Scale	Length feet (meters)	Ship Speed knots	Froude No.	Condition
DDG 2	4645	21.524	19.51 (5.95)	17.3	0.25	Drag
				18.4	0.268	"
				18.6	0.27	"
				19.3	0.28	"
				20.0	0.29	"
				20.7	0.30	"
				21.3	0.31	"
Destroyer	5415	24.824	18.77 (5.72)	18.1	0.25	Drag
				20.0	0.28	"
				30.0	0.41	"
CVN 68	5063	33.05	31.46 (9.60)	20.0	0.185	Drag
				27.0	0.25	"
CGN 38	5201	24.064	23.27 (7.09)	20.0	0.25	Drag Design trim
				"	"	Drag Trim by bow
				"	"	Drag Trim by stern
				"	"	Propelled Design trim
				"	"	Propelled Trim by bow

Table 2 (Continued)

Ship	Model	Scale	Length feet (meters)	Ship Speed knots	Froude No.	Condition
DD 993	5359	24.824	21.36 (6.51)	15.5	0.20	Drag
				17.0	0.22	"
				18.6	0.24	"
				19.3	0.25	"
				20.0	0.258	"
				21.7	0.28	"
				22.5	0.29	"
				23.2	0.30	"
				24.0	0.31	"
				24.8	0.32	"
				25.6	0.33	"
				26.3	0.34	"
				27.1	0.35	"
				27.9	0.36	"
				28.6	0.37	"
				29.4	0.38	"
				30.2	0.39	"
				31.0	0.40	"
				31.7	0.41	"

THIS PAGE INTENTIONALLY LEFT BLANK

INITIAL DISTRIBUTION

Copies

6 CONR
- 1 1121 S. Ramberg
- 1 1132F E. Rood
- 1 121 R.J. Hansen
- 1 1215 J. Fein
- 1 1223 D. Johnson
- 1 211 J. Gagorik

4 NAVSEA
- 1 501E W. Bauman
- 1 55W3 E. Comstock
- 1 55W3 A. Engle
- 1 55W3 H. Chatterton

2 NCSC
- 1 2210 R. Peterson
- 1 2210 M. Hyman

4 NRL
- 1 4420 G. Keramidas
- 1 4420 R. Peltzer
- 1 4420 H. Wang
- 1 4420 O. Griffin

2 NOAA, National Ocean Service
- 1 B. Baldwin
- 1 G. Snyder

2 USNA
- 1 R. Comstock
- 1 B. Johnson

12 DTIC

2 University of California
- 1 J. Wehausen
- 1 R. Yeung

1 University of Iowa
- 1 F. Stern

1 University of Maryland
- 1 J. Duncan

1 University of Maryland - Baltimore Campus
- 1 C. Von Kerczek

Copies

2 MIT
- 1 J. Milgram
- 1 N. Newman

2 University of Michigan
Department of Naval Architecture
- 1 R. Beck
- 1 A. Troesch

1 University of North Carolina
- 1 T. Lucas

1 Webb Institute of Naval Architecture
- 1 L. Ward

1 ARC Professional Services
- 1 J. Witting

1 LMSC
- 1 T. Schmidt

4 SAIC, Annapolis
- 1 C. Oliver
- 1 N. Salvesen
- 1 R. Skop
- 1 K. Weems

3 SAIC, San Diego
- 1 B. Hall
- 1 C. Scragg
- 1 D. Wyatt

INITIAL DISTRIBUTION (Continued)

CENTER DISTRIBUTION

Copies	Code	Name
1	015	S. Hawkins
1	1504	V. Monacella
1	1506	D. Walden
1	1521	P. Chang
1	1521	G. Karafiath
6	1521	W. Lindenmuth
1	1522	Y. Kim
6	1522	T. Ratcliffe
1	1522	M. Wilson
1	1542	F. Noblesse
1	1542	D. Hendrix
1	1543	P. Purtell
6	1544	A. Reed
1	1843	H. Cheng
1	1843	J. Dean
1	1843	J. Telste
1	522.1	TIC (C)
1	522.2	TIC (A)
10	522.6	Reports Control